Tampere University

JUSSI ISOKUORTTI

Triplet Energy Transfer in Photon Upconversion and Photoswitching

Tampere University Dissertations 627

Tampere University Dissertations 627

JUSSI ISOKUORTTI

Triplet Energy Transfer in Photon Upconversion and Photoswitching

ACADEMIC DISSERTATION
To be presented, with the permission of
the Faculty of Engineering and Natural Sciences
of Tampere University,
for public discussion in the auditorium Pieni sali 1
of the Festia building, Korkeakoulunkatu 8, Tampere,
on 10 June 2022, at 12 o'clock.

ACADEMIC DISSERTATION
Tampere University, Faculty of Engineering and Natural Sciences
Finland

Responsible supervisor and Custos	Professor Timo Laaksonen Tampere University University of Helsinki Finland	
Supervisors	Dr. Nikita Durandin Tampere University Finland	Professor Nikolai Tkachenko Tampere University Finland
Pre-examiners	Professor Bo Albinsson Chalmers University of Technology Sweden	Professor Sylvestre Bonnet Leiden University Netherlands
Opponent	Professor Kasper Moth-Poulsen ICREA and ICMAB-CSIC, Spain	

Cover design: Roihu Inc.

ISBN 978-952-03-2463-6 (print)
ISBN 978-952-03-2464-3 (pdf)
ISSN 2489-9860 (print)
ISSN 2490-0028 (pdf)
http://urn.fi/URN:ISBN:978-952-03-2464-3

PunaMusta Oy – Yliopistopaino
Joensuu 2022

ACKNOWLEDGEMENTS

The work for this thesis was performed in the Supramolecular chemistry of bio- and nanomaterials team at the Faculty of Engineering and Natural Sciences of Tampere University. The Academy of Finland (grant no. 316893), the European Research Council (decision no. 101001016) and Tekniikan edistämissäätiö are gratefully acknowledged for their funding and support of this work.

First, I want to thank my supervisors Prof. Timo Laaksonen and Dr. Nikita Durandin. I started working with Timo in 2016 and with Nikita in 2017 and I never looked back. You have instilled in me a great passion for research and given me all the support I could have wished for all the while trusting me to find my own way from early on. I can only hope you are as proud of me as I am of you as my mentors. I would also like to thank Profs. Nikolai Tkachenko and Arri Priimägi, Drs. Elina Vuorimaa-Laukkanen and Alexander Efimov, and Mr. Kim Kuntze for their invaluable support and friendship during these years. I want to also extend my gratitude to all my colleagues in Festia and Sähkötalo, whether it was about borrowing the beam profiler or having coffee. I am also grateful to my co-authors, here in Tampere and elsewhere, for their help with every project I have been involved with during my doctoral studies.

To my friends, the ones from childhood that also emigrated from Hyvinkää to Tampere and those that I have made during these wonderful years in Tampere, I want to say thank you. I am so fortunate to be able to call such brilliant and lovely people my friends.

I cannot express how much I want to thank my family for all their love and support. Äiti ja isä, I would not be here without you. Ever since I can remember, you have encouraged curiosity and supported the endeavors of us kids. Terhi ja Harri, how wonderful siblings I have been given. I have always admired your courage and the trails you have blazed. All I had to do was to follow your example. Cristina, a luz da minha vida, your love, resolve and brains amaze and inspire me every day. What a blessing it is to share the struggles and joys of studies, science, and more importantly, of life with you. Thank you for always being there.

Austin, Texas, May 2022
Jussi Isokuortti

ABSTRACT

Light-driven processes involving excited triplet states can be leveraged in numerous fields of science and technology to achieve for example more sustainable manufacturing and chemical syntheses, more efficient solar energy harvesting, safer and more potent therapies for diseases, more sensitive imaging and sensors, or more stable qubits for quantum information sciences. Knowledge of the origin and fate of triplet states is therefore fundamental in realizing these outcomes. This involves understanding triplet energy transfer (TET), an integral step in many of these processes.

In this thesis we explore TET, especially in the context of triplet fusion photon upconversion and photoswitching. Photon upconversion by triplet fusion is based on pooling the energy of photoexcitation in metastable triplet states that can fuse to generate singlet excited states with higher energy. Therefore, TET is an integral part of triplet fusion upconversion. Photoswitching or photoisomerization means control of the geometric structure and thus properties of molecules with light. In some photoswitches, such as azobenzenes that are used in this thesis, isomerization can be achieved by accessing their triplet states via TET.

After introducing the definition, generation and general properties of excited triplet states and the mechanism of TET, we focus on its role in triplet fusion upconversion and photoswitching systems. This involves investigating the properties of the engaged molecules, photosensitizers and acceptors, and how they affect the performance of these systems, allowing formulation of clear guidelines for designing them. Particularly, we consider the interplay of these properties and its effect on the thermodynamics of TET. Commonly efficient TET is ensured by employing photosensitizer-acceptor pairs with a large exothermic triplet energy gap. Here we investigate systems with small or even endothermic energy gap, how to make them efficient and uncover the possibilities they offer. This thesis deepens the understanding of TET and offers insight into controlling it in photon upconversion and photoswitching, which paves way for their implementation into practical applications.

TIIVISTELMÄ

Virittyneitä triplettitiloja hyödyntäviä valokäyttöisiä prosesseja voidaan käyttää lukuisilla tieteen ja teknologian aloilla esimerkiksi kestävämpien valmistusmenetelmien ja synteesien, tehokkaamman aurinkoenergian tuotannon, turvallisempien ja tehokkaampien hoitomuotojen, herkempien anturien ja kuvantamisen sekä vakaampien kvanttibittien aikaansaamiseksi. Triplettitilojen alkuperien ja kohtaloiden käsittäminen on siten perustavanlaatuista tietoa näiden saavutusten toteuttamiseksi. Tämä vaatii tietämystä triplettienergian siirrosta, joka on olennainen osa monia näitä prosesseja.

Tässä väitöskirjassa tarkastellaan triplettienergian siirtoa erityisesti triplettifuusioon perustuvan valon ylöskonversion ja valokytkemisen yhteydessä. Valon ylöskonversio triplettifuusiolla perustuu valon energian keräämiseen metastabiileihin triplettitiloihin, jotka voivat fuusioitua muodostaen korkeamman energian virittyneitä singlettitiloja. Triplettienergian siirto on siis erottamaton osa triplettifuusioon perustuvaa ylöskonversiota. Valokytkeminen tai valoisomerointi tarkoittaa molekyylien rakenteen ja siten niiden ominaisuuksien ohjaamista valolla. Joidenkin valokytkinten, kuten tässä väitöskirjassa käytettyjen atsobentseenien, isomerointi voidaan suorittaa triplettienergian siirron avulla.

Virittyneiden triplettitilojen määritelmän, muodostamisen ja yleisten ominaisuuksien sekä triplettienergian siirron mekanismin esittelyn jälkeen väitöskirjassa keskitytään triplettienergian siirtoon valon ylöskonversio- ja valokytkentäjärjestelmissä. Tämä käsittää osallistuvien molekyylien, valoherkistäjien ja akseptorien, ominaisuuksien tutkimista ja miten ne vaikuttavat näiden järjestelmien suorituskykyyn, mikä mahdollistaa selkeiden suunnitteluohjeiden muodostelun. Erityisesti huomioidaan näiden ominaisuuksien vuorovaikutukset ja sen seuraukset triplettienergian siirron termodynamiikkaan ja kinetiikkaan. Yleisesti tehokas triplettienergian siirto varmistetaan käyttämällä valoherkistimiä ja akseptoreja, joiden välillä on suuri eksoterminen energiaväli. Tässä väitöskirjassa tutkitaan järjestelmiä, joiden energiaväli on pieni tai jopa endoterminen, miten tällaisesta järjestelmästä tehdään tehokas ja avataan niiden mahdollistamia uusia näkymiä. Väitöskirja syventää tietoa triplettienergian siirrosta ja sen hallinnasta valon ylöskonversiossa ja valokytkemisessä, mikä viitoittaa niiden käyttöönottoa käytännön sovelluksissa.

CONTENTS

ABBREVIATIONS AND SYMBOLS

A	Acceptor
Azo	Azobenzene
CT	Charge transfer
D	Donor
dif	Diffusion
eT	Electron transfer
ET	Energy transfer
FRET	Förster resonance energy transfer
HO	Highest occupied molecular orbital
hT	Hole transfer
ISC	Intersystem crossing
LU	Lowest unoccupied molecular orbital
PS	Photosensitizer
RTET	Reverse triplet energy transfer
TET	Triplet energy transfer
TF	Triplet fusion
TFUC	Triplet fusion photon upconversion
SOC	Spin-orbit coupling

ΔE_T	Photosensitizer-acceptor triplet energy gap
ΔE_{S-T}	Singlet-triplet energy gap
ΔS	Entropy change
E	Energy
Φ	Efficiency or quantum yield
H	Hamiltonian
I_{exc}	Excitation power density
I_{th}	Excitation power density threshold
J	Coulomb integral
K	Exchange integral

k	Rate constant
k_B	Boltzmann constant
K_{SV}	Stern-Volmer rate constant
S_n	Singlet state, n = 0, 1, 2, 3, …
T_n	Triplet state, n = 0, 1, 2, 3, …
T	Temperature
τ	Lifetime

ORIGINAL PUBLICATIONS

Publication I Durandin, N. A.; Isokuortti, J.; Efimov, A.; Vuorimaa-Laukkanen, E.; Tkachenko, N. V.; Laaksonen, T. Efficient photon upconversion at remarkably low annihilator concentrations in a liquid polymer matrix: when less is more. *Chemical Communications* **2018**, 54, 14029.

Publication II Durandin, N. A.; Isokuortti, J.; Efimov, A.; Vuorimaa-Laukkanen, E.; Tkachenko, N. V.; Laaksonen, T. Critical Sensitizer Quality Attributes for Efficient Triplet-Triplet Annihilation Upconversion with Low Power Density Thresholds. *Journal of Physical Chemistry C.* **2019**, 123, 37, 22865

Publication III Isokuortti, J.; Allu, S. R.; Efimov, A.; Vuorimaa-Laukkanen, E.; Tkachenko, N. V.; Vinogradov, S. A.; Laaksonen, T.; Durandin, N. A. Endothermic and Exothermic Energy Transfer Made Equally Efficient for Triplet-Triplet Annihilation Upconversion. *Journal of Physical Chemistry Letters* **2020**, 11, 1, 318

Publication IV Isokuortti, J.; Kuntze, K.; Virkki, M.; Ahmed, Z.; Vuorimaa-Laukkanen, E.; Filatov, M. A.; Turshatov, A.; Laaksonen, T.; Priimägi, A.; Durandin, N. A. Expanding excitation wavelengths for azobenzene photoswitching into the near-infrared range *via* endothermic triplet energy transfer. *Chemical Science* **2021**, 12, 7504

AUTHOR'S CONTRIBUTION

Publication I The author carried out all the experiments and data analysis, except the titration studies that were performed by N. A. Durandin, and contributed to the writing of the manuscript. The manuscript was written together with all the coauthors.

Publication II The author carried out all the experiments, data analysis and kinetic modelling, and contributed to the design of the kinetic model with N. A. Durandin and T. Laaksonen. The manuscript was written together with all the coauthors.

Publication III The author actively participated in planning the experiments, performed all the experiments, modelling and data analysis, and wrote the first draft of the manuscript. The final manuscript was written together with all the coauthors.

Publication IV The author actively participated in planning the experiments and performed all the experiments and data analysis, and wrote the first draft of the manuscript. The final manuscript was written together with all the coauthors.

1 INTRODUCTION

Light is the energy source for life on Earth and the importance of its efficient harvesting and transforming is only increasing.[1–4] Even further, light is becoming more and more potent and common carrier of information and stimulus, which offers untold possibilities for fields of science and technology ranging from biomedicine and quantum technology to soft robotics and additive manufacturing.[5–16]

Many of these fields rely on light-driven processes that either depend on or suffer from the involvement of triplet states. Thus, understanding the generation and fate of triplet states is essential for leveraging such processes. An excited triplet state may decay radiatively via thermally activated delayed fluorescence or phosphorescence, which can be utilized for example in light-emitting diodes, sensors or bioimaging.[17–23] It may react with molecular oxygen and generate reactive oxygen species that can be useful in cancer therapy and inactivating microbial pathogens or as reaction intermediates in synthesis, or contribute to the deterioration of the system.[24–26] More importantly, at least in the context of this thesis, the energy of the triplet excited state may be transferred to a triplet state of another molecule. Triplet energy transfer or photosensitization enables access to the triplet states of molecules that have a low triplet yield upon photoexcitation. This indirect excitation can be harnessed for example in photorelease of therapeutic molecules[27,28] or photocatalysis of organic syntheses[29–33] or photon upconversion and photoswitching.

Triplet fusion (or triplet-triplet annihilation) photon upconversion (TFUC) systems can generate high-energy excited states from low-energy, low-intensity and incoherent excitation.[34–36] TFUC systems have attracted considerable attention in the last 20 years due to their potential for improving solar energy harvesting by spectral conversion.[37–49] In addition to solar energy, TFUC has been implemented to a wide array of applications such as phototriggered drug release and targeting, bioimaging, optogenetics, sensing, 3D printing and photocatalysis.[50–68]

The other triplet energy transfer driven process we examine in this thesis is sensitized photoswitching or photoisomerization. Photoswitches, like the azobenzenes studied here, are used in solar energy conversion and as key tools for achieving non-invasive spatiotemporal control in photoactuation, photocatalysis,

magnetic resonance imaging, super-resolution microscopy, phototriggered drug release and photopharmacology.[9,69–79] Orthogonal or indirect excitation pathways, such as triplet energy transfer, offer photoswitching systems new or improved properties like more quantitative photoisomerization and extended excitation wavelengths.

Efficient red or even near infrared excitable photon upconversion and photoswitching systems are required for the aforementioned applications, especially for those pertaining to biology. As we will learn throughout this thesis, grasp of triplet energy transfer will enable taking these systems to their limits and realizing their full potential.

1.1 Aim and scope of this work

This thesis is about triplet energy transfer in the context of photon upconversion and photoswitching. After establishing the mechanism of triplet energy transfer (TET), the thesis focuses on how the photosensitizer and acceptor properties affect the energy transfer step and overall efficiency of triplet fusion photon upconversion (TFUC) and sensitized photoswitching. As such, the objectives of this thesis are to provide the reader with a theoretical context of TET, TFUC and sensitized photoswitching, and establish clear guidelines on how the photophysical properties of the photosensitizer/acceptor pairs and their operating conditions affect the thermodynamics, kinetics and overall performance of TFUC and sensitized photoswitching systems. We will also explore how these properties and conditions can be leveraged to approach the thermodynamic limits of TFUC and sensitized photoswitching systems and what possible benefits are realized by approaching these limits.

The objectives are achieved with a comprehensive literature review and the results of the four original publications presented in this thesis. **Publication I** demonstrates the importance of photosensitizer triplet state lifetime to the TET and TFUC process, especially in viscous media and when acceptor concentrations are limited. **Publication II** is a comprehensive study on the effect of the photosensitizer and acceptor properties and their concentrations on the performance of a TFUC system with focus on the photosensitizer lifetime and energy gap between the photosensitizer and acceptor triplet states. In Publication II we also postulate that in certain cases efficient TFUC is possible even when the triplet energy gap is close to zero or even positive (endothermic). **Publication III** verifies this hypothesis by

demonstrating that with careful design of the TFUC system and with superb photosensitizers, even substantially endothermic TET can drive the TFUC process efficiently and subsequently extend the excitation wavelength. In such case, the TET process becomes entropy driven. The entropy change can be maximized and utilized efficiently in systems that consume the transferred triplet states rapidly, such as some photoswitching systems. This concept is demonstrated in **Publication IV** that shows efficient azobenzene photoswitching by indirectly exciting azobenzene photoswitches via triplet energy transfer from photosensitizers possessing considerably lower triplet state energies than the acceptor azobenzene.

These results contribute to the field of photon upconversion by establishing directions for maximizing TET efficiency when, for example, the acceptor concentration is limited or even for "energetically non-favorable", i.e. less than 4 k_bT exothermic triplet energy gap, photosensitizer-acceptor pairs. Such guidelines are important when designing upconversion systems in nanoconfinement and solid state or when maximized upconversion energy shift is desired. In addition to photon upconversion, the thesis highlights the utility of TET as an alternative excitation pathway for azobenzene photoswitching systems. The realization that even substantially endothermic TET is capable of driving azobenzene isomerization effectively paves way for near-infrared excitable photoswitching systems that are required in, for example, biomedical applications.

1.2 Outline

This thesis consists of five chapters. Chapter 1 is the introduction and provides the reader the background and motivation for these studies. In Chapter 2, after establishing the principal properties of electronic triplet state, the focus is on the mechanism, thermodynamics and kinetics of triplet energy transfer, and how it can be studied experimentally. Chapter 3 introduces the process of triplet-fusion photon upconversion and establishes the connection between the efficiency of triplet energy transfer and triplet-fusion photon upconversion. Chapter 4 outlines (azobenzene) photoswitching, its different indirect or orthogonal excitation pathways and why endothermic triplet energy transfer is especially viable for azobenzene photoswitching. Chapter 5 draws the conclusions of this thesis and offers some prospects for research in future.

2 TRIPLET ENERGY TRANSFER

After the absorption of a photon, the created excited state of a molecule faces multiple possible fates. It may decay to the ground state non-radiatively or by emitting another photon. The excited molecule may change its spin state from a singlet to a triplet via a process called intersystem crossing. It may interact with another molecule by transferring a charge or the excitation energy. If this interaction results in the donation of energy from a triplet excited state to a triplet state of the acceptor, the process is called triplet energy transfer. In this Chapter we shall work through from the definition and general properties of triplet state to how it is generated after photoexcitation and eventually to triplet energy transfer – its mechanism, what sets it apart from charge and other energy transfer processes, and the thermodynamics involved. The final two shorter sections are devoted to the experimental aspects of triplet energy transfer and the relationship between oxygen and triplet excited states. As expressed in the introduction, the grasp of these fundamentals is paramount to understand triplet energy transfer driven processes like photon upconversion (Chapter 3) and sensitized photoswitching (Chapter 4) and achieve their full potential.

2.1 Triplet state – definition, formation, and general properties

To define "triplet state", we will first take a brief excursion to the 1920s that experienced one of the golden ages of physics with an astonishing number of revolutionary discoveries and theories that lead to the conception of quantum mechanics.[80] One of these discoveries was the spin, the inherent angular moment of a particle or atom, its influence on for example spectroscopy[81] and the periodic table of elements and chemical bonding under the Aufbau principle[82].

The electron, being a fermion with an electric charge, has three fundamental properties in the context of this thesis: 1) it has a spin of ½, 2) its spin and electric charge give it a magnetic dipole moment and angular moment and 3) its wavefunction is antisymmetric. This antisymmetry invokes the Pauli exclusion principle[83], which states that two electrons cannot occupy the same quantum state.

In terms of atoms and molecules, two electrons sharing an orbital are required to have opposite spins, ½ and -½. As most molecules do not possess unpaired electrons in ground state (molecular dioxygen being an exception, vide infra), their total spin quantum number is zero (½ + (-½) = 0). However, especially in some cases of excited states, the two electrons that once shared an orbital may be separated and no longer constrained by their fermionic nature of maintaining opposite spins. In such a case, the total spin quantum number can be -1, 0, or 1. Thus, the spin multiplicity is three, when in the case of paired electrons in the same orbital, the spin multiplicity is naturally one. As is probably already evident, a system with spin multiplicity of one is a singlet state and with three a triplet state. To conclude this brief history lesson, it has to be noted that this terminology of singlet and triplet states first originated from the observation of spectral lines splitting under an external magnetic field, which was satisfactorily explained with the concept of spin in, you guessed it, the 1920s.[84]

How are triplet states then formed if most molecules have a singlet ground state? This question is especially prudent due to the conservation of spin angular momentum, which makes transitions from singlet to triplet state and vice versa forbidden and thus typically improbable.[85,86] However, in addition to their inherent spin angular momentum, the electrons in atoms and molecules are in orbit and therefore possess orbital angular momentum. These two momenta acting on the electrons are coupled to a varying a degree via a relativistic effect called the spin-orbit coupling (SOC). The magnitude of SOC and consequently the probability of intersystem crossing (ISC) between two different spin multiplicities can be evaluated by considering the integral of the two states involved in the transition (here from singlet to triplet state as an example):

$$\left[\hat{H}_{SOC}\right]_{ij} = \left\langle \psi_{S_i} \middle| \hat{H}_{SOC} \middle| \psi_{T_j} \right\rangle \tag{1}$$

where $\hat{H}_{SOC}$ is the SOC operator (Hamiltonian), ψ is the electronic wavefunction of the initial singlet (S) and the resulting triplet state (T). In qualitative terms, the magnitude of SOC and therefore the probability of multiplicity mixing is dependent on the $\hat{H}_{SOC}$ and the character of the states involved. First, let us consider the SOC operator that can be approximated[a] as

[a] For details, see Penfold et al.[90] and Baryshnikov et al.[100].

$$\hat{H}_{SOC} = \frac{1}{2m_e^2c^2}\sum_I \sum_i \frac{Z_I^{eff}}{r_{iI}^3}\hat{\boldsymbol{l}}_i \cdot \hat{\boldsymbol{s}}_i \quad (2)$$

where m_e is the mass of the electron, c is the speed of light, Z_I^{eff} is the effective nuclear charge of the nucleus I, r is distance and $\hat{\boldsymbol{l}}_i$ is the angular momentum and $\hat{\boldsymbol{s}}_i$ is the spin operator of electron i. From Eq. 2 we can draw the first simple conclusion that SOC and consequently ISC is enhanced by the nuclear charge. This is called the heavy atom effect[87] and it is utilized in many triplet photosensitizers (PS) i.e. molecules that are capable of generating an excited triplet state upon excitation with light.

While it is useful for depicting the coupling of spin and orbital angular moment and the heavy atom effect, Eq. 2 in its simplicity is a very limited description of the formation of a triplet state. The fact of the matter is that the Born-Oppenheimer approximation[88] is liable to break down in excited molecules, which necessitates the inclusion of the vibrational contributions to ISC. Fermi's golden rule[89] is often utilized in describing the rate of population transfer between states as the function of the coupling strength between the initial and final states and the number of ways the transition can occur i.e. density of (final) states. For ISC this can be written (with the electronic and vibrational contributions separated) as[90]

$$k_{ISC} = \frac{2\pi}{\hbar}\sum\left|\langle\psi_S|\hat{H}_{SOC}|\psi_T\rangle\right|^2 \sum|\langle\nu_S|\nu_T\rangle|^2\,\delta(E_S - E_T), \quad (3)$$

where ν_T and ν_S are the vibrational wavefunctions, E_S is the energy of the singlet state and E_T is the energy of the triplet state and the δ function ensures the conservation of energy. The vibrational term is often called the Franck-Condon factor or Franck-Condon weighted density of states.[91] The coupling and thus transfer rate between two states depends on the energy gap between them – the smaller the energy gap, the higher the transfer rate – which is why the application of Fermi's golden rule is sometimes called the energy gap law.[92]

Eq. 3 underpins the vibrational contributions to ISC but for the sake of simplicity, the electronic and vibrational terms were separated, which can be reasonable for rigid molecules with localized electronic states. However, for molecules with high flexibility and density of states, such simplistic approaches as the heavy atom effect, the energy gap law or El-Sayed rules[93] occasionally fail to describe ISC and the use of a more holistic, spin-vibronic (vibrational and electronic) approach is required.[90] This means that the wavefunctions in Eq. 1 need to be replaced by the electronic, vibrational and spin wavefunctions and perturbations thereof. A sound example of

a molecule where the electronic, vibrational and spin cannot be treated separately is porphyrin and its derivatives that are common PSs and also employed in every publications presented in this thesis. Free-base porphyrin has no heavy atoms in its structure, the electronic transitions are almost purely of $\pi - \pi^*$ character meaning that the change in the spin is not accompanied by changes in the angular momentum (El-Sayed rules) and the energy difference between the first singlet (S_1) and triplet (T_1) states is large yet somehow the efficiency of the singlet-to-triplet ISC can be as high as 90 %.[94] In such a case, the ISC from S_1 to T_1 in free-base porphyrin can only be explained with spin-vibronic coupling, which is the result of out-of-plane vibrations of the porphyrin macrocycle.[95] This causes spin-vibrational coupling between the S_1 and T_1 by mixing some $\sigma - \pi^*$ character in to the electronic wavefunctions allowing efficient ISC.[96]

Having outlined the somewhat complicated nature of the formation of triplet states from originally singlet state molecules, we shall conclude this chapter by considering some of the interesting properties of triplet states. One of the pioneers of molecular spectroscopy, Aleksander Jabłoński, proposed in 1933 the existence of a metastable energy level between the ground state and the prompt excited state in some common dye molecules and that the probability of the transition from this metastable state to the ground state is small.[97] Ten years later, the pioneers Terenin and Lewis & Kasha recognized this low lying metastable state as a triplet.[98,99] Thus, again with a little historic context, we come to recognize some of the most important properties of molecular triplet excited states:

1) They have lower energy than their respective singlet state, i.e. $E(\mathrm{T_n}) < E(\mathrm{S_n})$.[b]
2) The probability of spontaneous transition from a triplet excited state to the singlet ground state is low, thus the lifetimes of excited triplet states are long, typically several orders of magnitude longer than excited singlet states.
3) They are paramagnetic due to the nonzero total spin and thus having a net magnetic dipole moment.
4) They are quenched by molecular dioxygen, which yields highly reactive singlet oxygen.

We shall now dedicate the rest of Chapter 2 to elaborate on these properties. Some of these processes and properties related to triplet states are summarized in Fig. 1.

[b] Possibly the first exception was reported in 2021.[370]

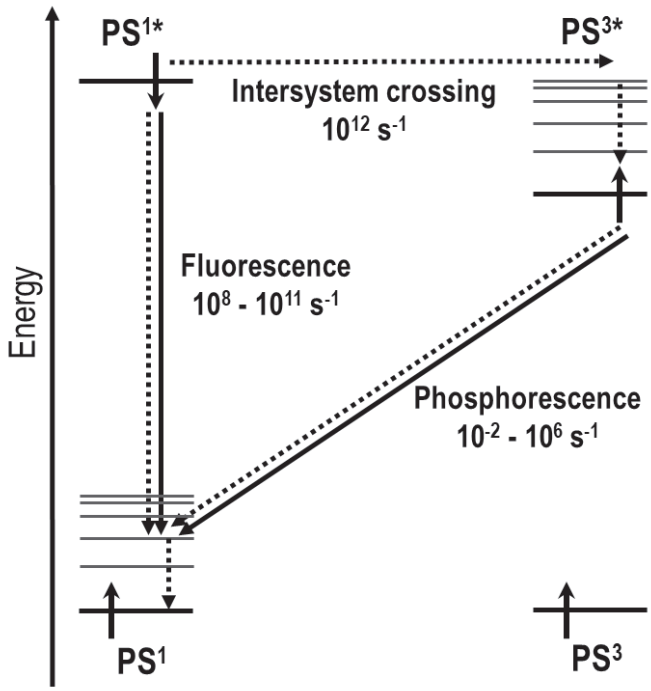

Figure 1. The unimolecular processes involved with excited singlet and triplet states. The arrows represent the spin of the electrons. The solid lines represent radiative transitions while the dashed lines represent non-radiative processes, such as internal conversion (occurs without change in spin multiplicity) or intersystem crossing (occurs with change in spin multiplicity). The typical rate constants of the processes are from Baryshnikov et al.[100]

To explain why the energy of the triplet state is lower than the corresponding singlet state, a chemist may remember the Hund's rules[101], the first one of which postulates that the electronic state with the largest total spin has the lowest energy.[102] This is the result of exchange interaction[103,104] that leads to repulsion between electrons due to the Pauli exclusion principle. For a two-electron system with orthogonal orbitals a and b the total energy is

$$E = E_a + E_b + J \pm K \tag{4}$$

where E_a and E_b are the unperturbed energies, J is the Coulomb integral and K is the exchange integral. A positive sign is assigned to the singlet and a negative sign to the triplet state.[102,105] Therefore, the energy difference between the singlet and triplet states is

$$\Delta E_{S-T} = 2K. \quad (5)$$

For the electrons 1 and 2 occupying the orbitals, K can be evaluated by the overlap of the orbitals in space:

$$K \sim \frac{1}{r_{12}} \langle a(1)b(2)|a(2)b(1)\rangle. \quad (6)$$

Thus, ΔE_{S-T} of a molecule depends on two factors, the distance separating the electrons and the overlap of the orbitals occupied in the excited state. For $\pi - \pi^*$ systems, such as anthracene (1.5 eV[106]) or perylene (1.4 eV[107]), ΔE_{S-T} tends to be large whereas in $n - \pi^*$ systems, such as benzophenone (0.2 eV[106]), it is small as a result of smaller overlap between the orthogonal n and π^* orbitals.

Manipulation of the exchange integral of molecular systems has led to the breakthrough of the thermally activated delayed fluorescence (TADF) materials.[17] When the ΔE_{S-T} of a molecule is low enough (typically in the order of 0.1 eV), reverse ISC from the triplet state back to the more emissive singlet state may occur by thermal excitation. This results in delayed fluorescence[c] and can be used for example in organic light emitting diodes (OLEDs) to increase their efficiency by promoting some of the triplet excitons to the singlet state after charge recombination.[108] In TADF dyes, ΔE_{S-T} is reduced by introducing charge transfer character to the excited states using electron donor and acceptor moieties, which increases the separation of the electrons in the excited state and decreases the orbital overlap. The orbital overlap can be further decreased by twisting the moieties in respect to each other with sterically bulky substituents.[109,110] The small ΔE_{S-T} allows efficient ISC and several TADF molecules have been used as PSs.[111,112]

Another interesting class of materials with low exchange energies are semiconductor quantum dots/nanocrystals. In these materials, the high dielectric constant attenuates the electron-electron repulsion and spatial confinement of the exciton (electron-hole pair) result in small exchange integrals (typically called bright-dark state splitting in semiconductors) in the order of 1-100 meV and thus effective mixing of the singlet and triplet states.[113] In fact, the SOC is so strong in such materials that total angular momentum should be used as the defining quantum number instead of spin. This enables the use of semiconductor quantum dots/nanocrystals as PSs, a research topic that has received much attention in the last few years.[112,114–117]

---

[c] Occasionally, or more historically, called E-type delayed fluorescence after eosin was discovered to undergo temperature dependent reverse ISC and delayed fluorescence by Parker & Hatchard.[371]

Until this point, we have only considered transition from the triplet state to be improbable and thus longer living, especially when compared to fluorescence from the excited singlet state due to the forbidden nature of transitions involving change in the spin multiplicity. Prior to the establishment of quantum theory, phosphorescence was typically differentiated from fluorescence only by the fact that it was more persistent. For example, TADF was considered to be a form of phosphorescence until the 1940s and the works of Terenin and Lewis & Kasha, who identified triplet state as "phosphorescent state unique"[99] in molecules. This led to the modern definition[d] of phosphorescence that IUPAC designates as "luminescence involving change in spin multiplicity, typically from triplet to singlet or vice versa".[118] For the context of this thesis this definition works well. However, it should be noted that due to SOC being non-zero in practically every system, all electronic states have mixed singlet and triplet state character. As was the case with semiconductor nanocrystals, even in some molecules, especially those that contain heavy elements like Ir or Pt, SOC is so strong that S and T states become quasi-degenerate and distinction between fluorescence and phosphorescence becomes convoluted.[100] In many systems, fortunately, singlet and triplet states are spectrally and temporally well-resolved, which enables the detection of phosphorescence as a powerful tool, used in every publication of this thesis, to examine the triplet state, its energy, lifetime and character. For example, in Publication II, the phosphorescence spectra of the PSs, tetraphenylporphyrins metalated with Zn, Pd or Pt ions, were used to evaluate their triplet energies that are shown in Fig. 2.

[d] Here we are concerned about molecular phosphorescence, not for example phosphorescence originating from electron-hole recombination in semiconductors.

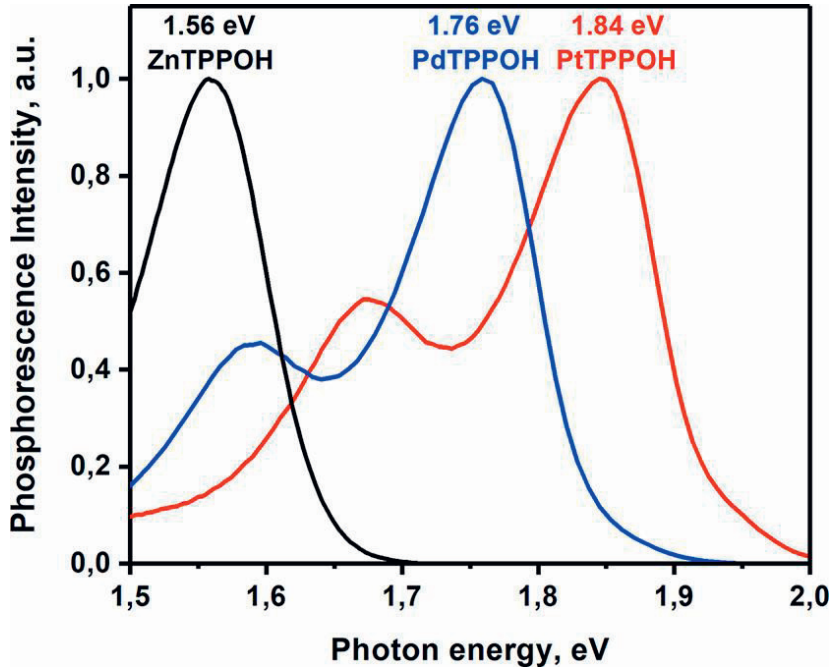

Figure 2. Intensity normalized phosphorescence spectra of the PSs used in Publication II. The triplet state energy was assigned by the maximum of each spectrum. Reprinted with permission from Publication II.[119] Copyright 2019, ACS.

2.2 Mechanism and thermodynamics of triplet energy transfer

Quenching of excited states was briefly mentioned in the previous section. Now we shall take a closer look at different quenching, i.e. energy or charge transfer, mechanisms between different molecules and states. After establishing these mechanisms, we will focus on triplet energy transfer (TET) and its parameters.

To determine whether charge transfer (CT) or energy transfer (ET) occurs between two molecules, we first need to introduce the term frontier molecular orbitals (FMO) that includes the highest occupied molecular orbital (HO) and lowest unoccupied molecular orbital (LU) of the ground state of a molecule. This makes the notation of electron configurations simple for molecules as the ground state can be expressed as $(HO)^2$ and an excited molecule as $(HO)^1(LU)^1$. In most cases, the extent (probability) and mechanism of the quenching reaction can be determined by examining the FMO interaction between the donor (D)[c] and acceptor (A) of the

[c] A photosensitizer is a donor in its triplet state.

system.[106] The interactions that can occur in ET are dipole-dipole and electron exchange interaction and in CT solely electron exchange. These (simplified) interactions are illustrated in Fig. 3. ET may also occur by a trivial or radiative mechanism, i.e. the donor emits a photon that is absorbed by the acceptor. This, however, is not considered a quenching mechanism since it does not result in shorter excited state lifetime. It is also worth mentioning that, since direct singlet-to-triplet excitation is improbable due to its spin-forbidden nature and therefore low absorption cross section, TET cannot occur via the radiative mechanism.

The overall electronic coupling that results in ET can be expressed as[120]

$$V = V_{Coul} + V_{exch} + V_{ovlp}, \tag{7}$$

where V_{Coul} is the Coulomb interaction between electronic transitions, V_{ecxh} is the exchange coupling that arises from the indistinguishability of electrons in many-electron wavefunctions and V_{ovlp} depicts the overlap between the donor and acceptor orbitals. Over large distances (we shall give some context on what is a large distance a bit later), only Coulomb interaction can take place. This Coulombic interaction was approximated as the dipole-dipole coupling between the transition states of D and A by Theodor Förster[121,122], which is why the dipole-dipole ET is often called Förster resonance energy transfer (FRET).

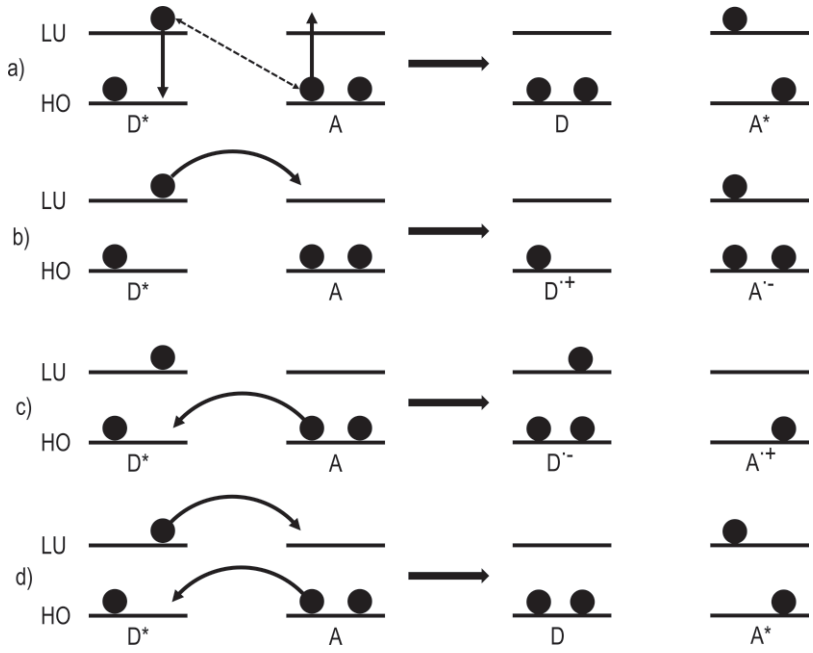

Figure 3. Schematic mechanisms of a) resonance energy transfer (dashed arrow represents dipole-dipole interaction), b) electron (charge) transfer, c) hole (charge) transfer and d) exchange electron transfer.

Thus, the Coulombic coupling can be approximated with dipole-dipole interaction[123]:

$$V_{Coul} \approx V_{dd} = \frac{1}{4\pi\varepsilon_0}\left[\frac{3(\boldsymbol{\mu_D}\cdot\boldsymbol{R_{DA}})(\boldsymbol{\mu_A}\cdot\boldsymbol{R_{DA}})-\boldsymbol{\mu_D}\cdot\boldsymbol{\mu_A}}{R_{DA}^3}\right], \quad (8)$$

where $\boldsymbol{\mu}$ is the transition dipole moment and $\boldsymbol{R_{DA}}$ is the separation between the D and A. The square of the transition dipole moment is proportional to the oscillator strength of the electronic transition. Experimentally, the oscillator strength is directly proportional to the extinction coefficient of absorption and radiative constant of emission.[106] In the Förster theory, these quantities are related to the emission (fluorescence) lifetime of D and the overlap of emission spectrum of D and absorption spectrum of A, resulting in the well-known relation between the dipole-dipole coupling and rate of FRET:[120,122]

$$V_{dd}^2 \propto k_{FRET} \propto \frac{k_D^0}{R_{DA}^6} J(\epsilon_A), \quad (9)$$

where k_D^0 is the radiative lifetime of D and $J(\epsilon_A)$ is the overlap integral of D emission and A absorption where the extinction coefficient of A is included in the integration. The overlap integral of emission and absorption spectra gives notion to the similarity between the radiative ET and FRET. Indeed, they are a unified process in terms of quantum electrodynamics, where FRET is mediated by virtual photons and radiative ET by real photons.[124]

Typically, the Coulombic coupling is considered to occur between two singlet states as these transitions are allowed with discernible transition dipole moments and thus V_{Coul} been regarded to become zero if either D or A undergoes a change in multiplicity.[125] However, strong SOC can promote large enough transition dipole moment between the triplet excited state and singlet ground state of D for triplet-singlet FRET to occur between D and A.[126,127] In principle, triplet-triplet and singlet-triplet ET can occur via SOC-mediated FRET but even in theory this pathway is negligible (approx. $10^{-6} \times V_{Coul}$ when compared to singlet-singlet FRET)[123] and experimentally energy transfer from excited triplet states has been found to be independent of A singlet-triplet oscillator strengths.[128] As neither radiative ET nor FRET can be considered as a plausible mechanism of yielding a triplet excited acceptor from an excited donor,[f] we need to consider a third mechanism.

It was already mentioned that the Coulomb interaction dominates at large distances between the molecules. Rightfully one begins to wonder what occurs when the distance between D and A becomes small. And by small we mean so small that the orbitals of D and A begin to overlap, i.e. D and A come into contact. At such distances, the electron exchange and orbital overlap coupling (see Eq. 7) cannot be neglected. Moreover, they naturally become the predominant coupling modes for forbidden transitions as the Coulomb coupling vanishes,. The theory of ET occurring at such small distances was first introduced by David Dexter[129] and thus ET via electron exchange is often called Dexter energy transfer. The coupling in this case can be written as[123]

$$V \approx \frac{2\beta_{eT}\beta_{hT}}{\Delta E} - K, \tag{10}$$

where β_{eT} and β_{hT} are the electron and hole transfer matrix elements between D and A, ΔE is the energy difference between the charge-separated (D^+A^-) and locally excited (D*A) configurations and K is the exchange integral. Eq. 10 highlights the

[f] Perhaps a trivial mechanism of yielding a triplet excited A is FRET from singlet excited D to A that immediately undergoes ISC.[372]

contribution of eT and hT to the exchange ET and the fact that exchange ET can be considered simultaneous[g] eT and hT (see Fig. 3).[130–133] Owing to the exponential spatial distribution of orbital wavefunctions, the exchange coupling also attenuates exponentially in space.[123,134] Thus, in the Dexter theory, the rate of exchange ET has the following proportionality to D-A separation:[129,134]

$$k_{ET} \propto K^2 J \propto \exp\left(-\frac{2R_{DA}}{L}\right) J, \tag{11}$$

where L is the effective average (Bohr) radius of the D and A wave functions, which has been estimated to be, for example, 1.3-1.4 Å for naphtalenes[135] and 4.8 Å for porphyrin[136]. Thus, besides the D-A separation, the magnitude of K depends strongly on the spatial distribution of the D and A orbitals, i.e. molecular shape, size and orientation.[130,131,137] Altogether, for efficient exchange ET to occur, much shorter distance (<10 Å) between D and A is typically required than in FRET (<100 Å).[138]

It should be noted that both the Förster and the Dexter theory are based on the Fermi's golden rule (one may notice the similarity between Eqs. 3, 9 and 11). Thus, the overlap integral J can be considered to account for the Franck-Condon factors in ET.[120] In case of FRET, J is scaled by the extinction coefficient of A, while in exchange ET the overlap integral is normalized.[125,129] Therefore, as opposed to k_{FRET}, k_{ET} has no dependence on the transition dipole moment of A (nor D). This implies that exchange ET can promote even forbidden transitions, provided that the total spin multiplicity of D and A is remains constant in the process,[139,140] which the electron exchange ensures as it conserves the electron spin (see Fig. 4).[125,129] In the context of this thesis, this means that a triplet excited D (PS) can transfer its energy to a singlet ground state A to yield a singlet ground state D (PS) and a triplet excited A, i.e. triplet-triplet energy transfer that we will call triplet energy transfer (TET) henceforth. Other transitions can also occur via exchange ET, such as doublet-triplet energy transfer[141] as long as the total spin multiplicity is conserved.

[g] While typically exchange ET is regarded as simultaneous eT and hT, there has been discussion whether exchange ET can also occur with distinctive eT and hT steps from semiconductor nanocrystals.[115,373–375]

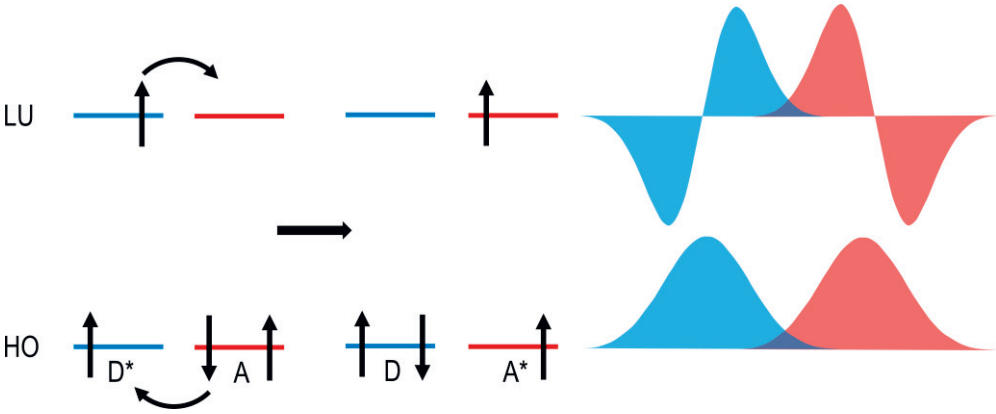

Figure 4. Exchange energy transfer conserves the spin of the transferred electrons and requires orbital overlap between the donor and the acceptor.

So far, we have discussed that PS and A need to be in contact for TET. This can be achieved either by bridging the chromophores together or collisions. In bridged systems (D-bridge-A, where bridge is either a solvent molecule(s) or a covalently linked moiety), the bridge can mediate the energy transfer by mechanisms such as superexchange or hopping.[138,142] However, in this thesis PS and A are separate molecules in a solvent, which makes their collisions and thus TET dependent on the rate of diffusion. As the PS and A begin to collide, they form an encounter complex. Within the encounter complex, the orbital overlap between PS and A occurs as they form a collision complex and TET may occur between them. The dissociation of PS and A is then again diffusion controlled. Thus, the observable rate of TET (k_{TET}) depends on the rate of diffusion (k_{dif}) and rate of the exchange ET (Eq. 11). This overall process[29] is depicted in Fig. 5.

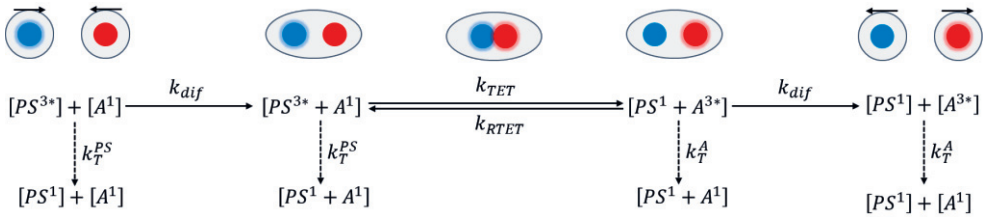

Figure 5. Formation of an encounter complex between PS and A leads to TET. The solvent cages of the individual molecules and the complexes are shown in grey. The competing process, spontaneous decay of the excited triplet state, is shown for both PS and A with the dashed arrows and the corresponding rate constants.

Diffusion is microscopically related to Brownian motion and macroscopically can be treated with the Stokes-Einstein equation[143], where the diffusion coefficient and consequently the rate of diffusion has an inverse dependence on the solvent viscosity.[144] After the diffusion limited encounter complex formation, PS and A share a solvent cage, where they may undergo multiple collisions before energy transfer occurs. As the dissociation of the encounter complex is also diffusion limited, the encounter complex lives longer in viscous solvents. Therefore in low-viscosity solvents the lifetime of the encounter complex may be too short for TET to occur and the apparent k_{TET} may differ substantially from k_{dif}.[106,145,146]

However, diffusion is not always the limiting factor for TET in solutions, the actual coupling between PS and A naturally affects k_{TET} as well. Besides the spatial separation, the coupling depends on the orbital overlap between PS and A, which can be estimated using the $PS^{3*} \rightarrow PS^{1}$ emission spectrum and $A^{1} \rightarrow A^{3*}$ absorption spectrum (Eq. 11). Owing to the forbidden nature of these transitions (especially direct singlet-to-triplet absorption), the direct determination of the spectral overlap can be challenging or even experimentally impossible,[134] while some computational approaches for evaluating the coupling have been developed by simulating the corresponding spectra[147,148] or potential energy surfaces[149,150]. Thus, the rate of TET is often estimated by examining its thermodynamic feasibility using the triplet energies of the sensitizer and the acceptor.[29,151]

When TET is observed in a solvent with a large population of PS and A, the triplet state population between the PS and A molecules follows the Boltzmann distribution and thus k_{TET} can be evaluated using an Arrhenius-type[152] equation:[153]

$$k_{TET} = \frac{k_{dif}}{1+\exp\left(\frac{\Delta E_T}{k_B T}\right)}, \tag{12}$$

where ΔE_T is the energy gap between the triplet states of PS and A, i.e. $\Delta E_T = E(A^{3*}) - E(PS^{3*})$, k_B is the Boltzmann constant and T is the temperature. Here the PS and A triplet state energies correspond to their vertical (0-0) transitions, meaning the emission energy of PS (phosphorescence) and singlet-to-triplet absorption of A. As such (and for now), ΔE_T can be considered as the enthalpy change in the energy transfer reaction.[154,155] Therefore, when $\Delta E_T < 0$, energy transfer is exothermic and when $\Delta E_T > 0$, it is endothermic. Consequently, if ΔE_T is highly exothermic (ΔE_T < -4 k_BT or 100 meV at room temperature), k_{TET} is essentially diffusion limited ($k_{TET} \rightarrow k_{dif}$). Another trivial consequence is naturally $k_{TET}(\Delta E_T = 0) = \frac{1}{2} k_{dif}$. As ΔE_T becomes more positive, the rate of TET from

the sensitizer to the acceptor becomes smaller and the reverse TET (RTET, see Fig. 5) from the acceptor back to the sensitizer becomes more probable. The ratio between forward TET (FTET, from sensitizer to acceptor) and RTET depends again on ΔE_T:[153]

$$\frac{k_{FTET}}{k_{RTET}} = \exp\left(\frac{-\Delta E_T}{k_B T}\right). \tag{13}$$

Eq. 13 depicts the energy transfer dynamics between sensitizer and acceptor with close triplet energies. These dynamics, however, cannot be depicted only with enthalpy change, as we know from chemical equilibrium, and the use of (Gibbs) free energy change should be used instead to take the entropy change into account:

$$\Delta G = \Delta H - T\Delta S, \tag{14}$$

where ΔH is the enthalpy change (ΔE_T) and ΔS is the entropy change. Thus, in an endothermic TET system, FTET needs to be driven by the entropy change as RTET is largely enthalpy driven. To efficiently populate the acceptor triplet states, ΔS needs to be maximized by ensuring large population or concentration between the ground and triplet excited states of both PS and A as depicted in the following equation:[154]

$$\Delta S = k_B \ln\left(\frac{[PS^{3*}][A^1]}{[PS^1][A^{3*}]}\right), \tag{15}$$

where the brackets indicate the concentrations of the singlet ground state and triplet excited state PS and A. Eq. 15 gives straightforward rules for maximizing ΔS and making endothermic TET spontaneous and efficient: The PS manifold (total number of PS molecules, ground and excited state) should be limited and as occupied as possible by excited triplet states. The opposite is required for the A manifold, i.e. it should be large and unoccupied. This is illustrated in Fig. 6.

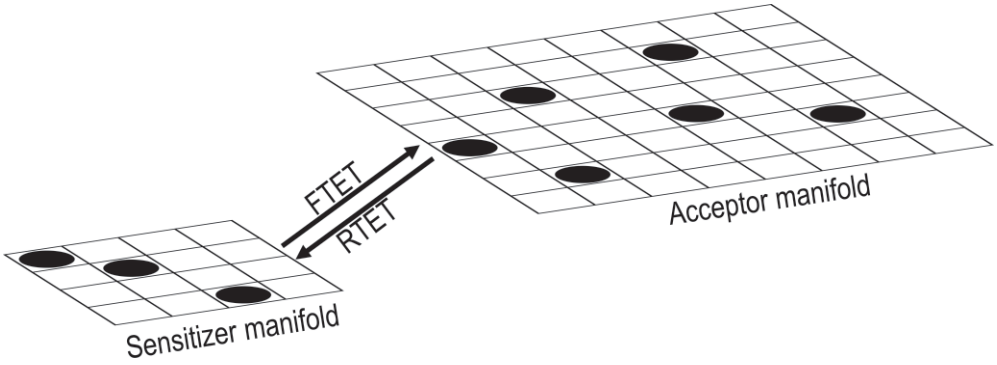

Figure 6. Photosensitizer and acceptor manifolds in TET. The black dot indicates a site occupied by an excited (triplet) state. Intuitively, by limiting the size of the S manifold and keeping it occupied, RTET becomes less probable.

Eq. 15 depicts the "mixing" entropy change involved in TET. Other contributions to ΔS in TET are 1) changes in dipole moment and therefore solvation, 2) changes in orbital and spin degeneracy and 3) changes in the degrees of freedom of the molecule, i.e. changes in conformations.[155] However, if there is no substantial CT involved in the states and considering that spin multiplicity is conserved in TET, 1) and 2) can be considered negligible. In nonrigid molecules, such as biphenyl, benzophenone or stilbenes, there may be substantial conformational differences between the ground and excited states, which can invoke substantial ΔS in the TET process.[156–158]

Molecules that possess substantially different geometries in ground and excited states are often regarded to undergo so-called non-vertical electronic transitions since the ground and excited state potential energy surfaces are strongly displaced. This notion has also been adopted to ET systems where the donor/sensitizer and/or acceptor undergoes a non-vertical transition and consequently the ET process is also called non-vertical[155,159,160] or "hot-band" assisted[160,161]. Such terms underline the importance of the vibrational contributions to the ET process (see Eq. 11!). These vibrational features may be especially significant in endothermic TET as the electronic transitions are strongly coupled with the conformational changes and substantial discrepancy between the energy values yielded by "spectroscopic" vertical (T_1-S_0) and the sensitized (S_0-T_1) transitions may be observed.[160]

To conclude this chapter, the author would like to reiterate the fascinating quantum mechanical (electron exchange) and thermodynamic (Gibbs free energy, mixing entropy) aspects of TET and emphasize their often-intertwined nature (non-vertical ET and its observable effects on the thermodynamics of ET). Their

collective understanding is therefore required for designing new TET-based systems and can lead to exciting and unexpected discoveries.[154,162–172]

2.3 Quenching studies of triplet energy transfer

TET is considered a quenching process as the PS triplet state is quenched by the acceptor. The quenching can be observed by monitoring the lifetime of the PS triplet. Lifetime measurements can be performed by measuring the phosphorescence decay or transient triplet-triplet (T_1-T_n, n = 2 , 3, …) absorption of the PS after pulsed excitation. Since every PS used in this thesis exhibit observable phosphorescence even at room temperature, quenching studies were performed measuring PS phosphorescence lifetime in presence of A. Quenching studies can be performed also by monitoring the steady-state intensity of phosphorescence as the lifetime and intensity are directly proportional. Time-resolved measurements are however often preferred over steady-state ones due to the ability to, for example, resolve dynamic and static quenching processes.[173] Another method for elucidating TET kinetics is observing the rise of the triplet-triplet absorption of A or, in certain cases as we will outline in Chapter 3, the delayed fluorescence of A.

Quenching is quantified by the ratio between the unquenched PS lifetime in absence of A (τ_0) and in presence of A (τ). The dependence of this ratio to [A] is called the Stern-Volmer relationship:[174]

$$\frac{\tau_0}{\tau} = 1 + K_{SV}[A], \tag{16}$$

where K_{SV} is the Stern-Volmer constant with a unit of M^{-1}. K_{SV} is the product of τ_0 and the quenching rate constant, which in case of TET is naturally k_{TET}:

$$\frac{\tau_0}{\tau} = 1 + k_{TET}\tau_0[A]. \tag{17}$$

The quenching rate constants, either K_{SV} or k_{TET} are typically determined by titrating the phosphorescence sample with A and fitting the rate constant to the quenching data as shown in Fig. 7.

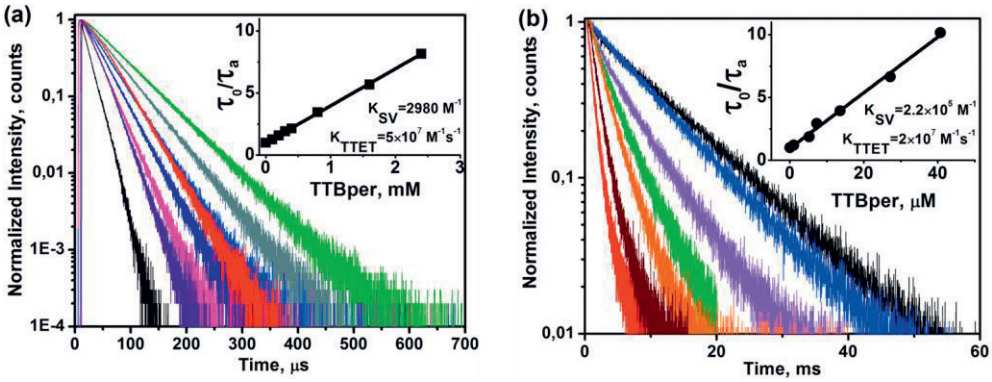

Figure 7. Phosphorescence decays of (a) Pt-tetraphenylporhyrin (PtTPPOH) and (b) Zn-tetraphenylporphyrin (ZnTPPOH) with tetra(tert-butyl)perylene (TTBper) as A in polyethylene glycol. The insets show the resulting Stern-Volmer plots with the quenching rate constants (here TTET is TET). Reprinted with permission from Publication I.[175] Copyright 2018, RSC.

The probability of (triplet) energy transfer from the excited state, i.e. the efficiency of quenching, is the ratio between the energy transfer rate and the sum of the rates of every decay process. For a PS-A system it is thus

$$\Phi_{TET} = 1 - \frac{\tau}{\tau_0} = \frac{k_{TET}[A]}{\frac{1}{\tau_0} + k_{TET}[A]}, \tag{18}$$

which is expressed with the reciprocal of the spontaneous decay rate i.e. the lifetime of the excited state. This emphasizes the effect of the PS lifetime to the quenching process, which is also evident in the K_{SV} values for the PS-A pairs shown above in Fig. 7 as the unquenched triplet state lifetime of PtTPPOH is 61 μs and ZnTPPOH is 11 ms in polyethylene glycol. If the quenching efficiency is plotted as the function of [A] (tetra(tert-butyl)perylene) for these two PSs used in Publication I, the effect of τ_0 becomes even more striking as shown in Figure 8. For example, to yield 0.9 quenching efficiency, only 40 μM of A is required for ZnTPPOH, whereas 3 mM is required for PtTPPOH even though the ZnTPPOH/tetra(tert-butyl)perylene pair exhibits smaller k_{TET} due to the considerably lower triplet energy of ZnTPPOH (see Fig. 2).

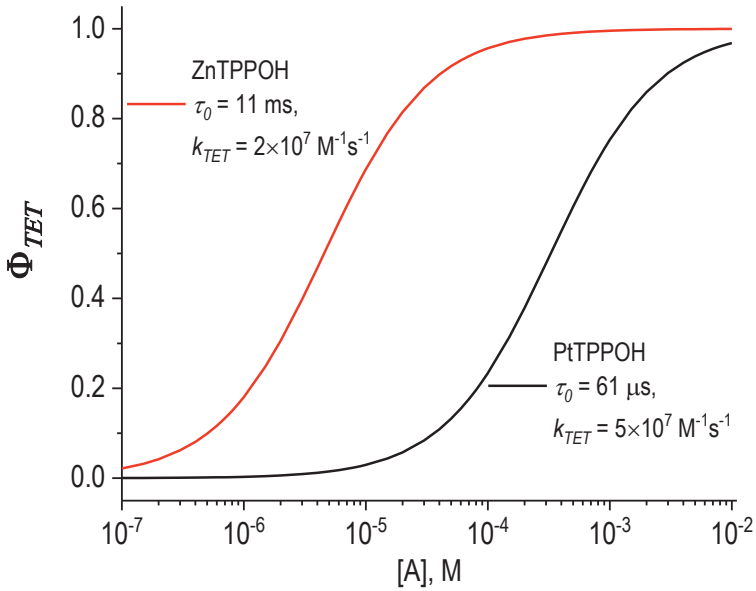

Figure 8. The quenching efficiency Φ_{TET} of PSs ZnTPPOH and PtTPPOH in polyethylene glycol as a function of quencher tetra(tert-butyl)perylene concentration [A].

Quenching studies provide essential insight into the kinetics and dynamics of photochemical processes like TET and can be implemented to estimate for example ΔE_T between PS and A. If the triplet energy of the PS is known (by for example measuring its phosphorescence spectrum, see Fig. 2), the triplet energy of A can then be evaluated indirectly with quenching studies, an approach commonly used, also in Publications II-IV, for molecules that do not exhibit observable phosphorescence or direct singlet-to-triplet absorption. For example, in Publications III-IV the k_{TET} values obtained from quenching studies were used to evaluate the previously unknown triplet energies of the acceptors and the thermodynamic nature of TET with Eq. 12.

2.4 Oxygen and triplet states

The rest of this chapter is dedicated to molecular dioxygen (O_2). Excited triplet states and dioxygen share such an inseparable relationship that, at least in the humble opinion of the author, they should be introduced simultaneously. Ground state dioxygen has two electrons occupying doubly degenerate antibonding π orbitals and per Hund's rules, these electrons are unpaired, which results in a triplet ground state.[176] This biradical electron configuration of dioxygen gives it peculiar properties[177,178] as a reactant and would be worth their own dissertation. However, here we shall limit the discussion on the interaction of dioxygen and excited states.

Singlet (di)oxygen is generally produced by triplet ground state dioxygen quenching excited molecules due to 1) ET from both excited singlet and triplet states being spin-allowed, 2) the excitation energy of singlet oxygen (0.98 eV) being substantially lower than most triplet photosensitizers, which makes the ET fast and irreversible and 3) small size of the dioxygen molecule enabling rapid diffusion.[179,180] As the high atmospheric concentration of dioxygen also ensures its abundancy in most media, intermolecular processes can rarely compete with oxygen quenching.

The photosensitization of singlet oxygen is often regarded to occur via exchange ET, although some discrepancies with pure Dexter theory have been reported.[181] As already mentioned, both excited singlet and triplet states may undergo quenching to yield singlet oxygen:

$$PS^{1*} + O_2^3 \rightarrow PS^{3*} + O_2^{1*} \tag{19}$$

$$PS^{3*} + O_2^3 \rightarrow PS^{1} + O_2^{1*} \tag{20}$$

The process depicted in Eq. 19 is often considered to be limited to PS whose $\Delta E_{S-T} \geq 0.98$ eV and is sometimes called oxygen mediated or enhanced ISC. More often singlet oxygen generation is associated with excited triplet state quenching (Eq. 20) due to the longer lifetime and thus more probable collision between the excited molecule and dioxygen.

Due to the proficiency of dioxygen to quench excited triplet states and therefore ability to compete with for example TET, its removal is often necessary from the medium. Another detrimental aspect of dioxygen in the medium is the high reactivity

of singlet oxygen,[182] which can lead to oxidation ("photobleaching") and degradation of the dye molecules involved in triplet state processes. The reactivity of photosensitized singlet oxygen can also be beneficial for some applications, such as synthetic chemistry[26], photopolymerization[183], photoisomerization[184] or photodynamic therapy[185,186].

Different strategies have thus been developed to overcome the quenching and oxidation caused by dioxygen. Arguably the most straightforward approach is removal of dioxygen from the medium by, for example, freeze-pump-thaw degassing or purging with an inert gas such as nitrogen, helium or argon. However, complete deoxygenation is often challenging and leaking of oxygen back into the medium may perturb especially long-lasting measurements. Diffusion of dioxygen back into the medium can be hindered by employing materials with barrier properties against dioxygen, such as high viscosity solvents[146] and rubbery polymeric materials[187], or encapsulating the system in macro and micro[188] or nanoscale[189]. Oxygen can also be removed chemically by employing oxygen scavengers. Oxygen scavengers, like sodium sulfite[190], may react with ground state triplet dioxygen or photosensitized singlet oxygen, like oleic acid[146] or dimethyl thiomethane[191].

Combinations of these strategies have been used in this thesis: The solvents, polyethylene glycols (PEGs) in Publications I-III and dimethyl sulfoxide in Publication IV, were thoroughly purged with nitrogen. Furthermore, the high viscosity of polyethylene glycol makes it an efficient barrier for oxygen diffusion, enabling long lasting oxygen sensitive measurements. In addition to removing oxygen, the solvents were doped with singlet oxygen scavengers: oleic acid in Publications I-III and dimethyl thiomethane in Publication IV. Oxygen scavengers enable oxygen sensitive processes to occur even without prior removal of oxygen, which is shown in Publication IV.

3 TRIPLET FUSION UPCONVERSION

Until this point, although interesting in its own right as a physical phenomenon, the utility of TET may seem unclear. In this Chapter we shall delve into triplet fusion upconversion, one of the two processes driven by TET we will explore in this Thesis. After introducing the mechanism and overall process of triplet fusion upconversion, we focus on the factors that influence its efficiency, especially in relation to TET. Let's get to the good stuff.

3.1 Mechanism of triplet fusion

In 1962, one year after reporting the eosin or E-type (thermally activated) delayed fluorescence, Parker & Hatchard recognized another type of delayed fluorescence.[192–194] While the E-type delayed fluorescence originates from a single triplet excited state undergoing reverse intersystem crossing to the fluorescent singlet state, this new type of delayed fluorescence, called P-type[195,196] (for pyrene) or triplet-triplet annihilation[197,198], resulted from interaction between two triplet excited states yielding one fluorescent singlet excited and one singlet ground state. This was indicated by, for example, the quadratic dependence of the intensity of the delayed fluorescence to the excitation rate.[199]

After these seminal discoveries, the overall process of triplet-triplet annihilation or triplet fusion[h] (TF) has become established:[34] Photoexcitation of a PS molecule generates a triplet excited state that undergoes TET to an A molecule. When two triplet excited A molecules come into contact, triplet fusion may occur and result in one singlet excited and one singlet ground state. This overall process is shown in Fig. 9. Naturally, the TET step is not required as TF may occur for example between two triplet excited PS molecules like porphyrins.[58,200,201] However, an efficient TF system typically requires the TET step, as we will see in the next section. The whole TF

[h] The term triplet fusion is preferred by the author due to the conformity with its inverse process, singlet fission.

process from photoexcitation of PS to emission from A is called photon upconversion if the energy of the emissive state of A is higher than the initial photoexcited state of PS, for example $E(A^{1*}) > E(PS^{1*})$.

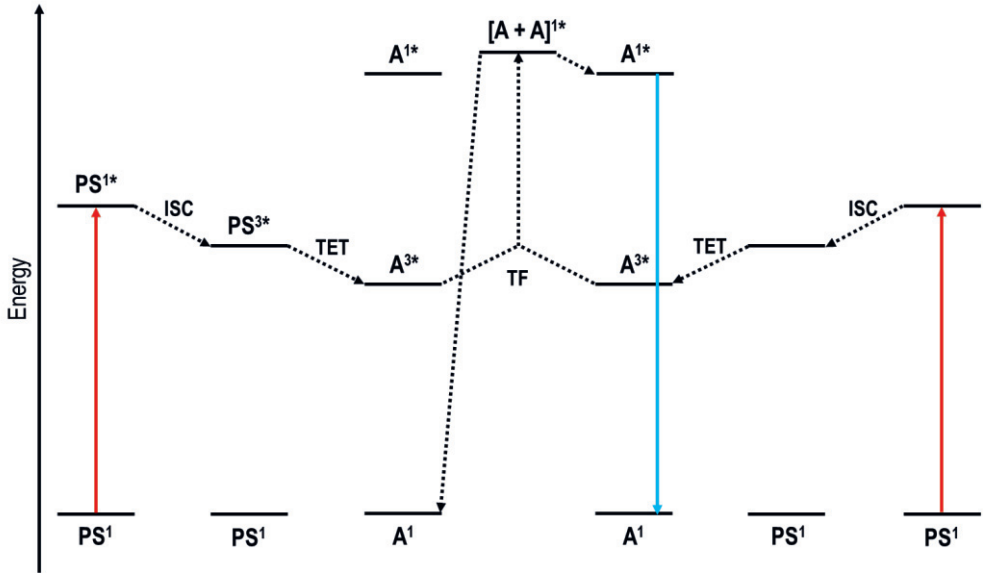

Figure 9. Jablonski diagram of the overall process of triplet fusion photon upconversion. The solid red arrow represents the photoexcitation of PSs that undergo ISC and TET to A triplet states. When in contact, two excited A molecules may undergo triplet fusion (TF) that results in one singlet excited A molecule while the other is reverted to its ground state. The solid blue arrow represents upconverted delayed fluorescence from the singlet excited A molecule.

As was the case with exchange ET, TF requires contact or orbital overlap between the excited molecules and the underlying mechanism was early on recognized as exchange interaction between two triplet state wavefunctions,[197,202,203] which can be examined as a four-electron state of the encounter complex.[204] The exchange interaction between the triplets breaks down their degeneracy and results in nine (three times three) possible combinations of the spin states in the encounter complex: one with singlet, three with triplet and five with quintet state character (see Fig. 10).[205,206] The probability of yielding a certain spin state after dissociation of the encounter complex is called spin statistics.[207] Often the spin-statistics are reduced to one number, *f*, that denotes the probability of yielding an excited singlet states by fusing two excited triplet states.[208,209]

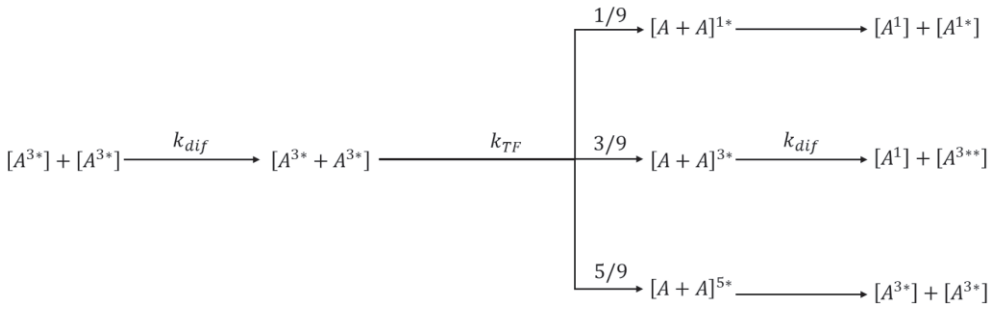

Figure 10. Possible spin state combinations resulting from triplet fusion and based on the spin tensor product (Glebsch-Gordan coefficients) of the interacting individual spin states.[210]

With the statistics presented above, the simple assumption[211] would be that TF has the probability of 11 % (1/9) to yield an excited singlet state. However, excited singlet yields above 11 % are routinely achieved experimentally as in for example Publications I-III. This discrepancy between the experimental and purely statistical singlet yields is often attributed to the energetics of the molecules involved in TF. Firstly, a quintet state is generally unattainable for a single molecule due to its high energy[212,213] and thus the quintet encounter complex is thought to revert back to its starting species ($2 \times A^{3*}$) that are "recycled" back to the triplet population and may yield a singlet state upon TF.[214,215] The higher triplet excited state (for example T_2, denoted by the double asterisk in the middle channel in Fig. 10), undergoes rapid internal conversion to A^{3*} that can take part in TF making the singlet yield 40 %.[216–218] This is the expected fate of the T_2 state per Kasha's rule[219], however in some systems the T_2 state can undergo competing ISC to the S_1 state increasing the S_1 yield. [220–222] The 40 % limit stands only if the formation of a higher excited state is possible upon TF, i.e. the combined energies of the two T_1 states are higher than the T_2 state. Naturally, this is also a requirement if the S_1 state is to form upon TF.[217,223,224] Some acceptors, such as rubrene[216,225], tetracene[226], TIPS-anthracene[227] and perylene[209], have been demonstrated to have singlet yields well above 40 %. This is attributed to the combined energy of two T_1 states to lie in between the S_1 and T_2 states, i.e.

$$E(S_1) < 2 \times E(T_1) < E(T_2). \tag{21}$$

This would effectively leave only the singlet channel open for TF as both the quintet and triplet channels are energetically inaccessible and allow 100 % singlet yield upon TF, which is why the conditions presented in Eq. 21 are often considered to be one of the criteria for efficient acceptors for TF.[48,228] It should also be noted that the

energetics outlined in Eq. 21 are naturally subject to thermal effects that may have significant contribution to the geometry of A and therefore the energy levels of its excited states.[229]

The above presented mechanism of singlet state generation upon TF has been shown to be somewhat simplistic and therefore quite limited by the current boom of studies in singlet fission.[204,230,231] As the aim of singlet fission is to produce two triplet states from one singlet state – the exact reverse of the aims of TF – the entanglement between the rules governing both processes is integral. Bossanyi et al.[231] attribute these shortcomings to the assumption of the triplet pairs undergoing TF are strongly exchange coupled, which leads to neglect of such factors as inter-molecular orientation in the encounter complex and internal conversion and intersystem crossing between the T_1, T_2 and S_1 states. In such case, the upper limit of $E(T_1)$ presented in Eq. 21 may no longer benefit the TF system. This disruption of the 1:3:5 spin statistics is exciting for the field of TF as it will inspire new studies into the mechanism of TF and likely realization of more efficient TF upconversion systems.

3.2 Efficiency of triplet fusion upconversion

The efficiency of TF upconversion (TFUC) systems can be quantified using three figures of merit: 1) quantum yield, 2) excitation power density threshold and 3) anti-Stokes shift or upconversion energy shift. Respectively, these figures of merit translate in a good TFUC system as the capability to yield upconverted photons from absorbed photons with high probability, under low excitation power density and with a large energy difference between the upconverted and absorbed photons. However, these requirements may vary between different application areas as we will discover with some examples in the following sections.

First and arguably the most important figure of merit for any TFUC system is the quantum yield of upconversion, Φ_{UC}, for which the simplest and most common definition is the number of emitted upconverted photons per number of photons absorbed by the photosensitizer. If the aim of the TFUC system is not to emit photons rather than create higher energy excited states that are harvested to drive a process, such as a photovoltaics or photochemical organic synthesis, Φ_{UC} is the ratio of upconverted excited states and photons absorbed by PS.[232] As TFUC is cascade of several processes, Φ_{UC} can be expressed as the product of the quantum yields or efficiencies of each process:

$$\Phi_{UC} = \frac{1}{2}\Phi_{ISC}\Phi_{TET}f\Phi_{TF}\Phi_{fluo}, \quad (22)$$

where Φ_{ISC} is the quantum yield of intersystem crossing, Φ_{TET} is the efficiency of TET, f is the spin statistical factor discussed above, Φ_{TF} is the quantum yield of TF (occasionally f is included in Φ_{TF}), and Φ_{fluo} is the fluorescence quantum yield of A. Maximum theoretical Φ_{UC} cannot exceed 50 % due to the inherent two-to-one photon nature of TFUC. Therefore a "multiplication factor" of two is sometimes used in Eq. 22 to normalize the maximum theoretical Φ_{UC} to 100 %. This practise is however becoming less prevalent and the normalized results are recommended to be called efficiency instead of quantum yield.[228,232] It is worth noticing that in the original publications of this thesis still report normalized quantum yields.

PS initiates the TFUC process by absorbing a photon and undergoing ISC to yield an excited triplet state. Φ_{ISC} depends on the strength of spin-orbit coupling in the PS molecule as discussed in Chapter 2. The maturation of TF from a curiosity to a useful tool in so many application fields in 21st century has been attributed to the introduction of efficient PSs based on metal-containing chromophores such as porphyrins or phthalocyanines.[34] The heavy metal ion, most often Zn, Pd or Pt, enhances SOC via the heavy atom effect and enables Φ_{ISC} to reach close unity values. All PSs used in this thesis are metalated porphyrins with $\Phi_{ISC} \gtrsim 90$ %.

The efficiency of the next step, TET, is determined by the combined properties of PS, A and the medium. Already expressed in Eq. 18 in Chapter 2.3 as quenching efficiency, Φ_{TET} can be considered as a function of PS triplet lifetime τ_0, [A] and rate constant of TET k_{TET}. As we also recall, k_{TET} depends on the rate of diffusion in the medium and the triplet energy gap ΔE_T between PS and A. Thus, there are generally three approaches for achieving high Φ_{TET}: 1) employ a PS-A pair with a large ΔE_T to maximize k_{TET}, 2) utilize high [A] and/or 3) employ PS with long τ_0, all of which were employed in this thesis.

Relying on a large exothermic ΔE_T between PS and A is often the strategy to ensure efficient TET. However, increasing the energy gap much below -4 k_BT offers no enhancement as k_{TET} has already reached its maximum value, i.e. k_{dif}. This may suffice for TFUC systems operating in low viscosity solvents to achieve high Φ_{TET} with low [A] and short τ_0. However, as many applications of TFUC require media, such as polymeric materials, where diffusion is hindered, the other two strategies need to be leveraged.[233–235] Although increasing [A] seems the most straightforward strategy, it may be limited by the medium due to aggregation or phase separation of

the dye molecules or overall loading capacity, a common issue[i] in polymeric and self-assembled materials.[37,56,236–238]

Therefore, utilizing PSs with long τ_0 presents a prudent approach for ensuring efficient Φ_{TET} even with low [A] and slow diffusion. This was explored in Publication I, where two PSs with considerably different triplet lifetimes were employed for TFUC in highly viscous polyethylene glycol. The 11 ms triplet lifetime of ZnTPPOH enabled over 10 % upconversion quantum yield already at 400 μM [A] and maximum Φ_{UC} of 13 % was reached at 1.5 mM [A]. PtTTPOH with substantially shorter τ_0, 61 μs, required 3 mM to reach 15 % upconversion quantum yield.

Similar [A] titration was performed for Publication III to explore the extent of reverse triplet energy transfer in a TFUC system where the triplet energy gap between PS and A is positive i.e. endothermic. Projection of Φ_{TET} based on PS phosphorescence lifetime quenching (see Fig. 8 for example) is prone to overestimation as it reflects the forward TET (PS to A, FTET). The equilibrium between FTET and RTET can thus be revealed by monitoring Φ_{UC} as a function of [A], which is illustrated in Fig. 11. The titration curves were used to find the [A] that yielded maximum Φ_{UC} and therefore comparable Φ_{TET} for two different TFUC systems, one with exothermic PS/A pair (ΔE_T = -0.4 k_BT) and the other with endothermic PS/A pair (ΔE_T = 3 k_BT). For the (slightly) exothermic pair, the [A] to yield 90 % Φ_{TET} projected by phosphorescence quenching results and Eq. 18 (Φ_{FTET}) was 0.7 mM while the apparent maximum Φ_{UC} was reached at 1.2 mM. Strikingly, the respective values for the endothermic pair were 0.35 mM and 5 mM, even when PS of the endothermic pair had over 20 times longer τ_0 (440 μs vs. 10.3 ms). As such, the endothermic PS/A pair makes a sound example of a TFUC system where both high [A] and long τ_0 are required for high Φ_{TET}.

[i] Although aggregation is often considered deleterious to TF-UC systems, A dyes exhibiting aggregation induced emission or co-aggregation of PS and A may be utilized for TF-UC operating in solid-state conditions.[376,377]

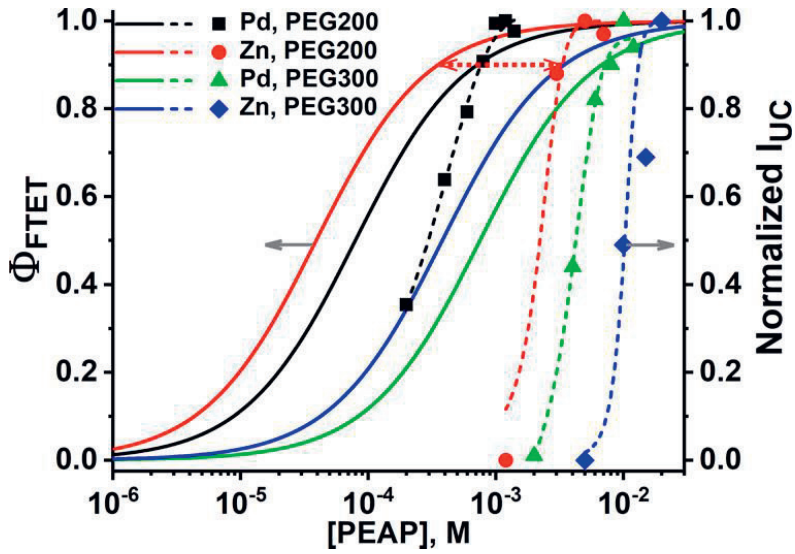

Figure 11. Comparison between TET efficiency yielded by phosphorescence quenching results (Φ_{FTET}, solid lines) and (normalized) upconversion emission intensities (symbols and dashed lines) of PdTAPIP (Pd, exothermic) and ZnTAPIP (Zn, endothermic). The red dashed arrow highlights the discrepancy between the methods to evaluate [A] needed for 90 % TET efficiency. Reprinted with permission from Publication III.[165] Copyright ACS 2020.

Similarly to Φ_{TET}, the efficiency of TF can be expressed in (steady-state) kinetic terms as[46]

$$\Phi_{TF} = \frac{k_{TF}[A^{3*}]^2}{k_{TET}[PS^{3*}][A^1]} = \frac{k_{TF}[A^{3*}]}{k_{TF}[A^{3*}]+\frac{1}{\tau_0^A}}, \quad (23)$$

where [A^1] and [A^{3*}] are the concentration of ground state and triplet excited A molecules, respectively, τ_0^A is the triplet lifetime of A and k_{TF} is the rate constant of TF. Investigating this equation, one notices that Φ_{TF} depends on the [A^{3*}], which is the product of the chain of processes prior to the formation of A^{3*} beginning from the absorption of photon. This dependency of Φ_{TF} and consequently of Φ_{UC} on the rate or intensity of excitation is explored more in depth later in this chapter.

As TF requires contact between the triplet excited A molecules, Φ_{TF} is dictated by the rate (or probability) of these contacts. In TFUC systems where the A molecules are initially separated, k_{TF} is thus essentially diffusion-limited.[239,240] Therefore, long triplet state lifetime is paramount for TF systems relying on molecular or exciton diffusion.[235,241–243] The limitations imposed by the medium to k_{TF} has prompted studies to achieve intramolecular TF between covalently linked

chromophores in either dimers or larger oligomeric or even polymeric molecules instead of intermolecular TF.[242,244–250]

The spin-statistical factor f, i.e. the probability of yielding an excited singlet state upon TF, was already introduced and discussed in the previous section, ergo we shall concentrate on the fate of that newly generated singlet state and how to ensure its radiative decay. As such, dyes with high intrinsic Φ_{fluo} are preferred choices for A. However, there are several processes that arise from the operating conditions of TFUC systems and reduce Φ_{fluo}, such as excimer formation, aggregation, and FRET from A back to PS.

Excimer (excited dimer) formation is somewhat innate to TF systems as the solvent cage where TF has occurred contains one excited and one ground state A molecule.[251] Excimers may reduce the TFUC efficiency either by introducing a non-radiative pathway for A^{1*} thereby decreasing Φ_{fluo} or red-shifting the emission.[252] Excimer formation can be mitigated by introducing moieties, such as alkyl groups, that sterically alter the stacking interaction between A molecules.[253,254] Optimizing [A] is also important as overly high ground state concentration increases the probability of excimer formation.[254] This was achieved in Publications I and III by titrating the TFUC system with A to find the concentration that yielded maximum Φ_{UC}. Parenthetically, dimerization of anthracene, one of the most iconic photochemical reactions, can occur via the excimer formed upon TF.[255,256]

As discussed above, reverse triplet energy transfer from A to PS can lead to lower Φ_{TET} and therefore lower Φ_{UC}. Energy transfer from the singlet excited state of A to PS can also occur via the FRET mechanism (see Chapter 2.2) if the emission spectrum of A overlaps the absorption spectrum of PS. For example, the so-called Soret band of porphyrin PSs often overlaps with the A fluorescence spectrum. This causes reabsorption of the upconverted light and may even enable FRET in TFUC systems with either spatially confined PS and A or high [PS] resulting in reduced Φ_{fluo}.[228,257–259] On the other hand, FRET from A can facilitate the harvesting of the upconverted excited states to, for example, drive drug release via photodissociation[260] or outcompete singlet fission[259,261]. Incidentally on this note, the realization that FRET efficiency is not limited by Φ_{fluo} of the donor, a common misconception,[262] could widen the A selection for FRET-based TFUC systems as currently the choice of A molecules is typically restricted to ones exhibiting high Φ_{fluo}.

Experimentally Φ_{UC} is typically determined by using so-called relative actinometry, where the UC emission intensity is compared to the fluorescence intensity of a reference whose fluorescence quantum yield is known.[263] For example,

the reference dyes used in this thesis were the widely utilized Rhodamine 6G in ethanol (Φ_{fluo} = 95 %[264], Publications I and II) for the green light absorbing TFUC systems and methylene blue in water (Φ_{fluo} = 4 %[265], Publication III) for the red light absorbing systems. PSs with non-unity Φ_{ISC} present an interesting variation of the relative actinometry as their fluorescence can be utilized as an internal quantum yield reference.[266] In addition to reference-based methods, determination of absolute Φ_{UC} using an integrating sphere are becoming more common.[267,268]

As was briefly mentioned above, Φ_{UC} depends on the excitation power density (I_{exc}), which was already observed in the first TF studies by Parker and Hatchard. This quadratic dependence of the UC emission intensity to I_{exc}, rationalized by the requirement of two triplet excited to generate one emissive singlet state, has often been used as proof of TF being the underlying mechanism for delayed fluorescence.[269–274] The rate of excited singlet state ($[A^{1*}]$) generation upon TF can be expressed with three coupled rate equations that were also used as the basis for the kinetic model used in Publications II and III:[275–277]

$$\frac{\partial[PS^{3*}]}{\partial t} = \alpha I_{exc}[PS^1] - k_T^{PS}[PS^{3*}] - k_{TET}[PS^{3*}][A^1] \tag{24a}$$

$$\frac{\partial[A^{3*}]}{\partial t} = k_{TET}[PS^{3*}][A^1] - k_T^A[A^{3*}] - k_{TF}[A^{3*}]^2 \tag{24b}$$

$$\frac{\partial[A^{1*}]}{\partial t} = \frac{1}{2} f k_{TF}[A^{3*}]^2 - k_S^A[A^{1*}], \tag{24c}$$

where α is the extinction coefficient of PS at the excitation wavelength(s) (later we will use absorption a that is the product of α and $[PS^1]$) and k_S^A is the excited singlet state decay rate of A. Under low power density excitation $[A^{3*}]$ is small, which implies that $k_T^A[A^{3*}] \gg k_{TF}[A^{3*}]^2$, i.e. most of the triplet excited A molecules decay spontaneously instead of undergoing TF. Monguzzi et al. called this condition the case of slow TF and solved Eq. 24 under steady-state conditions showing the expected $[A^{1*}] \propto (I_{exc})^2$.[275] In the case of fast TF, I_{exc} is so high that $[A^{3*}]$ is large and results in $k_{TF}[A^{3*}]^2 \ll k_T^A[A^{3*}]$, i.e. the main decay path for A^{3*} is via TF. In such case, solving Eq. 24 under steady-state conditions yields $[A^{1*}] \propto I_{exc}$. The linear dependence thus indicates that the TFUC system is operating at its maximum Φ_{UC}. The kinetic investigation of TF by Monguzzi et al. however culminates in the recognition of a specific I_{exc} that results in $k_{TF}[A^{3*}]^2 = k_T^A[A^{3*}]$ and is aptly named the power density threshold or I_{th}. This represents a tipping point of a TF

system where Φ_{TF} is half of its maximum (see Eq. 23) and can be expressed in terms of the kinetic parameters as

$$I_{th} \propto \frac{\left(k_T^A\right)^2}{\Phi_{TET} k_{TF} a}. \tag{25}$$

Consequently, I_{th} has become the definition of the lowest I_{exc} required to operate a TFUC system efficiently and therefore an important figure of merit that facilitates objective comparison between different systems as it ties together parameters from multiple steps of the TFUC process. For most applications minimizing I_{th} is desirable, however the ability to manipulate I_{th} may become an important feature for TFUC-based applications that require localized photochemistry such as light-driven 3D printing.[55]

I_{th} can be determined with two different methods, either by finding the crossing point of UC emission intensity between the linear and quadratic dependence on I_{exc} (Fig. 12a) or finding I_{exc} that yields half of the maximum Φ_{UC} (Fig. 12b). The first method can be visualized by plotting the UC emission intensity and I_{exc} in a double logarithmic scale and fitting two lines to the data, one with a slope of one and another with a slope of two. The intersection of these (extrapolated) linear fits is equal to the I_{th}. The second method is based on the fact that at I_{th} the TFUC is operating at half of its maximum Φ_{UC} due to the only power density dependent process of TFUC being the TF.

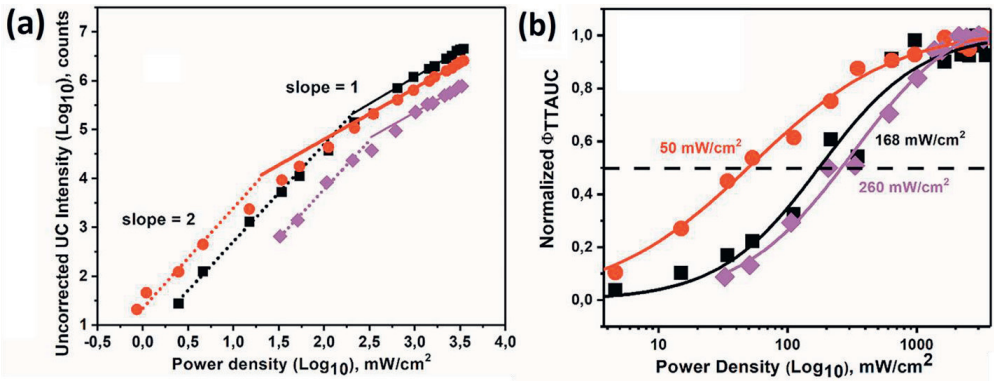

Figure 12. The power density dependence of 532 nm excitation of three TFUC systems photosensitized by PdTPPOH (red dots), PtTPPOH (black squares) and ZnTPPOH (magenta diamonds). Reprinted with permission from Publication II.[119] Copyright ACS 2019.

In Fig. 12 we see the power density dependence of three TFUC systems with clearly different I_{th} values. To explain these differences, we will first take another

look at Eq. 25 that shows the influence of the triplet lifetime of A, rate of TF, absorption, and efficiency of TET. In Publication II, the TFUC systems employed the same A and equal [A], 3 mM of tetra(tert-butyl)perylene, and equal absorption (the optical density was 1 over the 1 cm path length at the excitation wavelength of 532 nm). Thus, the variation in I_{th} between the systems is the result of different Φ_{TET}. As we have seen earlier in Eq. 18, Φ_{TET} depends on k_{TET}, τ_0 of PS and [A]. According to the phosphorescence quenching results, 3 mM of tetra(tert-butyl)perylene should result in over 90 % Φ_{TET} for each system and due to exhibiting the longest τ_0, the ZnTPPOH sensitized system should prevail with the lowest I_{th}. This is however in stark contrast with the experimentally determined I_{th}, which revealed that something had been overlooked in the evaluation of TET efficiency.

Besides τ_0, there were two major differences that set the ZnTPPOH-sensitized system apart from the others: the triplet energy of PS and its concentration. E_T of ZnTPPOH is substantially lower, $\geq$ 0.2 eV, than the other PSs (see Fig. 2) and results in a very small energy gap between ZnTPPOH and A. Moreover, to obtain optical density of one at 532 nm, [ZnTPPOH] = 294 μM was required, almost three and six times higher than PtTPPOH and PdTPPOH, respectively. Altogether this indicated that reverse TET from A to PS is probable in the ZnTPPOH system.[239]

This sparked an investigation into the interplay of ΔE_T, [PS], [A] and τ_0, which determines the equilibrium between the forward and reverse TET and consequently influences heavily the I_{th} of a TFUC system. Due to the number of variables, the tool of choice for this investigation was kinetic rate modelling. The model was fundamentally based on Eq. 24 with additional terms to account for RTET and its task was to solve the excitation intensity (or photon flux) that yielded half of the maximum Φ_{UC}, i.e. I_{th}. In terms of [A], the results were quite straightforward, as high [A] is beneficial for attaining low I_{th}, especially with short living PS and negligibly exothermic ΔE_T. Initially, with highly exothermic ΔE_T (≤ -4 k_BT) the choice of [PS] seems as trivial as [A] – high [PS] increases the absorption and therefore lowers I_{th} per Eq. 25 (see Fig. 13a). The kinetic landscape changes however dramatically, when ΔE_T approaches zero or even becomes endothermic. In such case, the I_{th} has a clear parabolic behavior in respect to [PS], especially with shorter τ_0 (see Figs. 13c and d). This clearly demonstrates the effect of RTET, especially prominent with endothermic PS/A pairs and short living PSs, as it begins to compete with TF with higher [PS] and thus reduces its efficiency.[278,279] This was verified also experimentally, as in the absence of significant RTET, decreasing [PS] should result in higher I_{th}, whereas three times lower [ZnTPPOH] = 100 μM resulted in decrease of I_{th} from 260 to 200 mW/cm^2.

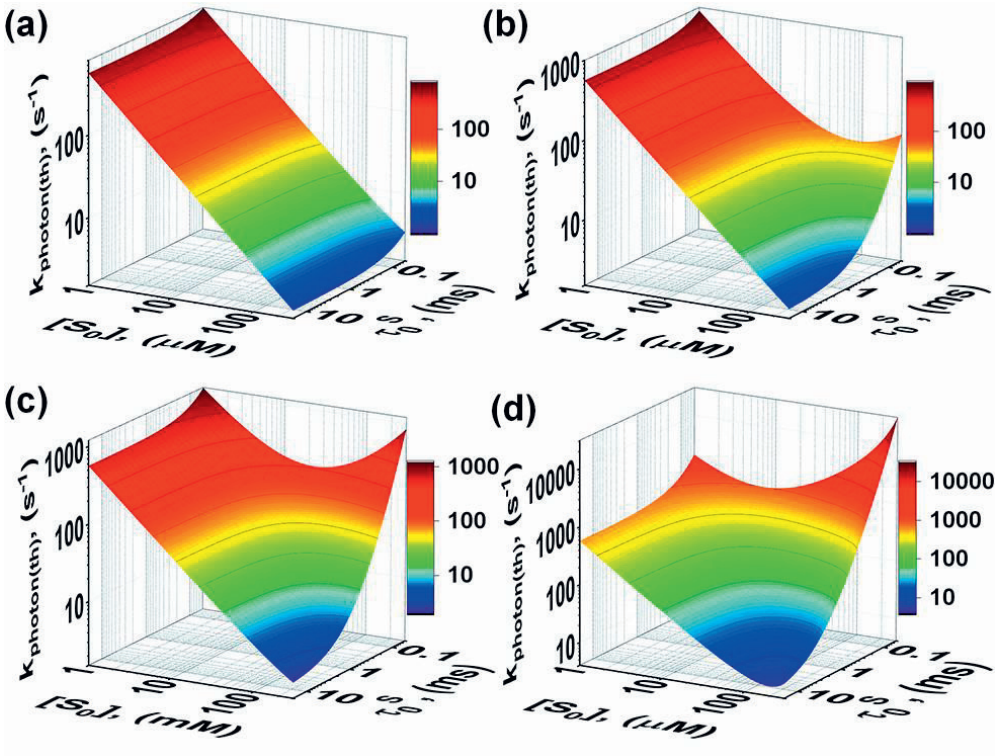

Figure 13. Power density thresholds as excitation photon rates of TFUC systems with ΔE_T of −4 k_BT (a), −1 k_BT (b), 0 k_BT (c) and 0.8 k_BT (d) as a function of PS concentration ([S_0]) and PS triplet lifetime (τ_0^S, note the superscript S for sensitizer). Here photon rate of 10 s^{-1} corresponds approx. to 290 mW/cm^2 of 532 nm excitation. Reprinted with permission from Publication II.[119] Copyright ACS 2019.

Indicated by the results of the kinetic model, it became apparent that through judicious planning, even endothermic PS/A pairs can be used for efficient TFUC. This however requires certain properties from the PS: long τ_0 and high molar extinction coefficient. The latter requirement stems from the need of strong absorption (Eq. 25) with low [PS] that will minimize the probability of RTET. Coupling a PS that exhibits such properties with A of sufficiently high concentration suppresses RTET and allows the realization of an efficient TFUC system driven by endothermic TET.

To test this hypothesis in Publication III, we mobilized two PSs, Pd and Zn-tetraarylphthalimidoporphyrins (Pd and ZnTAPIP), that boast long triplet lifetimes, 0.44 and 10.3 ms, and ultrahigh molar extinction coefficients, 264000 and 199000 M^{-1} cm^{-1}, respectively. The PSs were paired with an acceptor, 9-(4-phenylethynyl)-

10-phenylanthracene (PEAP), in viscous PEG200 and PEG300. The phosphorescence quenching studies revealed slightly exothermic (-0.4 k_BT) and substantially endothermic (3 k_BT) energy gaps between PdTAPIP/PEAP and ZnTAPIP/PEAP, respectively. [PS] that yielded optical density of 1 or 2 at the excitation wavelength in PEG200 or PEG300 were chosen, which required only 4.2/8.4 μM of PdTAPIP or 5.1/10.2 μM of ZnTAPIP in 1 cm path length, thanks to their outstanding molar extinction coefficients. [A] for each system was based on the titration results that yielded the highest Φ_{UC} (Fig. 11). The resulting TFUC performance of each system is shown in Figs. 14a and b.

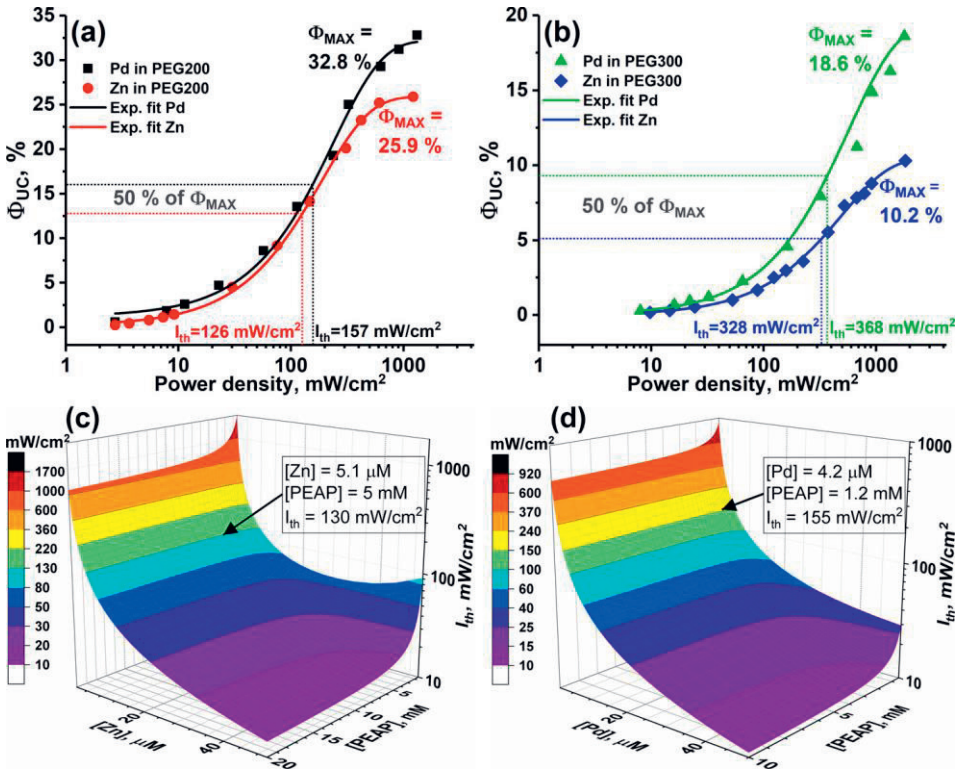

Figure 14. Φ_{UC} of PdTAPIP (Pd) and ZnTAPIP (Zn) sensitized upconversion in PEG200 (a) and PEG300 (b) as a function of excitation power density. The I_{th} values were determined as the power density that yielded half of the maximum Φ_{UC}. Note that Φ_{UC} have been multiplied by 2 (i.e. out of 100 % theoretical maximum). The modelled I_{th} values with varied [PS] and [A] are shown in (c) and (d) for both PS in PEG200 with the corresponding experimental parameters and results highlighted by arrows. Reprinted with permission from Publication III.[165] Copyright ACS 2020.

Remarkably, the TFUC systems sensitized by ZnTAPIP exhibit lower I_{th} than PdTAPIP. This can be attributed to the suppression of RTET due to long τ_0 and

high [A]/[PS] (see Chapter 2.2 with Fig. 6 and the "mixing" entropy change involved in TET) as a result of increased [A] and high molar extinction coefficients that enabled high optical densities with very low [PS]. Kinetic rate modelling (Fig. 14 c and d) was performed to test the systems beyond the experimental conditions, which demonstrated the comparable TFUC performance between the highly endothermic ZnTAPIP/PEAP and exothermic PdTAPIP/PEAP systems.

Publications II and III outline guidelines for achieving efficient TFUC even with endothermic PS/A pairs. This requires certain properties, such as long τ_0 or high molar extinction coefficients, from PS and/or increased [A]. At this point it is also fair to raise the question why one should go through all this trouble in designing the TFUC system if efficient TFUC can be achieved with a highly exothermic PS/A pair in a more straightforward manner. One way of justifying this is to draw the attention to the third and last figure of merit introduced in the beginning of this Chapter – the upconversion energy shift. Decreasing the triplet energy of PS, making ΔE_T more endothermic, often translates also in lower singlet state energy of PS. This naturally permits the use of lower energy excitation and results in a larger upconversion energy shift,[154,162,280,281] which was also realized in Publication III as replacing PdTAPIP with ZnTAPIP increased the upconversion energy shift from 0.80 to 0.89 eV (see Fig. 15). Red-shifting or even extending the excitation wavelengths of TFUC into near infrared is being pursued actively for many photonic applications as it offers for example deeper tissue penetration or broader harvesting of the solar spectrum.[50]

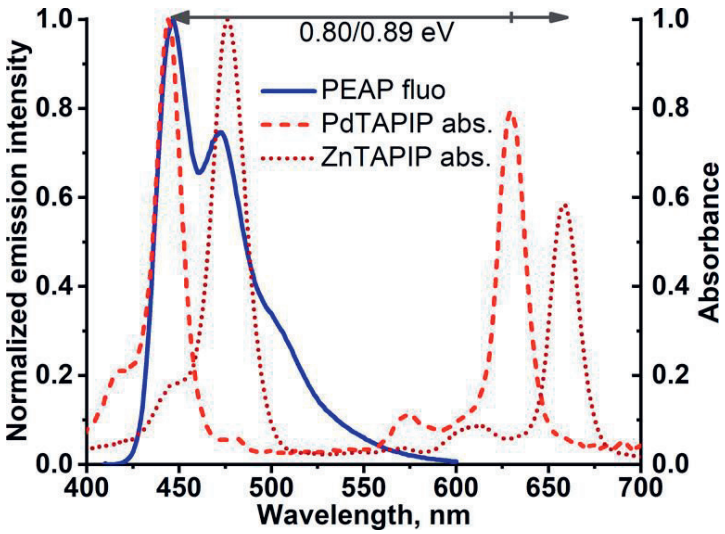

Figure 15. The fluorescence spectrum of PEAP and the absorption spectra of PdTAPIP and ZnTAPIP. The upconversion energy shift for both PdTAPIP and ZnTAPIP-sensitized TFUC systems is shown as the energy difference between PEAP emission maximum and PS absorption maxima. Reprinted with permission from Publication III.[165] Copyright ACS 2020.

Increasing the endothermicity of TET is only one of many approaches for increasing the upconversion energy shift by minimizing the so-called enthalpic or thermalization losses of TFUC as enthalpy change is often involved also in TF and ISC. Minimizing these losses during TF would require modifying either the singlet or triplet energy of the A chromophore while maintaining the general condition of $2 \times E(T_1) > E(S_1)$. While promising, only recently TFUC studies have shown deliberate control of the energies of these states over the other.[223,224,282–284] Decreasing the singlet-triplet energy gap of PS is arguably the most common approach for increasing the upconversion energy shift,[112] which can be achieved by employing TADF dyes or semiconductor nanocrystals/quantum dots as already discussed in Chapter 2. However, many of TADF PSs utilized in TFUC systems have been originally designed for organic light emitting diodes, where low molar extinction coefficients are not a concern and efficient fluorescence and reverse ISC is beneficial, which necessitates new PS designs and synthesis.[285–287] One of the outstanding challenges for using semiconductor nanocrystals as PSs to expand the upconversion energy shift is the requirement of exothermic ΔE_T between the nanocrystal and the surface-bound so-called bridge or transmitter ligands that harvest the triplet excitons and transfer them to the unbound A molecules.[288–291] Another concept for minimizing the losses involved in ISC is to bypass it completely. Although still more of a curiosity, osmium complexes exhibit appreciable extinction

coefficients for direct singlet-triplet absorption owing to extremely strong spin-orbit coupling.[292] While exhibiting impressive upconversion energy shifts (~1 eV), these systems are otherwise still lacking in upconversion efficiency mostly due to very short triplet lifetimes (<1 μs) caused by said strong SOC.[293–295]

Considering these unresolved limitations, engaging an endothermic PS/A pair is a sound approach for expanding the upconversion shift. In fact and in more general terms, provided that the TFUC system is properly designed with PSs exhibiting suitable properties such as long τ_0 and high molar extinction coefficient, this Chapter is concluded with the overall notion that endothermic TET need not necessarily imply inefficient TFUC as reverse TET can be controlled with relatively simple measures like the concentration ratio of PS and A. Moreover, the lessons learned about harnessing endothermic TET in this chapter will come in handy when designing other photosensitized systems, like sensitized photoswitching.

4 SENSITIZED PHOTOSWITCHING

Photoswitches are molecules that convert reversibly between isomers under excitation.[14] A common example of photoswitching or photoisomerizable molecule is retinal or retinaldehyde that undergoes *cis*-to-*trans* isomerization upon absorbing a photon, which initiates the cellular signalling cascade responsible for vision.[296] Hundreds of millions of years of evolution later, several other types of photoswitches have been discovered: azobenzenes[297,298], norbornadienes/quadricyclanes[299], spiropyrans/merocyanines[300], donor-acceptor Stenhouse adducts[301], diarylethenes[302], overcrowded alkenes[303], indigos[304], and stilbenes[305] and other olefins[306], to name a few. Arguably, the most common class of photoswitches is azobenzenes due to their stability, reliability, efficiency (high quantum yields of isomerization and large molar extinction coefficients) and tunability.[15,307–309]

Photoswitching of azobenzenes (Azo) between the *trans* (*E*) and *cis* (*Z*) isomers causes significant changes in the molecular geometry shown in Fig. 16. The

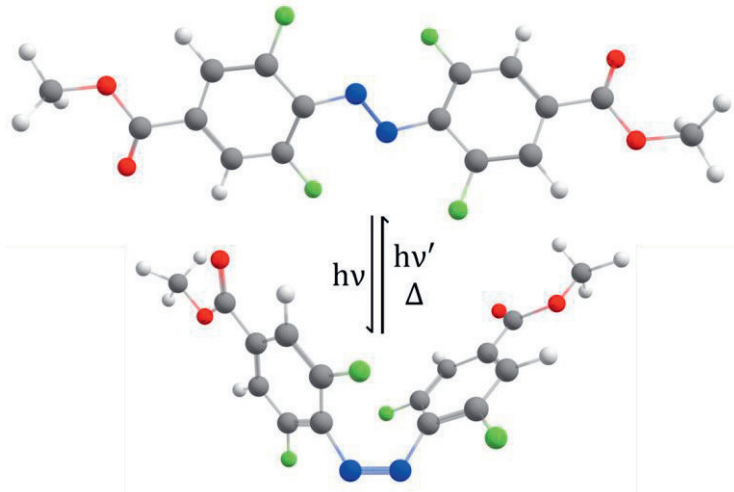

Figure 16. *E* (above) and *Z*-isomers (below) of an *ortho*-tetrafluoroazobenzene (TFA), one of the two azobenzene photoswitches used in Publication IV (here methyl-terminated instead of ethyl). *E*-isomer assumes a planar geometry, whereas the phenyl rings of the *Z*-isomer are highly twisted. The geometries were optimized using B3LYP/6-31G(d) level of theory on Gaussian 16 (revision C.01)[310].

isomerization naturally affects the electronic properties of the molecule, which imparts different absorption spectra to the isomers giving rise to the photochromism of the photoswitch. Thus, if the absorption bands of the isomers are separated enough, their selective photoexcitation at different wavelengths results in back-and-forth photoswitching. Here we will call this direct excitation. Isomerization from the *Z*-isomer to the thermodynamically more stable *E*-isomer also occurs in the dark via thermal excitation.

The properties of azobenzenes, such as absorption spectra, photoisomerization quantum yields and rates of thermal isomerization, depend on the molecular structure and are therefore highly tuneable by substitutions of the phenyl rings. Unsubstituted azobenzene possesses fairly strong absorption in the UV range ($\pi - \pi^*$) and weaker absorption in the blue range of visible spectrum ($n - \pi^*$) while exhibiting a long half-life of two days for the *Z*-isomer at room temperature.[307] Altogether the unsubstituted azobenzene shows robust and efficient photoswitching as excitation at 313 nm or 436 nm yields so-called photostationary states of 20 % or 90 % of *E*-isomer, respectively.[311] However, the requirement of short wavelength excitation hampers the utility of the unsubstituted azobenzene in many applications, especially biological ones where green or preferably red or near infrared excitation is desired.[312–314] Thus, considerable synthetic efforts have been made to red-shift the absorption of azobenzenes, which include *para* and *ortho*-substitution and protonation.[315–324] However, these approaches usually coincide with substantial shortening of the *Z*-isomer half-life, down to minutes or even microseconds for the near-infrared absorbing azobenzenes, a trait often considered deleterious for the said biological applications as it prevents control over the isomer composition and necessitates high-intensity excitation and/or long exposure.[325–328] New approaches are therefore needed to yield bistable azobenzene photoswitching systems operating in the red or near-infrared range of the spectrum.

This leads us to indirect excitation that leaves the intrinsic properties (such as long half-life) of the azobenzene photoswitch intact but expands the excitation modality beyond its capabilities by introducing a proxy system responsible for harvesting the excitation and transferring it to the photoswitch. Several concepts for indirect excitation of azobenzenes have been demonstrated: two-photon excitation of an antenna molecule or moiety and subsequent (singlet) energy transfer to the azobenzene,[329–331] upconverted excitation,[332–334] photoinduced electron or hole transfer,[335–339] and the most established approach of these – triplet sensitization.[340–346]

Triplet sensitization of azobenzenes yields selectively the *E*-isomer,[340,344,348] which can be elucidated by examining the potential energy curves (Fig. 17) of different electronic states of azobenzene. T_1 state crosses S_0 at two N=N twist angles, approx. 65 and 120 degrees, with the T_1 minimum (110 degrees) close to the latter. Furthermore, the crossing point at 120 degrees and the T_1 minimum are nearly degenerate, while a small energy barrier exists between the 65-degree crossing and T_1 minimum. This clearly indicates that isomerization via excitation of the T_1 strongly favors the *E*-isomer.[347–349] Naturally, the crossing between the T_1 and S_0

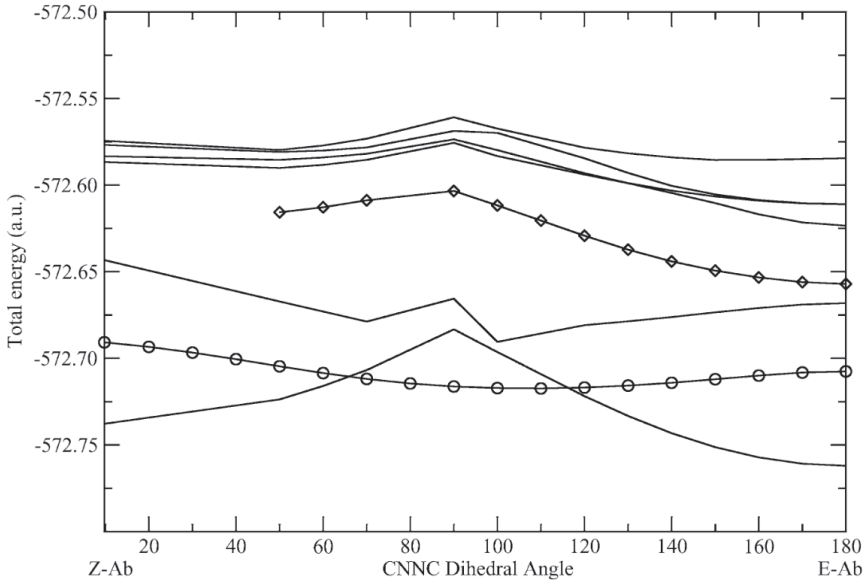

Figure 17. Potential energy curves of unsubstituted azobenzene singlet (solid line) and triplet (T_1 and T_2, circles and diamonds) states along the N=N twist ("CNNC Dihedral Angle"). Reprinted with permission from Gagliardi et al.[347] Copyright Springer Nature 2003.

manifolds requires spin-orbit coupling, which is considerable for azobenzene as one may expect for molecules with $n - \pi^*$ character. As the product of the almost negligible energy barrier and considerable spin-orbit coupling, overall T_1-S_0 intersystem crossing in azobenzene is very rapid (see Fermi's golden rule, Eq. 3) with an estimated[i] rate of 10^{11} s^{-1}.[348] Against this backdrop, triplet sensitization of azobenzene offers an efficient mode for rapid and selective *Z*-to-*E* isomerization.

[i] This estimate is based on computational studies. The triplet state of azobenzene has so far evaded direct experimental observation, which also testifies for its ultrashort lifetime. Triplet lifetimes in the 10-100 ns range have been measured in viscous solvents at low temperatures for azobenzenes with electron donating and withdrawing *para*-substitution (sometimes called push-pull azobenzenes or pseudostilbenes).[378] Their prolonged and thus observable triplet kinetics are assigned to the $\pi - \pi^*$ character of their T_1 state caused by the strong push-pull effect.

Triplet sensitized isomerization of azobenzenes was discovered already in 1960s by George S. Hammond.[340] Much like triplet fusion, until the turn of the millennium it was mostly studied by using organic photosensitizers with absorption in the shorter wavelength range of the visible spectrum. We set out to investigate the potential of strongly red-light absorbing photosensitizers, Pd and Pt-tetraphenyltetrabenzoporphyrin (PdP and PtP) for azobenzene photoswitching in Publication IV. These PSs were paired with two bistable azobenzenes, TFA[323] and FPA (bearing an *ortho*-fluorine and *ortho*-pyrrolidine)[319]. The structures of the PSs and azobenzenes are shown in Fig. 18.

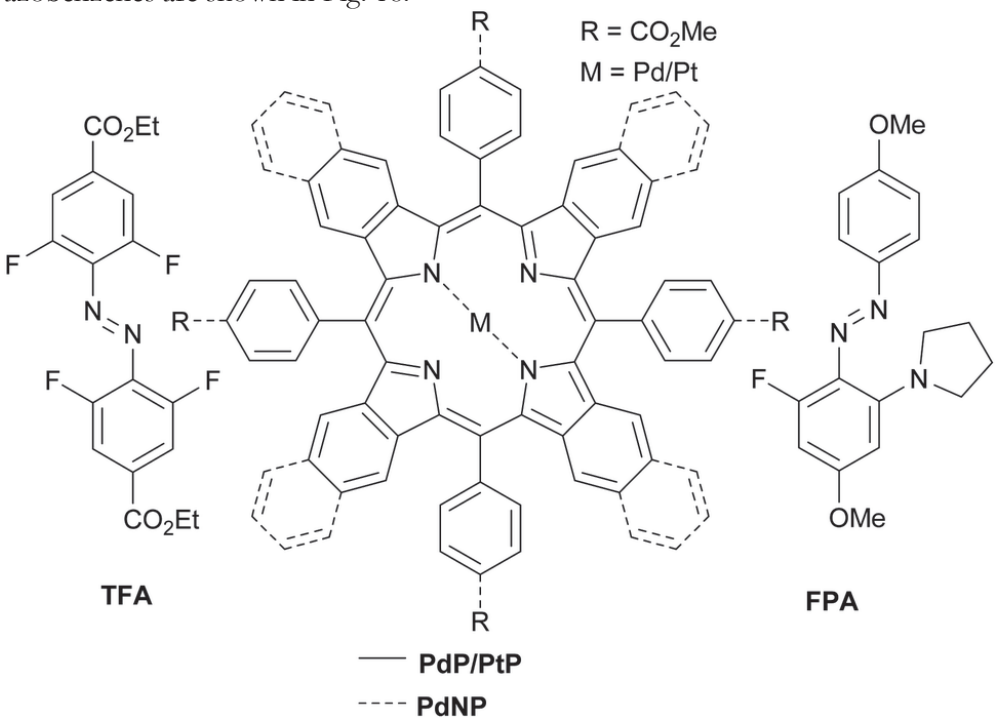

Figure 18. The structures of the photosensitizers (PdP/PtP and Pd-tetraphenyltetranaphthoporhyrin, PdNP) and the azobenzenes TFA and FPA used in this thesis. Reprinted with permission from Publication IV.[166] Copyright RSC 2021.

The TET kinetics between these porphyrin photosensitizers and azobenzene acceptors were studied by phosphorescence quenching using both *E* and *Z*-isomers of the azobenzenes as acceptors. The resulting TET rate constants, shown in Table 1, revealed with Eq. 12 that TET from both PSs was exothermic to TFA and endothermic to FPA.

Table 1. Triplet energies of *E*- and *Z*-isomers of the azobenzene triplet energy acceptors TFA and FPA in DMSO ($k_{dif} \approx 1.1 \times 10^9$ $M^{-1}s^{-1}$). The triplet energies of the PSs PdP and PtP were determined to be 1.55 eV and 1.61 eV, respectively, by phosphorescence measurements. The measurements were performed at room temperature.

PS/A pair	k_{TET} ($M^{-1}s^{-1}$)	ΔE_T (k_BT)	ΔE_T (meV)	E_T (eV)
PdP/*E*-TFA	8.7×10^8	-1.3	-34	1.49-1.52
PtP/*E*-TFA	1.1×10^9	-4.7	-120	
PdP/*Z*-TFA	8.1×10^8	-1.0	-26	1.52-1.56
PtP/*Z*-TFA	9.7×10^8	-2.0	-52	
PdP/*E*-FPA	2.8×10^8	1.1	29	1.58-1.63
PtP/*E*-FPA	3.6×10^8	0.7	18	
PdP/*Z*-FPA	2.4×10^8	1.3	34	1.58-1.65
PtP/*Z*-FPA	2.2×10^8	1.4	36	

Sensitized photoswitching was studied by initial direct excitation of the azobenzenes to yield *Z*-isomers in the system followed by excitation of PS to drive the triplet sensitized *Z*-to-*E* isomerization. The absorption spectra with the excitation wavelengths and photoisomerization curves of these systems are shown in Fig. 19. Remarkably, the sensitized isomerization was equally fast for both azobenzenes despite the substantial differences in the triplet energies and TET rate constants yielded by the phosphorescence quenching studies.

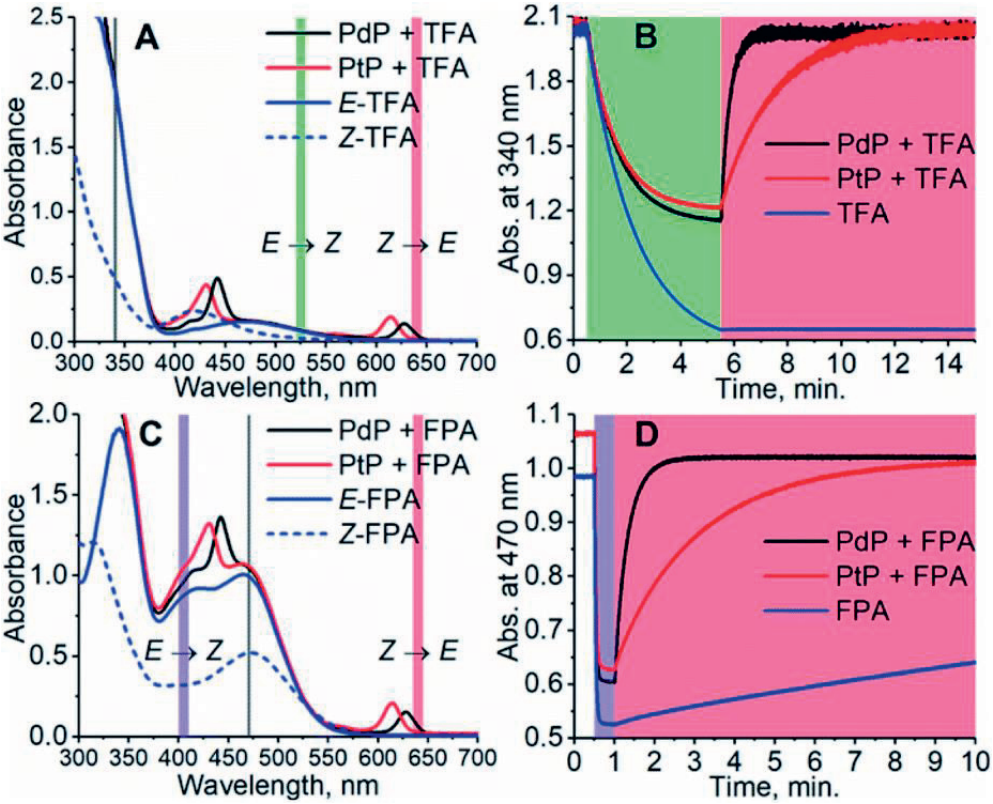

Figure 19. Absorption spectra (A and C) and photoisomerization curves (B and D) of the sensitized photoswitching systems. The slower isomerization rate afforded by PtP is mostly the result of smaller spectral overlap between the excitation source (640 nm LED) and the absorption. The direct *E*-to-*Z* photoisomerization was excited with either a 525 nm (TFA) or 405 nm (FPA) LED. Reprinted with permission from Publication IV.[166] Copyright RSC 2021.

To put the quenching and sensitized isomerization results into context, we can examine the overall kinetic scheme of the process:[344,350]

$$PS^{3*} + (E\text{-}Ab)^1 \xrightarrow{k_{TET-E}} PS^1 + Ab^{3*} \quad (26)$$

$$PS^{3*} + (Z\text{-}Ab)^1 \xrightarrow{k_{TET-Z}} PS^1 + Ab^{3*} \quad (27)$$

$$Ab^{3*} \xrightarrow{k_{ISC-E}} (E\text{-}Ab)^1 \quad (28)$$

$$Ab^{3*} \xrightarrow{k_{ISC-Z}} (Z\text{-}Ab)^1, \quad (29)$$

where Ab means azobenzene and sensitization of either isomer yields the same triplet state as both isomers revert to the same triplet state minimum (see Fig. 17). As the sensitization results selectively to *Z*-to-*E* isomerization, the kinetic scheme implies that $k_{ISC-E} \gg k_{ISC-Z}$, which was also inferred from the potential energy curves with the relative energies of the T_1-S_0 crossings in respect to the T_1 minimum. The kinetic scheme also reveals that TET must be the rate limiting step in the sensitized isomerization process as the rate of ISC is estimated to be extremely high from T_1 to S_0 of the *E*-isomer. Nevertheless, the rate of isomerization for both azobenzenes appears equal despite the large differences in the TET rate constants triplet energy gaps between PSs and the azobenzenes. This indicates that TET resulting in isomerization must have a substantial positive entropy component as the rate of isomerization is apparently decoupled from the TET rate constants yielded by quenching studies. The "mixing" entropy change in TET can be evaluated as previously with

$$\Delta S = k_B \ln\left(\frac{[(Z\text{-}Ab)^1][PS^{3*}]}{[Ab^{3*}][PS^1]}\right), \tag{30}$$

where the ultrashort triplet lifetime of azobenzene ensures $[Ab^{3*}] \ll [(Z\text{-}Ab)^1]$, $[PS^{3*}]$, $[PS^1]$ and a negligible probability of reverse TET. Combined with the possibility of non-vertical energy transfer (see Chapter 2.2) due to the large geometric distortion[345] involved in the isomerization, we can postulate that PSs with substantially lower triplet energies than the acceptor azobenzene can still effectively sensitize azobenzene photoswitching.

To test this hypothesis, TFA was paired with another PS, namely Pd-tetraphenyltetranaphthoporhyrin or PdNP, that exhibits absorption in the near-infrared region (maximum absorption at 712 nm) and low triplet energy (1.3 eV vs. 1.55/1.61 eV of PdP/PtP). As a result, the triplet energy gap between PdNP and *Z*-TFA was 8.5 k_BT or 220 meV at room temperature. Despite this formidable endothermic barrier for TET, PdNP was capable of sensitizing isomerization of TFA efficiently under 740 nm (shown in see Fig. 20) and even 770 nm near infrared excitation. As such, this was the first demonstration of triplet sensitized photoisomerization with beyond visible wavelengths. Furthermore, it offers the benefit of low-power incoherent excitation over the other indirect excitation approaches operating in the near infrared range like two-photon absorption and upconversion nanoparticles that require high-intensity laser light sources. To further highlight the utility of triplet sensitized near infrared photoswitching, we performed stepwise photoisomerization of bistable TFA with dosed excitation (see Fig. 20) as

such control over the isomer composition is not achievable with near infrared absorbing azobenzenes due to their shortened *Z*-half-lives.

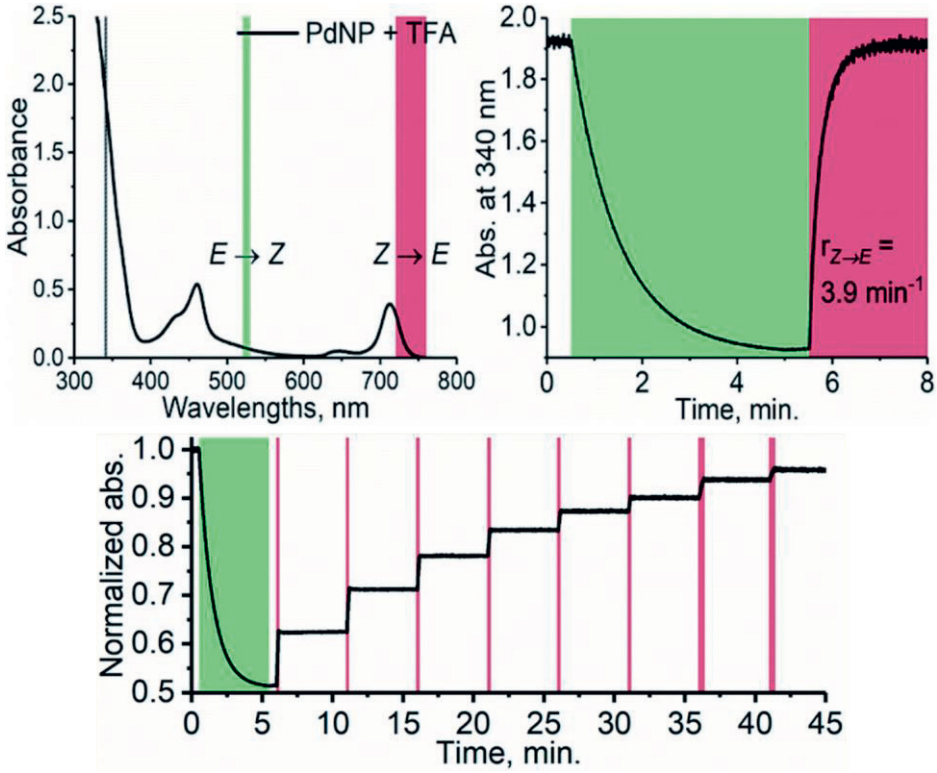

Figure 20. The absorption spectrum (top left) and the photoisomerization (740 nm LED excitation, top right) curve of the PdNP/TFA photoswitching system. The direct *E*-to-*Z* photoisomerization was excited with a 525 nm LED. Stepwise photoisomerization with 10 and 20 s near infrared excitation doses (bottom). Reprinted with permission from Publication IV.[166] Copyright RSC 2021.

As a conclusion, it should be mentioned that triplet sensitized photoswitching is not unique to azobenzenes as many other types of photoswitches, such as stilbenes[156,159,351,352], overcrowded alkenes[353], diarylethenes[354–356], indigos[357], spiropyrans[358] and norbornadienes[359,360] undergo isomerization when their triplet states are populated. Triplet sensitized isomerization has also its uses in enantioselective catalysis.[361,362] Thus, it would be interesting to investigate if endothermic TET can be utilized to push excitation wavelengths of these other types of photoswitches and photocatalysis beyond the visible wavelengths. As for sensitized photoswitching of azobenzenes, we conclude this chapter by highlighting some opportunities offered by near infrared photosensitized isomerization for

biomedical applications. For example, photocontrol of hydrogel stiffness by *Z*-to-*E* isomerization induced gel-to-sol transition, as demonstrated by the Kalow lab,[363,364] could be useful for dynamic cell cultures or light-triggered drug release. Another example comes from the field of photopharmacology, where replacing the core of a small molecule drug by an azobenzene or "azologization" is a common method to achieve optical control over function. However, most drug azologs are active as their *E*-isomers, which hampers their applicability as they are active by default and can only be deactivated by photoexcitation.[365] A possible solution to this are diazocines (cyclic/bridged azobenzenes) as their *Z*-isomer is the thermodynamically more stable isomer.[318,366–368] Thus, the diazocine-substituted drug is inactive in dark but can be activated by *Z*-to-*E* isomerization.[369] Whether triplet excited diazocines undergo *Z*-to-*E* isomerization has not been studied yet. However, if their sensitized behavior resembles that of conventional azobenzenes, photosensitized near infrared photoswitching of diazocines could have potential for *in vivo* photopharmacology.

5 CONCLUSIONS

In this thesis we have studied TET, first as a physical phenomenon on its own and then as an integral part of TFUC and sensitized photoswitching. The overarching method in these studies has been primary elucidation of the photosensitizer and acceptor properties followed by investigation of how these properties and their interaction affect the operating conditions and performance of these systems.

In Publication I we studied the effect of the photosensitizer triplet lifetime on the acceptor concentrations required for efficient TFUC. Long triplet lifetime enables high quantum yield of upconversion with lower acceptor concentrations, which is paramount in media, like polymeric and nanoscale materials, that restrict the dye concentrations due to for example limited solubility. Overly high dye concentrations are deleterious for TFUC performance also in general as they can induce additional loss channels like excimer formation and reverse energy transfer to the process.

In addition to high quantum yields, low power density thresholds are key feature of efficient TFUC systems. In Publication II we examined the collective influence of photosensitizer and acceptor triplet lifetimes, triplet energies and concentrations on the power density threshold. Due to the large number of variables, this was mostly achieved through kinetic rate modelling and corroborating the modelling results and trends with experimental determination of TFUC performance. Notably, these findings indicated that endothermic triplet energy transfer need not to lead to the demise of a TFUC if the system is designed judiciously.

Encouraged by this, we proceeded in Publication III to formulate TFUC systems with two photosensitizers exhibiting extraordinary molar extinction coefficients and long triplet lifetimes. The ultrahigh molar extinction coefficients enabled high acceptor/photosensitizer ratios as harvesting of excitation was effective even with micromolar photosensitizer concentrations. Combined with the long triplet lifetimes, reverse triplet energy transfer was suppressed even for the substantially endothermic photosensitizer/acceptor pair due to the large positive entropy change involved in the triplet energy transfer process. As a result, the exothermic and endothermic photosensitizer/acceptor pairs exhibited remarkably comparable TFUC performance. These findings also brought forward the idea that engaging in endothermic triplet energy transfer is a viable method for improving the

upconversion energy shift, the third figure of merit of photon upconversion systems, as it enables the utilization of photosensitizers with red-shifted absorption.

In Publications I-III we have mostly focused on the properties of the photosensitizers and for example in Publication III we elaborated on how these properties can be leveraged in efficient endothermic triplet energy transfer. What are then the acceptor properties that can be harnessed to push the limits of endothermic triplet energy transfer? To answer this, we widened the scope from photon upconversion to another photosensitizable process, photoswitching. Especially azobenzenes offer an appealing target for triplet sensitization as their triplet lifetime is ultrashort leading to negligible probability of reverse triplet energy transfer. This opportunity was capitalized in Publication IV that demonstrated endothermic triplet energy transfer as a potent approach for expanding the azobenzene photoisomerization wavelengths into the near infrared without altering the properties of the photoswitch itself and thus retaining its capabilities like bistability.

Overall, the objectives of this thesis have been to provide the reader with a broad context of triplet energy transfer and guidelines for controlling and implementing it in photon upconversion and photoswitching. The results presented here demonstrate means for approaching the thermodynamic limits of triplet energy transfer and highlight the potential of achieving these limits for photon upconversion and photoswitching. Fully realizing the potential triplet energy transfer will help implementing photon upconversion and sensitized photoswitching systems into practical applications ranging from solar energy to cancer therapies.

Thus, demonstrating these systems in a cuvette is not enough and realizing these outcomes onto rooftops and into clinics will require more than photochemists sitting in the lab and playing with their "toys" as the problems they envision to solve are not only formidable but truly multidisciplinary. Therefore, it is exciting to see photon upconversion systems increasingly applied to new fields of science and technology. Perhaps sensitized near infrared photoswitching will also find its uses. One thing is for sure, the potential of triplet states has barely been scratched and the photochemists too will have their hands full.

BIBLIOGRAPHY

1. Giacomo, C. The Photochemistry of the Future. *Science* **1912**, *36* (926), 385–394.
2. Zhang, B.; Sun, L. Artificial Photosynthesis: Opportunities and Challenges of Molecular Catalysts. *Chem. Soc. Rev.* **2019**, *48* (7), 2216–2264.
3. Rabaia, M. K. H. et al. Environmental Impacts of Solar Energy Systems: A Review. *Sci. Total Environ.* **2021**, *754*, 141989.
4. M., S. D.; P., Y. T. Solar Synthesis: Prospects in Visible Light Photocatalysis. *Science* **2014**, *343* (6174), 1239176.
5. Zhou, J. et al. Supramolecular Cancer Nanotheranostics. *Chem. Soc. Rev.* **2021**, *50* (4), 2839–2891.
6. Hüll, K.; Morstein, J.; Trauner, D. In Vivo Photopharmacology. *Chem. Rev.* **2018**, *118* (21), 10710–10747.
7. Shafranek, R. T. et al. Stimuli-Responsive Materials in Additive Manufacturing. *Prog. Polym. Sci.* **2019**, *93*, 36–67.
8. Ahn, D.; Stevens, L. M.; Zhou, K.; Page, Z. A. Rapid High-Resolution Visible Light 3D Printing. *ACS Cent. Sci.* **2020**, *6* (9), 1555–1563.
9. Pan, P. et al. Photosensitive Drug Delivery Systems for Cancer Therapy: Mechanisms and Applications. *J. Control. Release* **2021**, *338*, 446–461.
10. Lechner, V. M. et al. Visible-Light-Mediated Modification and Manipulation of Biomacromolecules. *Chem. Rev.* **2022**, *122* (2), 1752–1829.
11. MacFarlane, A. G. J.; Dowling, J. P.; Milburn, G. J. Quantum Technology: The Second Quantum Revolution. *Philos. Trans. R. Soc. London. Ser. A Math. Phys. Eng. Sci.* **2003**, *361* (1809), 1655–1674.
12. Wasielewski, M. R. et al. Exploiting Chemistry and Molecular Systems for Quantum Information Science. *Nat. Rev. Chem.* **2020**, *4* (9), 490–504.
13. Hiekkamäki, M.; Prabhakar, S.; Fickler, R. Near-Perfect Measuring of Full-Field Transverse-Spatial Modes of Light. *Opt. Express* **2019**, *27* (22), 31456–31464.
14. Goulet-Hanssens, A.; Eisenreich, F.; Hecht, S. Enlightening Materials with Photoswitches. *Adv. Mater.* **2020**, *32* (20), 1905966.
15. Dattler, D. et al. Design of Collective Motions from Synthetic Molecular Switches, Rotors, and Motors. *Chem. Rev.* **2020**, *120* (1), 310–433.
16. Costil, R. et al. Directing Coupled Motion with Light: A Key Step Toward Machine-Like Function. *Chem. Rev.* **2021**, *121* (21), 13213–13237.
17. Yang, Z. et al. Recent Advances in Organic Thermally Activated Delayed

Fluorescence Materials. *Chem. Soc. Rev.* **2017**, *46* (3), 915–1016.
18. Minaev, B.; Baryshnikov, G.; Agren, H. Principles of Phosphorescent Organic Light Emitting Devices. *Phys. Chem. Chem. Phys.* **2014**, *16* (5), 1719–1758.
19. Zhao, Q.; Li, F.; Huang, C. Phosphorescent Chemosensors Based on Heavy-Metal Complexes. *Chem. Soc. Rev.* **2010**, *39* (8), 3007–3030.
20. Spencer, J. A. et al. Direct Measurement of Local Oxygen Concentration in the Bone Marrow of Live Animals. *Nature* **2014**, *508* (7495), 269–273.
21. Xiang, H. et al. Near-Infrared Phosphorescence: Materials and Applications. *Chem. Soc. Rev.* **2013**, *42* (14), 6128–6185.
22. Chelushkin, P. S. et al. Phosphorescent NIR Emitters for Biomedicine: Applications{,} Advances and Challenges. *Dalt. Trans.* **2022**, *51* (4), 1257–1280.
23. Teng, J.-M.; Wang, Y.-F.; Chen, C.-F. Recent Progress of Narrowband TADF Emitters and Their Applications in OLEDs. *J. Mater. Chem. C* **2020**, *8* (33), 11340–11353.
24. Zhou, Z.; Song, J.; Nie, L.; Chen, X. Reactive Oxygen Species Generating Systems Meeting Challenges of Photodynamic Cancer Therapy. *Chem. Soc. Rev.* **2016**, *45* (23), 6597–6626.
25. Hamblin, M. R. Antimicrobial Photodynamic Inactivation: A Bright New Technique to Kill Resistant Microbes. *Curr. Opin. Microbiol.* **2016**, *33*, 67–73.
26. Ghogare, A. A.; Greer, A. Using Singlet Oxygen to Synthesize Natural Products and Drugs. *Chem. Rev.* **2016**, *116* (17), 9994–10034.
27. Askes, S. H. C. et al. Red Light-Triggered CO Release from Mn2(CO)10 Using Triplet Sensitization in Polymer Nonwoven Fabrics. *J. Am. Chem. Soc.* **2017**, *139* (43), 15292–15295.
28. Lv, W. et al. Upconversion-like Photolysis of BODIPY-Based Prodrugs via a One-Photon Process. *J. Am. Chem. Soc.* **2019**, *141* (44), 17482–17486.
29. Strieth-Kalthoff, F. et al. Energy Transfer Catalysis Mediated by Visible Light: Principles, Applications, Directions. *Chem. Soc. Rev.* **2018**, *47* (19), 7190–7202.
30. Strieth-Kalthoff, F.; Glorius, F. Triplet Energy Transfer Photocatalysis: Unlocking the Next Level. *Chem* **2020**, *6* (8), 1888–1903.
31. Albini, A. Photosensitization in Organic Synthesis. *Synthesis* **1981**, *1981* (04), 249–264.
32. Zhou, Q.-Q.; Zou, Y.-Q.; Lu, L.-Q.; Xiao, W.-J. Visible-Light-Induced Organic Photochemical Reactions through Energy-Transfer Pathways. *Angew. Chemie Int. Ed.* **2019**, *58* (6), 1586–1604.
33. Dantas, J. A.; Correia, J. T. M.; Paixão, M. W.; Corrêa, A. G. Photochemistry of Carbonyl Compounds: Application in Metal-Free Reactions. *ChemPhotoChem* **2019**, *3* (7), 506–520.

34. Singh-Rachford, T. N.; Castellano, F. N. Photon Upconversion Based on Sensitized Triplet-Triplet Annihilation. *Coord. Chem. Rev.* **2010**, *254* (21–22), 2560–2573.
35. Ehrler, B.; Yanai, N.; Nienhaus, L. Up- and down-Conversion in Molecules and Materials. *J. Chem. Phys.* **2021**, *154* (7), 70401.
36. Zhou, J. et al. Upconversion Luminescent Materials: Advances and Applications. *Chem. Rev.* **2015**, *115* (1), 395–465.
37. McCusker, C. E.; Castellano, F. N. Materials Integrating Photochemical Upconversion. *Top. Curr. Chem.* **2016**, *374* (2), 19.
38. Richards, B. S. et al. Photon Upconversion for Photovoltaics and Photocatalysis: A Critical Review. *Chem. Rev.* **2021**, *121* (15), 9165–9195.
39. VanOrman, Z. A.; Drozdick, H. K.; Wieghold, S.; Nienhaus, L. Bulk Halide Perovskites as Triplet Sensitizers: Progress and Prospects in Photon Upconversion. *J. Mater. Chem. C* **2021**, *9* (8), 2685–2694.
40. VanOrman, Z. A.; Nienhaus, L. Bulk Metal Halide Perovskites as Triplet Sensitizers: Taking Charge of Upconversion. *ACS Energy Lett.* **2021**, *6* (10), 3686–3694.
41. Beery, D.; Schmidt, T. W.; Hanson, K. Harnessing Sunlight via Molecular Photon Upconversion. *ACS Appl. Mater. Interfaces* **2021**, *13* (28), 32601–32605.
42. Dilbeck, T.; Hanson, K. Molecular Photon Upconversion Solar Cells Using Multilayer Assemblies: Progress and Prospects. *J. Phys. Chem. Lett.* **2018**, *9* (19), 5810–5821.
43. Kimizuka, N.; Yanai, N.; Morikawa, M. Photon Upconversion and Molecular Solar Energy Storage by Maximizing the Potential of Molecular Self-Assembly. *Langmuir* **2016**, *32* (47), 12304–12322.
44. Frazer, L.; Gallaher, J. K.; Schmidt, T. W. Optimizing the Efficiency of Solar Photon Upconversion. *ACS Energy Lett.* **2017**, *2* (6), 1346–1354.
45. Goldschmidt, J. C.; Fischer, S. Upconversion for Photovoltaics – a Review of Materials, Devices and Concepts for Performance Enhancement. *Adv. Opt. Mater.* **2015**, *3* (4), 510–535.
46. Gray, V. et al. Triplet–Triplet Annihilation Photon-Upconversion: Towards Solar Energy Applications. *Phys. Chem. Chem. Phys.* **2014**, *16* (22), 10345–10352.
47. Börjesson, K.; Dzebo, D.; Albinsson, B.; Moth-Poulsen, K. Photon Upconversion Facilitated Molecular Solar Energy Storage. *J. Mater. Chem. A* **2013**, *1* (30), 8521–8524.
48. Schulze, T. F.; Schmidt, T. W. Photochemical Upconversion: Present Status and Prospects for Its Application to Solar Energy Conversion. *Energy Environ. Sci.* **2015**, *8* (1), 103–125.
49. Gao, C. et al. Application of Triplet–Triplet Annihilation Upconversion in Organic Optoelectronic Devices: Advances and Perspectives. *Adv.*

Mater. **2021**, *33* (45), 2100704.
50. Bharmoria, P.; Bildirir, H.; Moth-Poulsen, K. Triplet–Triplet Annihilation Based near Infrared to Visible Molecular Photon Upconversion. *Chem. Soc. Rev.* **2020**, *49* (18), 6529–6554.
51. Yanai, N.; Kimizuka, N. Stimuli-Responsive Molecular Photon Upconversion. *Angew. Chemie Int. Ed.* **2020**, *59* (26), 10252–10264.
52. Duan, C. et al. Recent Progress in Upconversion Luminescence Nanomaterials for Biomedical Applications. *J. Mater. Chem. B* **2018**, *6* (2), 192–209.
53. Meir, R. et al. Photon Upconversion Hydrogels for 3D Optogenetics. *Adv. Funct. Mater.* **2021**, *31* (31), 2010907.
54. Sasaki, Y. et al. Near-Infrared Optogenetic Genome Engineering Based on Photon-Upconversion Hydrogels. *Angew. Chemie Int. Ed.* **2019**, *58* (49), 17827–17833.
55. Sanders, S. N. et al. Triplet Fusion Upconversion Nanocapsules for Volumetric 3D Printing. *arXiv* **2021**.
56. Healy, C.; Hermanspahn, L.; Kruger, P. E. Photon Upconversion in Self-Assembled Materials. *Coord. Chem. Rev.* **2021**, *432*, 213756.
57. Ahmad, W. et al. Strategies for Combining Triplet–Triplet Annihilation Upconversion Sensitizers and Acceptors in a Host Matrix. *Coord. Chem. Rev.* **2021**, *439*, 213944.
58. Awwad, N.; Bui, A. T.; Danilov, E. O.; Castellano, F. N. Visible-Light-Initiated Free-Radical Polymerization by Homomolecular Triplet-Triplet Annihilation. *Chem* **2020**, *6* (11), 3071–3085.
59. Ravetz, B. D. et al. Photoredox Catalysis Using Infrared Light via Triplet Fusion Upconversion. *Nature* **2019**, *565* (7739), 343–346.
60. Glaser, F.; Kerzig, C.; Wenger, O. S. Multi-Photon Excitation in Photoredox Catalysis: Concepts, Applications, Methods. *Angew. Chemie Int. Ed.* **2020**, *59* (26), 10266–10284.
61. Xiao, X. et al. Controlling the Triplet States and Their Application in External Stimuli-Responsive Triplet–Triplet-Annihilation Photon Upconversion: From the Perspective of Excited State Photochemistry. *Chem. Soc. Rev.* **2021**, *50* (17), 9686–9714.
62. Algar, W. R. et al. Photoluminescent Nanoparticles for Chemical and Biological Analysis and Imaging. *Chem. Rev.* **2021**, *121* (15), 9243–9358.
63. Askes, S. H. C.; Bonnet, S. Solving the Oxygen Sensitivity of Sensitized Photon Upconversion in Life Science Applications. *Nat. Rev. Chem.* **2018**, *2* (12), 437–452.
64. Baluschev, S.; Katta, K.; Avlasevich, Y.; Landfester, K. Annihilation Upconversion in Nanoconfinement: Solving the Oxygen Quenching Problem. *Mater. Horiz.* **2016**, *3* (6), 478–486.
65. Isokuortti, J. et al. Microfluidic Oxygen Tolerability Screening of

Nanocarriers for Triplet Fusion Photon Upconversion. *J. Mater. Chem. C* **2022**.
66. Zhu, X.; Su, Q.; Feng, W.; Li, F. Anti-Stokes Shift Luminescent Materials for Bio-Applications. *Chem. Soc. Rev.* **2017**, *46* (4), 1025–1039.
67. Huang, L. et al. Designing next Generation of Photon Upconversion: Recent Advances in Organic Triplet-Triplet Annihilation Upconversion Nanoparticles. *Biomaterials* **2019**, *201*, 77–86.
68. Dou, Q. et al. Bioimaging and Biodetection Assisted with TTA-UC Materials. *Drug Discov. Today* **2017**, *22* (9), 1400–1411.
69. Boelke, J.; Hecht, S. Designing Molecular Photoswitches for Soft Materials Applications. *Adv. Opt. Mater.* **2019**, *7* (16), 1900404.
70. Cheng, H.-B. et al. Advances in Application of Azobenzene as a Trigger in Biomedicine: Molecular Design and Spontaneous Assembly. *Adv. Mater.* **2021**, *33* (26), 2007290.
71. Welleman, I. M. et al. Photoresponsive Molecular Tools for Emerging Applications of Light in Medicine. *Chem. Sci.* **2020**, *11* (43), 11672–11691.
72. Li, J.; Zhou, X.; Liu, Z. Recent Advances in Photoactuators and Their Applications in Intelligent Bionic Movements. *Adv. Opt. Mater.* **2020**, *8* (18), 2000886.
73. Neilson, B. M.; Bielawski, C. W. Illuminating Photoswitchable Catalysis. *ACS Catal.* **2013**, *3* (8), 1874–1885.
74. Lu, P. et al. Wavelength-Selective Light-Matter Interactions in Polymer Science. *Matter* **2021**, *4* (7), 2172–2229.
75. Wang, Z. et al. Storing Energy with Molecular Photoisomers. *Joule* **2021**, *5* (12), 3116–3136.
76. Dong, L.; Feng, Y.; Wang, L.; Feng, W. Azobenzene-Based Solar Thermal Fuels: Design, Properties, and Applications. *Chem. Soc. Rev.* **2018**, *47* (19), 7339–7368.
77. Dommaschk, M. et al. Photoswitchable Magnetic Resonance Imaging Contrast by Improved Light-Driven Coordination-Induced Spin State Switch. *J. Am. Chem. Soc.* **2015**, *137* (24), 7552–7555.
78. Heilemann, M.; Dedecker, P.; Hofkens, J.; Sauer, M. Photoswitches: Key Molecules for Subdiffraction-Resolution Fluorescence Imaging and Molecular Quantification. *Laser Photon. Rev.* **2009**, *3* (1–2), 180–202.
79. Li, H.; Vaughan, J. C. Switchable Fluorophores for Single-Molecule Localization Microscopy. *Chem. Rev.* **2018**, *118* (18), 9412–9454.
80. Mehra, J.; Rechenberg, H. *The Historical Development of Quantum Theory 1-6*; Springer-Verlag: New York, 1982.
81. Gerlach, W.; Stern, O. Der Experimentelle Nachweis Der Richtungsquantelung Im Magnetfeld. *Zeitschrift für Phys.* **1922**, *9* (1), 349–352.
82. Lennard-Jones, J. E. The Electronic Structure of Some Diatomic

Molecules. *Trans. Faraday Soc.* **1929**, *25* (0), 668–686.
83. Pauli, W. Über Den Zusammenhang Des Abschlusses Der Elektronengruppen Im Atom Mit Der Komplexstruktur Der Spektren. *Zeitschrift für Phys.* **1925**, *31* (1), 765–783.
84. Uhlenbeck, G. E.; Goudsmit, S. Spinning Electrons and the Structure of Spectra. *Nature* **1926**, *117* (2938), 264–265.
85. Wigner, E. Ueber Die Erhaltungssätze in Der Quantenmechanik. *Nachrichten von der Gesellschaft der Wissenschaften zu Göttingen, Math. Klasse* **1927**, 375–381.
86. Wigner, E.; Witmer, E. E. Über Die Struktur Der Zweiatomigen Molekelspektren Nach Der Quantenmechanik. *Zeitschrift für Phys.* **1928**, *51* (11), 859–886.
87. McClure, D. S. Triplet-Singlet Transitions in Organic Molecules. Lifetime Measurements of the Triplet State. *J. Chem. Phys.* **1949**, *17* (10), 905–913.
88. Born, M.; Oppenheimer, R. Zur Quantentheorie Der Molekeln. *Ann. Phys.* **1927**, *389* (20), 457–484.
89. Dirac, P. A. M. The Quantum Theory of the Emission and Absorption of Radiation. *Proc. R. Soc. A Math. Phys. Eng. Sci.* **1927**, *114* (767), 243–265.
90. Penfold, T. J.; Gindensperger, E.; Daniel, C.; Marian, C. M. Spin-Vibronic Mechanism for Intersystem Crossing. *Chem. Rev.* **2018**, *118* (15), 6975–7025.
91. Siebrand, W. Franck—Condon Factors for Radiationless Transitions. *J. Chem. Phys.* **1971**, *55* (12), 5843.
92. Englman, R.; Jortner, J. The Energy Gap Law for Radiationless Transitions in Large Molecules. *Mol. Phys.* **1970**, *18* (2), 145–164.
93. El-Sayed, M. A. Spin—Orbit Coupling and the Radiationless Processes in Nitrogen Heterocyclics. *J. Chem. Phys.* **1963**, *38* (12), 2834–2838.
94. Pineiro, M. et al. Photoacoustic Measurements of Porphyrin Triplet-State Quantum Yields and Singlet-Oxygen Efficiencies. *Chem. – A Eur. J.* **1998**, *4* (11), 2299–2307.
95. Gentemann, S. et al. Photophysical Properties of Conformationally Distorted Metal-Free Porphyrins. Investigation into the Deactivation Mechanisms of the Lowest Excited Singlet State. *J. Am. Chem. Soc.* **1994**, *116* (16), 7363–7368.
96. Perun, S.; Tatchen, J.; Marian, C. M. Singlet and Triplet Excited States and Intersystem Crossing in Free-Base Porphyrin: TDDFT and DFT/MRCI Study. *ChemPhysChem* **2008**, *9* (2), 282–292.
97. Jablonski, A. Efficiency of Anti-Stokes Fluorescence in Dyes. *Nature* **1933**, *131* (3319), 839–840.
98. Terenin, A. Photochemical Processes in Aromatic Compounds. *Acta Physicochim. URSS* **1943**, *18* (4), 210–241.

99. Lewis, G. N.; Kasha, M. Phosphorescence and the Triplet State. *J. Am. Chem. Soc.* **1944**, *66* (12), 2100–2116.
100. Baryshnikov, G.; Minaev, B.; Ågren, H. Theory and Calculation of the Phosphorescence Phenomenon. *Chem. Rev.* **2017**, *117* (9), 6500–6537.
101. Hund, F. Atomtheoretische Deutung Des Magnetismus Der Seltenen. Erden. *Zeitschrift für Phys.* **1925**, *33* (1), 855–859.
102. Kutzelnigg, W.; Morgan, J. D. Hund's Rules. *Zeitschrift für Phys. D Atoms, Mol. Clust.* **1996**, *36* (3), 197–214.
103. Dirac, P. A. M.; Fowler, R. H. On the Theory of Quantum Mechanics. *Proc. R. Soc. London. Ser. A, Contain. Pap. a Math. Phys. Character* **1926**, *112* (762), 661–677.
104. Heisenberg, W. Mehrkörperproblem Und Resonanz in Der Quantenmechanik. *Zeitschrift für Phys.* **1926**, *38* (6), 411–426.
105. Atkins, P.; Friedman, R. *Molecular Quantum Mechanics*, 4th ed.; Oxford University Press Inc.: New York, 2005.
106. Turro, N.; Ramamurthy, V.; Scaiano, J. *Modern Molecular Photochemistry of Organic Molecules*; University Science Books: Sausalito, California, 2010.
107. Clarke, R. H.; Hochstrasser, R. M. Location and Assignment of the Lowest Triplet State of Perylene. *J. Mol. Spectrosc.* **1969**, *32* (2), 309–319.
108. Uoyama, H. et al. Highly Efficient Organic Light-Emitting Diodes from Delayed Fluorescence. *Nature* **2012**, *492* (7428), 234–238.
109. Dias, F. B.; Penfold, T. J.; Monkman, A. P. Photophysics of Thermally Activated Delayed Fluorescence Molecules. *Methods Appl. Fluoresc.* **2017**, *5* (1), 12001.
110. Im, Y. et al. Molecular Design Strategy of Organic Thermally Activated Delayed Fluorescence Emitters. *Chem. Mater.* **2017**, *29* (5), 1946–1963.
111. Wu, T. C.; Congreve, D. N.; Baldo, M. A. Solid State Photon Upconversion Utilizing Thermally Activated Delayed Fluorescence Molecules as Triplet Sensitizer. *Appl. Phys. Lett.* **2015**, *107* (3), 31103.
112. Yanai, N.; Kimizuka, N. New Triplet Sensitization Routes for Photon Upconversion: Thermally Activated Delayed Fluorescence Molecules, Inorganic Nanocrystals, and Singlet-to-Triplet Absorption. *Acc. Chem. Res.* **2017**, *50* (10), 2487–2495.
113. Scholes, G. D.; Rumbles, G. Excitons in Nanoscale Systems. *Nat. Mater.* **2006**, *5* (9), 683–696.
114. Huang, Z. et al. Hybrid Molecule–Nanocrystal Photon Upconversion Across the Visible and Near-Infrared. *Nano Lett.* **2015**, *15* (8), 5552–5557.
115. Luo, X. et al. Mechanisms of Triplet Energy Transfer across the Inorganic Nanocrystal/Organic Molecule Interface. *Nat. Commun.* **2020**, *11* (1), 28.
116. Hou, L. et al. Efficient Visible-to-UV Photon Upconversion Systems Based on CdS Nanocrystals Modified with Triplet Energy Mediators. *Adv. Funct. Mater.* **2021**, *31* (47), 2106198.

117. Gray, V.; Allardice, J. R.; Zhang, Z.; Rao, A. Organic-Quantum Dot Hybrid Interfaces and Their Role in Photon Fission/Fusion Applications. *Chem. Phys. Rev.* **2021**, *2* (3), 31305.
118. McNaught, A. D.; Wilkinson, A. *IUPAC. Compendium of Chemical Terminology (the "Gold Book")*, 2nd ed.; Blackwell Scientific Publications: Oxford, 2019.
119. Durandin, N. A. et al. Critical Sensitizer Quality Attributes for Efficient Triplet-Triplet Annihilation Upconversion with Low Power Density Thresholds. *J. Phys. Chem. C* **2019**, *123* (37), 22865–22872.
120. You, Z.-Q.; Hsu, C.-P. Theory and Calculation for the Electronic Coupling in Excitation Energy Transfer. *Int. J. Quantum Chem.* **2014**, *114* (2), 102–115.
121. Förster, T. Energiewanderung Und Fluoreszenz. *Naturwissenschaften* **1946**, *33* (6), 166–175.
122. Förster, T. Zwischenmolekulare Energiewanderung Und Fluoreszenz. *Ann. Phys.* **1948**, *437* (1-2), 55–75.
123. Scholes, G. D. Long-Range Resonance Energy Transfer in Molecular Systems. *Annu. Rev. Phys. Chem.* **2003**, *54* (1), 57–87.
124. Andrews, D. L. A Unified Theory of Radiative and Radiationless Molecular Energy Transfer. *Chem. Phys.* **1989**, *135* (2), 195–201.
125. Razi Naqvi, K.; Steel, C. Exchange-Induced Resonance Energy Transfer. *Chem. Phys. Lett.* **1970**, *6* (1), 29–32.
126. Kirch, A.; Gmelch, M.; Reineke, S. Simultaneous Singlet–Singlet and Triplet–Singlet Förster Resonance Energy Transfer from a Single Donor Material. *J. Phys. Chem. Lett.* **2019**, *10* (2), 310–315.
127. Cravcenco, A. et al. Multiplicity Conversion Based on Intramolecular Triplet-to-Singlet Energy Transfer. *Sci. Adv.* **2019**, *5* (9), eaaw5978.
128. Ermolaev, V. No Title. *Opt. Spektrosk.* **1959**, *6*, 642–647.
129. Dexter, D. L. A Theory of Sensitized Luminescence in Solids. *J. Chem. Phys.* **1953**, *21* (5), 836–850.
130. You, Z.-Q.; Hsu, C.-P.; Fleming, G. R. Triplet-Triplet Energy-Transfer Coupling: Theory and Calculation. *J. Chem. Phys.* **2006**, *124* (4), 44506.
131. Bai, S.; Zhang, P.; Beratan, D. N. Predicting Dexter Energy Transfer Interactions from Molecular Orbital Overlaps. *J. Phys. Chem. C* **2020**, *124* (35), 18956–18960.
132. Köhler, A.; Bässler, H. What Controls Triplet Exciton Transfer in Organic Semiconductors? *J. Mater. Chem.* **2011**, *21* (12), 4003–4011.
133. Closs, G. L.; Johnson, M. D.; Miller, J. R.; Piotrowiak, P. A Connection between Intramolecular Long-Range Electron, Hole, and Triplet Energy Transfers. *J. Am. Chem. Soc.* **1989**, *111* (10), 3751–3753.
134. Monguzzi, A.; Tubino, R.; Meinardi, F. Upconversion-Induced Delayed

Fluorescence in Multicomponent Organic Systems: Role of Dexter Energy Transfer. *Phys. Rev. B* **2008**, *77* (15), 155122–155124.
135. Inokuti, M.; Hirayama, F. Influence of Energy Transfer by the Exchange Mechanism on Donor Luminescence. *J. Chem. Phys.* **1965**, *43* (6), 1978–1989.
136. Faure, S.; Stern, C.; Guilard, R.; Harvey, P. D. Role of the Spacer in the Singlet−Singlet Energy Transfer Mechanism (Förster vs Dexter) in Cofacial Bisporphyrins. *J. Am. Chem. Soc.* **2004**, *126* (4), 1253–1261.
137. Mondal, J. A. et al. Ultrafast Intramolecular Electronic Energy-Transfer Dynamics in a Bichromophoric Molecule. *J. Phys. Chem. A* **2004**, *108* (39), 7843–7852.
138. Albinsson, B.; Mårtensson, J. Long-Range Electron and Excitation Energy Transfer in Donor–Bridge–Acceptor Systems. *J. Photochem. Photobiol. C Photochem. Rev.* **2008**, *9* (3), 138–155.
139. Naqvi, K. R. Spin Selection Rules Concerning Intermolecular Energy Transfer. Energy-Transfer Studies Using Doublet-State Acceptors. Comments. *J. Phys. Chem.* **1981**, *85* (15), 2303–2304.
140. Terenin, A.; Ermolaev, V. Sensitized Phosphorescence in Organic Solutions at Low Temperature. Energy Transfer between Triplet States. *Trans. Faraday Soc.* **1956**, *52*, 1042.
141. Han, J. et al. Doublet–Triplet Energy Transfer-Dominated Photon Upconversion. *J. Phys. Chem. Lett.* **2017**, *8* (23), 5865–5870.
142. Huang, Z. et al. Evolution from Tunneling to Hopping Mediated Triplet Energy Transfer from Quantum Dots to Molecules. *J. Am. Chem. Soc.* **2020**, *142* (41), 17581–17588.
143. Einstein, A. Über Die von Der Molekularkinetischen Theorie Der Wärme Geforderte Bewegung von in Ruhenden Flüssigkeiten Suspendierten Teilchen. *Ann. Phys.* **1905**, *322* (8), 549–560.
144. Debye, P. Reaction Rates in Ionic Solutions. *Trans. Electrochem. Soc.* **1942**, *82* (1), 265–272.
145. Saltiel, J.; Shannon, P. T.; Zafiriou, O. C.; Uriarte, A. K. A Case of Fully Diffusion-Controlled Exothermic Triplet Excitation Transfer. *J. Am. Chem. Soc.* **1980**, *102* (22), 6799–6808.
146. Mongin, C.; Golden, J. H.; Castellano, F. N. Liquid PEG Polymers Containing Antioxidants: A Versatile Platform for Studying Oxygen-Sensitive Photochemical Processes. *ACS Appl. Mater. Interfaces* **2016**, *8* (36), 24038–24048.
147. Serpa, C.; Arnaut, L. G.; Formosinho, S. J.; Naqvi, K. R. Calculation of Triplet–Triplet Energy Transfer Rates from Emission and Absorption Spectra. The Quenching of Hemicarcerated Triplet Biacetyl by Aromatic Hydrocarbons. *Photochem. Photobiol. Sci.* **2003**, *2* (5), 616–623.
148. You, Z.-Q.; Hsu, C.-P. Ab Inito Study on Triplet Excitation Energy

Transfer in Photosynthetic Light-Harvesting Complexes. *J. Phys. Chem. A* **2011**, *115* (16), 4092–4100.
149. Zapata, F. et al. Definition and Determination of the Triplet-Triplet Energy Transfer Reaction Coordinate. *J. Chem. Phys.* **2014**, *140* (3), 034102.
150. Frutos, L. M.; Castaño, O. A New Algorithm for Predicting Triplet-Triplet Energy-Transfer Activated Complex Coordinate in Terms of Accurate Potential-Energy Surfaces. *J. Chem. Phys.* **2005**, *123* (10), 104108.
151. Bryden, M. A.; Zysman-Colman, E. Organic Thermally Activated Delayed Fluorescence (TADF) Compounds Used in Photocatalysis. *Chem. Soc. Rev.* **2021**, *50* (13), 7587–7680.
152. Arrhenius, S. Über Die Dissociationswärme Und Den Einfluss Der Temperatur Auf Den Dissociationsgrad Der Elektrolyte. *Zeitschrift für Phys. Chemie* **1889**, *4U* (1), 96–116.
153. Sandros, K. Transfer of Triplet State Energy in Fluid Solutions. III. Reversible Energy Transfer. *Acta Chim. Scand.* **1964**, *18*, 2355–2374.
154. Cheng, Y. Y. et al. Entropically Driven Photochemical Upconversion. *J. Phys. Chem. A* **2011**, *115* (6), 1047–1053.
155. Balzani, V.; Bolletta, F.; Scandola, F. Vertical and "Nonvertical" Energy Transfer Processes. A General Classical Treatment. *J. Am. Chem. Soc.* **1980**, *102* (7), 2152–2163.
156. Saltiel, J. et al. Nonvertical Triplet Excitation Transfer to Cis- and Trans-Stilbene. *J. Am. Chem. Soc.* **1984**, *106* (11), 3144–3151.
157. Gessner, F.; Scaiano, J. C. Importance of Entropy Terms in Triplet Energy Transfer Equilibria. *J. Am. Chem. Soc.* **1985**, *107* (24), 7206–7207.
158. Zhang, D.; Closs, G. L.; Chung, D. D.; Norris, J. R. Free Energy and Entropy Changes in Vertical and Nonvertical Triplet Energy Transfer Processes between Rigid and Nonrigid Molecules. A Laser Photolysis Study. *J. Am. Chem. Soc.* **1993**, *115* (9), 3670–3673.
159. Saltiel, J.; Hammond, G. S. Mechanisms of Photochemical Reactions in Solution. XVII. Cis-Trans Isomerization of the Stilbenes by Excitation Transfer from Low Energy Sensitizers. *J. Am. Chem. Soc.* **1963**, *85* (16), 2515–2516.
160. Frutos, L. M. et al. A Theory of Nonvertical Triplet Energy Transfer in Terms of Accurate Potential Energy Surfaces: The Transfer Reaction from π,Π* Triplet Donors to 1,3,5,7-Cyclooctatetraene. *J. Chem. Phys.* **2004**, *120* (3), 1208–1216.
161. Ramamurthy, V.; Liu, R. S. H. Photochemistry of Polyenes. IX. Excitation, Relaxation, and Deactivation of Dienes, Trienes, and Higher Polyenes in the Vitamin A Series in the Sensitized Isomerization Reaction. *J. Am. Chem. Soc.* **1976**, *98* (10), 2935–2942.
162. Li, L. et al. Thermally Activated Delayed Fluorescence via Triplet Fusion. *J. Phys. Chem. Lett.* **2019**, 6239–6245.

163. He, S.; Han, Y.; Guo, J.; Wu, K. Long-Lived Delayed Emission from CsPbBr3 Perovskite Nanocrystals for Enhanced Photochemical Reactivity. *ACS Energy Lett.* **2021**, *6* (8), 2786–2791.
164. He, S.; Han, Y.; Guo, J.; Wu, K. Entropy-Gated Thermally Activated Delayed Emission Lifetime in Phenanthrene-Functionalized CsPbBr3 Perovskite Nanocrystals. *J. Phys. Chem. Lett.* **2021**, *12* (35), 8598–8604.
165. Isokuortti, J. et al. Endothermic and Exothermic Energy Transfer Made Equally Efficient for Triplet–Triplet Annihilation Upconversion. *J. Phys. Chem. Lett.* **2020**, *11* (1), 318–324.
166. Isokuortti, J. et al. Expanding Azobenzene Photoswitching into Near-Infrared via Endothermic Triplet Energy Transfer. *Chem. Sci.* **2021**.
167. Lai, R. et al. Shallow Distance-Dependent Triplet Energy Migration Mediated by Endothermic Charge-Transfer. *Nat. Commun.* **2021**, *12* (1), 1532.
168. Tabachnyk, M. et al. Resonant Energy Transfer of Triplet Excitons from Pentacene to PbSe Nanocrystals. *Nat. Mater.* **2014**, *13* (11), 1033–1038.
169. Thompson, N. J. et al. Energy Harvesting of Non-Emissive Triplet Excitons in Tetracene by Emissive PbS Nanocrystals. *Nat. Mater.* **2014**, *13* (11), 1039–1043.
170. Mongin, C. et al. Direct Observation of Triplet Energy Transfer from Semiconductor Nanocrystals. *Science* **2016**, *351* (6271), 369–372.
171. He, S.; Han, Y.; Guo, J.; Wu, K. Entropy-Powered Endothermic Energy Transfer from CsPbBr3 Nanocrystals for Photon Upconversion. *J. Phys. Chem. Lett.* **2022**, 1713–1718.
172. Yonemoto, D. T.; Papa, C. M.; Sheykhi, S.; Castellano, F. N. Controlling Thermally Activated Delayed Photoluminescence in CdSe Quantum Dots through Triplet Acceptor Surface Coverage. *J. Phys. Chem. Lett.* **2021**, *12* (15), 3718–3723.
173. Lakowicz, J. R. *Principles of Fluorescence Spectroscopy*, 3rd ed.; Springer: New York, 2006.
174. Stern, O.; Volmer, M. Über Die Abklingzeit Der Fluoreszenz. *Phys. Zeitschr.* **1919**, *20*, 183–188.
175. Durandin, N. A. et al. Efficient Photon Upconversion at Remarkably Low Annihilator Concentrations in a Liquid Polymer Matrix: When Less Is More. *Chem. Commun.* **2018**, *54* (99), 14029–14032.
176. Mulliken, R. S. The Interpretation of Band Spectra Part III. Electron Quantum Numbers and States of Molecules and Their Atoms. *Rev. Mod. Phys.* **1932**, *4* (1), 1–86.
177. Stuyver, T. et al. Do Diradicals Behave Like Radicals? *Chem. Rev.* **2019**, *119* (21), 11291–11351.
178. Borden, W. T.; Hoffmann, R.; Stuyver, T.; Chen, B. Dioxygen: What Makes This Triplet Diradical Kinetically Persistent? *J. Am. Chem. Soc.* **2017**,

139 (26), 9010–9018.
179. Schweitzer, C.; Schmidt, R. Physical Mechanisms of Generation and Deactivation of Singlet Oxygen. *Chem. Rev.* **2003**, *103* (5), 1685–1758.
180. Ogilby, P. R. Singlet Oxygen: There Is Indeed Something New under the Sun. *Chem. Soc. Rev.* **2010**, *39* (8), 3181–3209.
181. Schweitzer, C.; Schmidt, R. Physical Mechanisms of Generation and Deactivation of Singlet Oxygen. *Chem. Rev.* **2003**, *103* (5), 1685–1758.
182. DeRosa, M. C.; Crutchley, R. J. Photosensitized Singlet Oxygen and Its Applications. *Coord. Chem. Rev.* **2002**, *233–234*, 351–371.
183. Wu, C. et al. Unravelling an Oxygen-Mediated Reductive Quenching Pathway for Photopolymerisation under Long Wavelengths. *Nat. Commun.* **2021**, *12* (1), 478.
184. Kuntze, K. et al. Azobenzene Photoswitching with Near-Infrared Light Mediated by Molecular Oxygen. *J. Phys. Chem. B* **2021**, *125* (45), 12568–12573.
185. Dougherty, T. J. et al. Photodynamic Therapy. *JNCI J. Natl. Cancer Inst.* **1998**, *90* (12), 889–905.
186. Hamblin, M. R.; Hasan, T. Photodynamic Therapy: A New Antimicrobial Approach to Infectious Disease? *Photochem. Photobiol. Sci.* **2004**, *3* (5), 436–450.
187. Singh-Rachford, T. N.; Lott, J.; Weder, C.; Castellano, F. N. Influence of Temperature on Low-Power Upconversion in Rubbery Polymer Blends. *J. Am. Chem. Soc.* **2009**, *131* (33), 12007–12014.
188. Svagan, A. J. et al. Photon Energy Upconverting Nanopaper: A Bioinspired Oxygen Protection Strategy. *ACS Nano* **2014**, *8* (8), 8198–8207.
189. Monguzzi, A. et al. Low-Power-Photon Up-Conversion in Dual-Dye-Loaded Polymer Nanoparticles. *Adv. Funct. Mater.* **2012**, *22* (1), 139–143.
190. Askes, S. H. C. et al. Imaging Upconverting Polymersomes in Cancer Cells: Biocompatible Antioxidants Brighten Triplet-Triplet Annihilation Upconversion. *Small* **2016**, *12* (40), 5579–5590.
191. Dzebo, D.; Moth-Poulsen, K.; Albinsson, B. Robust Triplet–Triplet Annihilation Photon Upconversion by Efficient Oxygen Scavenging. *Photochem. Photobiol. Sci.* **2017**, *16* (8), 1327–1334.
192. Parker, C. A.; Hatchard, C. G. Sensitised Anti-Stokes Delayed Fluorescence. *Proc. Chem. Soc.* **1962**, 386–387.
193. Parker, C. A.; Hatchard, C. G. Delayed Fluorescence from Solutions of Anthracene and Phenanthrene. *Proc. R. Soc. London. Ser. A. Math. Phys. Sci.* **1962**, *269* (1339), 574–584.
194. Parker, C. A.; Hatchard, C. G. Delayed Fluorescence from Solutions of Anthracene and Phenanthrene. *Proc. Chem. Soc.* **1962**, 147.
195. Parker, C. A.; Hatchard, C. G. Delayed Fluorescence of Pyrene in Ethanol.

Trans. Faraday Soc. **1963**, *59* (0), 284–295.
196. Parker, C. A.; Bowen, E. J. Sensitized *P*-Type Delayed Fluorescence. *Proc. R. Soc. London. Ser. A. Math. Phys. Sci.* **1963**, *276* (1364), 125–135.
197. Sternlicht, H.; Nieman, G. C.; Robinson, G. W. Triplet—Triplet Annihilation and Delayed Fluorescence in Molecular Aggregates. *J. Chem. Phys.* **1963**, *38* (6), 1326–1335.
198. Parker, C. A. Transient Effects in Triplet-Triplet Annihilation. *Trans. Faraday Soc.* **1964**, *60* (0), 1998–2008.
199. Parker, C. A. Phosphorescence and Delayed Fluorescence from Solutions. *Advances in Photochemistry*. January 1, 1964, pp 305–383.
200. Sevchenko, A. N.; Stel'makh, G. F.; Tsvirko, M. P. No Title. *Opt. Spektrosk.* **1979**, *46*, 893–897.
201. O'Brien, J. A. et al. Efficient S2 State Production in ZnTPP–PMMA Thin Films by Triplet–Triplet Annihilation: Evidence of Solute Aggregation in Photon Upconversion Systems. *Chem. Phys. Lett.* **2009**, *475* (4), 220–222.
202. Nieman, G. C.; Robinson, G. W. Rapid Triplet Excitation Migration in Organic Crystals. *J. Chem. Phys.* **1962**, *37* (9), 2150–2151.
203. Azumi, T.; McGlynn, S. P. Delayed Fluorescence of Solid Solutions of Polyacenes. II. Kinetic Considerations. *J. Chem. Phys.* **1963**, *39* (5), 1186–1194.
204. Musser, A. J.; Clark, J. Triplet-Pair States in Organic Semiconductors. *Annu. Rev. Phys. Chem.* **2019**, *70* (1), 323–351.
205. Saltiel, J.; Atwater, B. W. Spin-Statistical Factors in Diffusion-Controlled Reactions. *Advances in Photochemistry*. January 1, 1988, pp 1–90.
206. Schmidt, T. W.; Castellano, F. N. Photochemical Upconversion: The Primacy of Kinetics. *J. Phys. Chem. Lett.* **2014**, *5* (22), 4062–4072.
207. Saltiel, J. et al. Spin-Statistical Factor in the Triplet-Triplet Annihilation of Anthracene Triplets. *J. Am. Chem. Soc.* **1981**, *103* (24), 7159–7164.
208. Groff, R. P.; Merrifield, R. E.; Avakian, P. Singlet and Triplet Channels for Triplet-Exciton Fusion in Anthracene Crystals. *Chem. Phys. Lett.* **1970**, *5* (3), 168–170.
209. Hoseinkhani, S.; Tubino, R.; Meinardi, F.; Monguzzi, A. Achieving the Photon Up-Conversion Thermodynamic Yield Upper Limit by Sensitized Triplet–Triplet Annihilation. *Phys. Chem. Chem. Phys.* **2015**, *17* (6), 4020–4024.
210. Sanders, S. N. et al. Understanding the Bound Triplet-Pair State in Singlet Fission. *Chem* **2019**, *5* (8), 1988–2005.
211. Singh-Rachford, T. N.; Haefele, A.; Ziessel, R.; Castellano, F. N. Boron Dipyrromethene Chromophores: Next Generation Triplet Acceptors/Annihilators for Low Power Upconversion Schemes. *J. Am. Chem. Soc.* **2008**, *130* (48), 16164–16165.
212. Froese, R. D. J.; Morokuma, K. Accurate Calculations of Bond-Breaking

Energies in C60 Using the Three-Layered ONIOM Method. *Chem. Phys. Lett.* **1999**, *305* (5), 419–424.
213. Dick, B.; Nickel, B. Accessibility of the Lowest Quintet State of Organic Molecules through Triplet-Triplet Annihilation; an Indo Ci Study. *Chem. Phys.* **1983**, *78* (1), 1–16.
214. Bachilo, S. M.; Weisman, R. B. Determination of Triplet Quantum Yields from Triplet−Triplet Annihilation Fluorescence. *J. Phys. Chem. A* **2000**, *104* (33), 7711–7714.
215. Cheng, Y. Y. et al. On the Efficiency Limit of Triplet–Triplet Annihilation for Photochemical Upconversion. *Phys. Chem. Chem. Phys.* **2010**, *12* (1), 66–71.
216. Cheng, Y. Y. et al. Kinetic Analysis of Photochemical Upconversion by Triplet−Triplet Annihilation: Beyond Any Spin Statistical Limit. *J. Phys. Chem. Lett.* **2010**, *1* (12), 1795–1799.
217. Wang, X. et al. An Energetics Perspective on Why There Are so Few Triplet–Triplet Annihilation Emitters. *J. Mater. Chem. C* **2020**, *8* (31), 10816–10824.
218. Helfrich, W.; Schneider, W. G. Transients of Volume-Controlled Current and of Recombination Radiation in Anthracene. *J. Chem. Phys.* **1966**, *44* (8), 2902–2909.
219. Kasha, M. Characterization of Electronic Transitions in Complex Molecules. *Discuss. Faraday Soc.* **1950**, *9* (0), 14–19.
220. Kobayashi, S.; Kikuchi, K.; Kokubun, H. Fluorescence of the Antharacenes Following Tn → T1 Excitation Studied by a Double Excitation Method. *Chem. Phys. Lett.* **1976**, *42* (3), 494–497.
221. Tang, X. et al. Achievement of High-Level Reverse Intersystem Crossing in Rubrene-Doped Organic Light-Emitting Diodes. *J. Phys. Chem. Lett.* **2020**, *11* (8), 2804–2811.
222. Zhao, Y. et al. The Second Excited Triplet-State Facilitates TADF and Triplet–Triplet Annihilation Photon Upconversion via a Thermally Activated Reverse Internal Conversion. *Adv. Opt. Mater.* **2022**, *n/a* (n/a), 2102275.
223. Weber, J. L. et al. In Silico Prediction of Annihilators for Triplet–Triplet Annihilation Upconversion via Auxiliary-Field Quantum Monte Carlo. *Chem. Sci.* **2021**, *12* (3), 1068–1079.
224. Pun, A. B.; Campos, L. M.; Congreve, D. N. Tunable Emission from Triplet Fusion Upconversion in Diketopyrrolopyrroles. *J. Am. Chem. Soc.* **2019**, *141* (9), 3777–3781.
225. Kondakov, D. Y.; Pawlik, T. D.; Hatwar, T. K.; Spindler, J. P. Triplet Annihilation Exceeding Spin Statistical Limit in Highly Efficient Fluorescent Organic Light-Emitting Diodes. *J. Appl. Phys.* **2009**, *106* (12),

124510.
226. Ern, V.; Saint-Clair, J. L.; Schott, M.; Delacote, G. Effects of Exciton Interactions on the Fluorescence Yield of Crystalline Tetracene. *Chem. Phys. Lett.* **1971**, *10* (3), 287–290.
227. Nishimura, N. et al. Photon Upconversion from Near-Infrared to Blue Light with TIPS-Anthracene as an Efficient Triplet–Triplet Annihilator. *ACS Mater. Lett.* **2019**, *1* (6), 660–664.
228. Gray, V.; Moth-Poulsen, K.; Albinsson, B.; Abrahamsson, M. Towards Efficient Solid-State Triplet–Triplet Annihilation Based Photon Upconversion: Supramolecular, Macromolecular and Self-Assembled Systems. *Coord. Chem. Rev.* **2018**, *362*, 54–71.
229. Gray, V. et al. Loss Channels in Triplet–Triplet Annihilation Photon Upconversion: Importance of Annihilator Singlet and Triplet Surface Shapes. *Phys. Chem. Chem. Phys.* **2017**, *19* (17), 10931–10939.
230. Miyata, K.; Conrad-Burton, F. S.; Geyer, F. L.; Zhu, X.-Y. Triplet Pair States in Singlet Fission. *Chem. Rev.* **2019**, *119* (6), 4261–4292.
231. Bossanyi, D. G. et al. Spin Statistics for Triplet–Triplet Annihilation Upconversion: Exchange Coupling, Intermolecular Orientation, and Reverse Intersystem Crossing. *JACS Au* **2021**, *1* (12), 2188–2201.
232. Zhou, Y.; Castellano, F. N.; Schmidt, T. W.; Hanson, K. On the Quantum Yield of Photon Upconversion via Triplet–Triplet Annihilation. *ACS Energy Lett.* **2020**, *5* (7), 2322–2326.
233. Kim, J.-H.; Deng, F.; Castellano, F. N.; Kim, J.-H. High Efficiency Low-Power Upconverting Soft Materials. *Chem. Mater.* **2012**, *24* (12), 2250–2252.
234. Wu, W. et al. Organic Triplet Sensitizer Library Derived from a Single Chromophore (BODIPY) with Long-Lived Triplet Excited State for Triplet–Triplet Annihilation Based Upconversion. *J. Org. Chem.* **2011**, *76* (17), 7056–7064.
235. Kashino, T. et al. Bulk Transparent Photon Upconverting Films by Dispersing High-Concentration Ionic Emitters in Epoxy Resins. *ACS Appl. Mater. Interfaces* **2021**, *13* (11), 13676–13683.
236. Huang, L. et al. Designing next Generation of Photon Upconversion: Recent Advances in Organic Triplet-Triplet Annihilation Upconversion Nanoparticles. *Biomaterials* **2019**, *201*, 77–86.
237. Simon, Y. C.; Weder, C. Low-Power Photon Upconversion through Triplet–Triplet Annihilation in Polymers. *J. Mater. Chem.* **2012**, *22* (39), 20817–20830.
238. Yun, Y. J. et al. Triplet-Triplet Annihilation Photon-Upconversion in Hydrophilic Media with Biorelevant Cholesteryl Triplet Energy Acceptors. *J. Photochem. Photobiol. A Chem.* **2021**, *418*, 113412.
239. Monguzzi, A. et al. Low Power, Non-Coherent Sensitized Photon up-

Conversion: Modelling and Perspectives. *Phys. Chem. Chem. Phys.* **2012**, *14* (13), 4322–4332.
240. Raišys, S. et al. Triplet Exciton Diffusion and Quenching in Matrix-Free Solid Photon Upconversion Films. *J. Phys. Chem. C* **2021**, *125* (7), 3764–3775.
241. Danos, A. et al. Deuteration of Perylene Enhances Photochemical Upconversion Efficiency. *J. Phys. Chem. Lett.* **2015**, *6* (15), 3061–3066.
242. Olesund, A.; Gray, V.; Mårtensson, J.; Albinsson, B. Diphenylanthracene Dimers for Triplet–Triplet Annihilation Photon Upconversion: Mechanistic Insights for Intramolecular Pathways and the Importance of Molecular Geometry. *J. Am. Chem. Soc.* **2021**, *143* (15), 5745–5754.
243. Monguzzi, A. et al. Unraveling Triplet Excitons Photophysics in Hyper-Cross-Linked Polymeric Nanoparticles: Toward the Next Generation of Solid-State Upconverting Materials. *J. Phys. Chem. Lett.* **2016**, *7* (14), 2779–2785.
244. Pun, A. B. et al. Annihilator Dimers Enhance Triplet Fusion Upconversion. *Chem. Sci.* **2019**, *10* (14), 3969–3975.
245. Imperiale, C. J. et al. Triplet-Fusion Upconversion Using a Rigid Tetracene Homodimer. *J. Phys. Chem. Lett.* **2019**, *10* (23), 7463–7469.
246. Dzebo, D. et al. Intramolecular Triplet–Triplet Annihilation Upconversion in 9,10-Diphenylanthracene Oligomers and Dendrimers. *J. Phys. Chem. C* **2016**, *120* (41), 23397–23406.
247. Edhborg, F. et al. Intramolecular Triplet–Triplet Annihilation Photon Upconversion in Diffusionally Restricted Anthracene Polymer. *J. Phys. Chem. B* **2021**, *125* (23), 6255–6263.
248. Gao, C. et al. Intramolecular Versus Intermolecular Triplet Fusion in Multichromophoric Photochemical Upconversion. *J. Phys. Chem. C* **2019**, *123* (33), 20181–20187.
249. Tilley, A. J.; Robotham, B. E.; Steer, R. P.; Ghiggino, K. P. Sensitized Non-Coherent Photon Upconversion by Intramolecular Triplet–Triplet Annihilation in a Diphenylanthracene Pendant Polymer. *Chem. Phys. Lett.* **2015**, *618*, 198–202.
250. Sun, W. et al. Highly Efficient Photon Upconversion Based on Triplet–Triplet Annihilation from Bichromophoric Annihilators. *J. Mater. Chem. C* **2021**, *9* (40), 14201–14208.
251. Bohne, C.; Abuin, E. B.; Scaiano, J. C. Characterization of the Triplet-Triplet Annihilation Process of Pyrene and Several Derivatives under Laser Excitation. *J. Am. Chem. Soc.* **1990**, *112* (11), 4226–4231.
252. Ye, C.; Gray, V.; Mårtensson, J.; Börjesson, K. Annihilation Versus Excimer Formation by the Triplet Pair in Triplet–Triplet Annihilation Photon Upconversion. *J. Am. Chem. Soc.* **2019**, *141* (24), 9578–9584.
253. Ye, C. et al. Optimizing Photon Upconversion by Decoupling Excimer

Formation and Triplet Triplet Annihilation. *Phys. Chem. Chem. Phys.* **2020**, *22* (3), 1715–1720.
254. Zhao, W.; Castellano, F. N. Upconverted Emission from Pyrene and Di-Tert-Butylpyrene Using Ir(Ppy)3 as Triplet Sensitizer. *J. Phys. Chem. A* **2006**, *110* (40), 11440–11445.
255. Charlton, J. L.; Dabestani, R.; Saltiel, J. Role of Triplet-Triplet Annihilation in Anthracene Dimerization. *J. Am. Chem. Soc.* **1983**, *105* (11), 3473–3476.
256. Islangulov, R. R.; Castellano, F. N. Photochemical Upconversion: Anthracene Dimerization Sensitized to Visible Light by a RuII Chromophore. *Angew. Chemie Int. Ed.* **2006**, *45* (36), 5957–5959.
257. Gray, V. et al. Singlet and Triplet Energy Transfer Dynamics in Self-Assembled Axial Porphyrin–Anthracene Complexes: Towards Supra-Molecular Structures for Photon Upconversion. *Phys. Chem. Chem. Phys.* **2018**, *20* (11), 7549–7558.
258. Gray, V. et al. Porphyrin–Anthracene Complexes: Potential in Triplet–Triplet Annihilation Upconversion. *J. Phys. Chem. C* **2016**, *120* (34), 19018–19026.
259. Radiunas, E. et al. Impact of T-Butyl Substitution in a Rubrene Emitter for Solid State NIR-to-Visible Photon Upconversion. *Phys. Chem. Chem. Phys.* **2020**, *22* (14), 7392–7403.
260. Askes, S. H. C.; Bahreman, A.; Bonnet, S. Activation of a Photodissociative Ruthenium Complex by Triplet-Triplet Annihilation Upconversion in Liposomes. *Angew. Chemie Int. Ed.* **2014**, *53* (4), 1029–1033.
261. Wieghold, S. et al. Is Disorder Beneficial in Perovskite-Sensitized Solid-State Upconversion? The Role of DBP Doping in Rubrene. *J. Phys. Chem. C* **2020**, *124* (33), 18132–18140.
262. Lindsey, J. S.; Taniguchi, M.; Bocian, D. F.; Holten, D. The Fluorescence Quantum Yield Parameter in Förster Resonance Energy Transfer (FRET)—Meaning, Misperception, and Molecular Design. *Chem. Phys. Rev.* **2021**, *2* (1), 11302.
263. Crosby, G. A.; Demas, J. N. Measurement of Photoluminescence Quantum Yields. Review. *J. Phys. Chem.* **1971**, *75* (8), 991–1024.
264. Kubin, R. F.; Fletcher, A. N. Fluorescence Quantum Yields of Some Rhodamine Dyes. *J. Lumin.* **1982**, *27* (4), 455–462.
265. Olmsted, J. Calorimetric Determinations of Absolute Fluorescence Quantum Yields. *J. Phys. Chem.* **1979**, *83* (20), 2581–2584.
266. Kiseleva, N. et al. Determination of Upconversion Quantum Yields Using Charge-Transfer State Fluorescence of Heavy-Atom-Free Sensitizer as a Self-Reference. *J. Phys. Chem. Lett.* **2020**, *11* (16), 6560–6566.
267. Yanai, N. et al. Absolute Method to Certify Quantum Yields of Photon

Upconversion via Triplet–Triplet Annihilation. *J. Phys. Chem. A* **2019**, *123* (46), 10197–10203.
268. Jones, C. M. S.; Gakamsky, A.; Marques-Hueso, J. The Upconversion Quantum Yield (UCQY): A Review to Standardize the Measurement Methodology, Improve Comparability, and Define Efficiency Standards. *Sci. Technol. Adv. Mater.* **2021**, *22* (1), 810–848.
269. Islangulov, R. R.; Kozlov, D. V; Castellano, F. N. Low Power Upconversion Using MLCT Sensitizers. *Chem. Commun.* **2005**, No. 30, 3776–3778.
270. Islangulov, R. R.; Lott, J.; Weder, C.; Castellano, F. N. Noncoherent Low-Power Upconversion in Solid Polymer Films. *J. Am. Chem. Soc.* **2007**, *129* (42), 12652–12653.
271. Kozlov, D. V; Castellano, F. N. Anti-Stokes Delayed Fluorescence from Metal–Organic Bichromophores. *Chem. Commun.* **2004**, No. 24, 2860–2861.
272. Singh-Rachford, T. N.; Islangulov, R. R.; Castellano, F. N. Photochemical Upconversion Approach to Broad-Band Visible Light Generation. *J. Phys. Chem. A* **2008**, *112* (17), 3906–3910.
273. Singh-Rachford, T. N.; Castellano, F. N. Low Power Visible-to-UV Upconversion. *J. Phys. Chem. A* **2009**, *113* (20), 5912–5917.
274. Haefele, A.; Blumhoff, J.; Khnayzer, R. S.; Castellano, F. N. Getting to the (Square) Root of the Problem: How to Make Noncoherent Pumped Upconversion Linear. *J. Phys. Chem. Lett.* **2012**, *3* (3), 299–303.
275. Monguzzi, A. et al. Upconversion-Induced Fluorescence in Multicomponent Systems: Steady-State Excitation Power Threshold. *Phys. Rev. B* **2008**, *78* (19), 195112.
276. Auckett, J. E. et al. Efficient Up-Conversion by Triplet-Triplet Annihilation. *J. Phys. Conf. Ser.* **2009**, *185*, 12002.
277. Murakami, Y.; Kamada, K. Kinetics of Photon Upconversion by Triplet–Triplet Annihilation: A Comprehensive Tutorial. *Phys. Chem. Chem. Phys.* **2021**, *23* (34), 18268–18282.
278. Gholizadeh, E. M. et al. Photochemical Upconversion Is Suppressed by High Concentrations of Molecular Sensitizers. *Phys. Chem. Chem. Phys.* **2018**, *20* (29), 19500–19506.
279. Jefferies, D.; Schmidt, T. W.; Frazer, L. Photochemical Upconversion Theory: Importance of Triplet Energy Levels and Triplet Quenching. *Phys. Rev. Appl.* **2019**, *12* (2), 24023.
280. Meroni, D.; Monguzzi, A.; Meinardi, F. Photon Upconversion in Multicomponent Systems: Role of Back Energy Transfer. *J. Chem. Phys.* **2020**, *153* (11), 114302.
281. Imperiale, C. J.; Green, P. B.; Hasham, M.; Wilson, M. W. B. Ultra-Small PbS Nanocrystals as Sensitizers for Red-to-Blue Triplet-Fusion

Upconversion. *Chem. Sci.* **2021**, *12* (42), 14111–14120.
282. Zähringer, T. J. B.; Bertrams, M.-S.; Kerzig, C. Purely Organic Vis-to-UV Upconversion with an Excited Annihilator Singlet beyond 4 EV. *J. Mater. Chem. C* **2022**.
283. Fallon, K. J. et al. Molecular Engineering of Chromophores to Enable Triplet–Triplet Annihilation Upconversion. *J. Am. Chem. Soc.* **2020**, *142* (47), 19917–19925.
284. Harada, N. et al. Discovery of Key TIPS-Naphthalene for Efficient Visible-to-UV Photon Upconversion under Sunlight and Room Light**. *Angew. Chemie Int. Ed.* **2021**, *60* (1), 142–147.
285. Olesund, A. et al. Approaching the Spin-Statistical Limit in Visible-to-Ultraviolet Photon Upconversion. *J. Am. Chem. Soc.* **2022**.
286. Wei, Y. et al. Multiple Resonance TADF Sensitizers Enable Green-to-UV Photon Upconversion: Application in Photochemical Transformations. *CCS Chem.* **2022**.
287. Fan, C. et al. Efficient Triplet–Triplet Annihilation Upconversion with an Anti-Stokes Shift of 1.08 EV Achieved by Chemically Tuning Sensitizers. *J. Am. Chem. Soc.* **2019**, *141* (38), 15070–15077.
288. Huang, Z.; Tang, M. L. Designing Transmitter Ligands That Mediate Energy Transfer between Semiconductor Nanocrystals and Molecules. *J. Am. Chem. Soc.* **2017**, *139* (28), 9412–9418.
289. Huang, T. et al. Bidirectional Triplet Exciton Transfer between Silicon Nanocrystals and Perylene. *Chem. Sci.* **2021**, *12* (19), 6737–6746.
290. Imperiale, C. J.; Green, P. B.; Hasham, M.; Wilson, M. W. B. Ultra-Small PbS Nanocrystals as Sensitizers for Red-to-Blue Triplet-Fusion Upconversion. *Chem. Sci.* **2021**, *12* (42), 14111–14120.
291. Nishimura, N. et al. Photon Upconversion Utilizing Energy beyond the Band Gap of Crystalline Silicon with a Hybrid TES-ADT/PbS Quantum Dots System. *Chem. Sci.* **2019**, *10* (18), 4750–4760.
292. Kinoshita, T. et al. Enhancement of Near-IR Photoelectric Conversion in Dye-Sensitized Solar Cells Using an Osmium Sensitizer with Strong Spin-Forbidden Transition. *J. Phys. Chem. Lett.* **2012**, *3* (3), 394–398.
293. Amemori, S.; Sasaki, Y.; Yanai, N.; Kimizuka, N. Near-Infrared-to-Visible Photon Upconversion Sensitized by a Metal Complex with Spin-Forbidden yet Strong S0–T1 Absorption. *J. Am. Chem. Soc.* **2016**, *138* (28), 8702–8705.
294. Sasaki, Y. et al. Near Infrared-to-Blue Photon Upconversion by Exploiting Direct S–T Absorption of a Molecular Sensitizer. *J. Mater. Chem. C* **2017**, *5* (21), 5063–5067.
295. Sasaki, Y.; Amemori, S.; Yanai, N.; Kimizuka, N. Singlet-to-Triplet Absorption for Near-Infrared-to-Visible Photon Upconversion. *Bull. Chem. Soc. Jpn.* **2021**, *94* (6), 1760–1768.

296. Kiser, P. D.; Golczak, M.; Palczewski, K. Chemistry of the Retinoid (Visual) Cycle. *Chem. Rev.* **2014**, *114* (1), 194–232.
297. Hartley, G. S. The Cis-Form of Azobenzene. *Nature* **1937**, *140* (3537), 281.
298. Mitscherlich, E. Ueber Das Stickstoffbenzid. *Ann. Phys.* **1834**, *108* (15), 225–227.
299. Cristol, S. J.; Snell, R. L. Bridged Polycyclic Compounds. VI. The Photoisomerization of Bicyclo [2,2,1]Hepta-2,5-Diene-2,3-Dicarboxylic Acid to Quadricyclo [2,2,1,02,6,03,5]Heptane-2,3-Dicarboxylic Acid1,2. *J. Am. Chem. Soc.* **1958**, *80* (8), 1950–1952.
300. Hirshberg, Y.; Fischer, E. Photochromism and Reversible Multiple Internal Transitions in Some Spiropyrans at Low Temperatures. Part I. *J. Chem. Soc.* **1954**, No. 0, 297–303.
301. Helmy, S. et al. Photoswitching Using Visible Light: A New Class of Organic Photochromic Molecules. *J. Am. Chem. Soc.* **2014**, *136* (23), 8169–8172.
302. Irie, M.; Mohri, M. Thermally Irreversible Photochromic Systems. Reversible Photocyclization of Diarylethene Derivatives. *J. Org. Chem.* **1988**, *53* (4), 803–808.
303. Koumura, N. et al. Light-Driven Monodirectional Molecular Rotor. *Nature* **1999**, *401* (6749), 152–155.
304. Brode, W. R.; Pearson, E. G.; Wyman, G. M. The Relation between the Absorption Spectra and the Chemical Constitution of Dyes. XXVII. Cis-Trans Isomerism and Hydrogen Bonding in Indigo Dyes1. *J. Am. Chem. Soc.* **1954**, *76* (4), 1034–1036.
305. Waldeck, D. H. Photoisomerization Dynamics of Stilbenes. *Chem. Rev.* **1991**, *91* (3), 415–436.
306. Wyman, G. M. The Cis-Trans Isomerization of Conjugated Compounds. *Chem. Rev.* **1955**, *55* (4), 625–657.
307. Bandara, H. M. D.; Burdette, S. C. Photoisomerization in Different Classes of Azobenzene. *Chem. Soc. Rev.* **2012**, *41* (5), 1809–1825.
308. Jerca, F. A.; Jerca, V. V.; Hoogenboom, R. Advances and Opportunities in the Exciting World of Azobenzenes. *Nat. Rev. Chem.* **2022**, *6* (1), 51–69.
309. Crespi, S.; Simeth, N. A.; König, B. Heteroaryl Azo Dyes as Molecular Photoswitches. *Nat. Rev. Chem.* **2019**, *3* (3), 133–146.
310. Frisch, M. J. et al. Gaussian 16. Gaussian, Inc. Wallingford, CT 2016.
311. Fischer, E. Temperature Dependence of Photoisomerization Equilibria. Part I. Azobenzene and the Azonaphthalenes. *J. Am. Chem. Soc.* **1960**, *82* (13), 3249–3252.
312. Bléger, D.; Hecht, S. Visible-Light-Activated Molecular Switches. *Angew. Chemie Int. Ed.* **2015**, *54* (39), 11338–11349.
313. Dong, M. et al. Red-Shifting Azobenzene Photoswitches for in Vivo Use. *Acc. Chem. Res.* **2015**, *48* (10), 2662–2670.

314. Beharry, A. A.; Woolley, G. A. Azobenzene Photoswitches for Biomolecules. *Chem. Soc. Rev.* **2011**, *40* (8), 4422–4437.
315. Samanta, S.; Babalhavaeji, A.; Dong, M.; Woolley, G. A. Photoswitching of Ortho-Substituted Azonium Ions by Red Light in Whole Blood. *Angew. Chemie Int. Ed.* **2013**, *52* (52), 14127–14130.
316. Dong, M. et al. Near-Infrared Photoswitching of Azobenzenes under Physiological Conditions. *J. Am. Chem. Soc.* **2017**, *139* (38), 13483–13486.
317. Hansen, M. J.; Lerch, M. M.; Szymanski, W.; Feringa, B. L. Direct and Versatile Synthesis of Red-Shifted Azobenzenes. *Angew. Chemie Int. Ed.* **2016**, *55* (43), 13514–13518.
318. Siewertsen, R. et al. Highly Efficient Reversible Z−E Photoisomerization of a Bridged Azobenzene with Visible Light through Resolved S1(Nπ*) Absorption Bands. *J. Am. Chem. Soc.* **2009**, *131* (43), 15594–15595.
319. Ahmed, Z.; Siiskonen, A.; Virkki, M.; Priimagi, A. Controlling Azobenzene Photoswitching through Combined Ortho-Fluorination and -Amination. *Chem. Commun.* **2017**, *53* (93), 12520–12523.
320. Konrad, D. B. et al. Computational Design and Synthesis of a Deeply Red-Shifted and Bistable Azobenzene. *J. Am. Chem. Soc.* **2020**, *142* (14), 6538–6547.
321. Kuntze, K. et al. Towards Low-Energy-Light-Driven Bistable Photoswitches: Ortho-Fluoroaminoazobenzenes. *Photochem. Photobiol. Sci.* **2021**.
322. Lameijer, L. N. et al. General Principles for the Design of Visible-Light-Responsive Photoswitches: Tetra-Ortho-Chloro-Azobenzenes. *Angew. Chemie Int. Ed.* **2020**, *59* (48), 21663–21670.
323. Bléger, D.; Schwarz, J.; Brouwer, A. M.; Hecht, S. O-Fluoroazobenzenes as Readily Synthesized Photoswitches Offering Nearly Quantitative Two-Way Isomerization with Visible Light. *J. Am. Chem. Soc.* **2012**, *134* (51), 20597–20600.
324. Knie, C. et al. Ortho-Fluoroazobenzenes: Visible Light Switches with Very Long-Lived Z Isomers. *Chem. – A Eur. J.* **2014**, *20* (50), 16492–16501.
325. Jia, S.; Sletten, E. M. Spatiotemporal Control of Biology: Synthetic Photochemistry Toolbox with Far-Red and Near-Infrared Light. *ACS Chem. Biol.* **2021**.
326. Sadovski, O.; Beharry, A. A.; Zhang, F.; Woolley, G. A. Spectral Tuning of Azobenzene Photoswitches for Biological Applications. *Angew. Chemie Int. Ed.* **2009**, *48* (8), 1484–1486.
327. Velema, W. A.; Szymanski, W.; Feringa, B. L. Photopharmacology: Beyond Proof of Principle. *J. Am. Chem. Soc.* **2014**, *136* (6), 2178–2191.
328. Szymański, W. et al. Reversible Photocontrol of Biological Systems by the Incorporation of Molecular Photoswitches. *Chem. Rev.* **2013**, *113* (8),

6114–6178.
329. Croissant, J. et al. Two-Photon-Triggered Drug Delivery in Cancer Cells Using Nanoimpellers. *Angew. Chemie Int. Ed.* **2013**, *52* (51), 13813–13817.
330. Moreno, J. et al. Sensitized Two-NIR-Photon Z→E Isomerization of a Visible-Light-Addressable Bistable Azobenzene Derivative. *Angew. Chemie Int. Ed.* **2016**, *55* (4), 1544–1547.
331. Izquierdo-Serra, M. et al. Two-Photon Neuronal and Astrocytic Stimulation with Azobenzene-Based Photoswitches. *J. Am. Chem. Soc.* **2014**, *136* (24), 8693–8701.
332. Jiang, Z.; Xu, M.; Li, F.; Yu, Y. Red-Light-Controllable Liquid-Crystal Soft Actuators via Low-Power Excited Upconversion Based on Triplet–Triplet Annihilation. *J. Am. Chem. Soc.* **2013**, *135* (44), 16446–16453.
333. Wang, L. et al. Reversible Near-Infrared Light Directed Reflection in a Self-Organized Helical Superstructure Loaded with Upconversion Nanoparticles. *J. Am. Chem. Soc.* **2014**, *136* (12), 4480–4483.
334. Liu, J.; Bu, W.; Pan, L.; Shi, J. NIR-Triggered Anticancer Drug Delivery by Upconverting Nanoparticles with Integrated Azobenzene-Modified Mesoporous Silica. *Angew. Chemie Int. Ed.* **2013**, *52* (16), 4375–4379.
335. Goulet-Hanssens, A. et al. Electrocatalytic Z → E Isomerization of Azobenzenes. *J. Am. Chem. Soc.* **2017**, *139* (1), 335–341.
336. Goulet-Hanssens, A. et al. Hole Catalysis as a General Mechanism for Efficient and Wavelength-Independent Z → E Azobenzene Isomerization. *Chem* **2018**, *4* (7), 1740–1755.
337. Hallett-Tapley, G. L. et al. Gold Nanoparticle Catalysis of the Cis–Trans Isomerization of Azobenzene. *Chem. Commun.* **2013**, *49* (86), 10073–10075.
338. Moreno, J. et al. Efficient Sensitized Z→E Photoisomerization of an Iridium(III)-Azobenzene Complex over a Wide Concentration Range. *Chem. – A Eur. J.* **2017**, *23* (56), 14090–14095.
339. Kuntze, K. et al. Azobenzene Photoswitching with Near-Infrared Light Mediated by Molecular Oxygen. *J. Phys. Chem. B* **2021**, *125* (45), 12568–12573.
340. Jones, L. B.; Hammond, G. S. Mechanisms of Photochemical Reactions in Solution. XXX.1 Photosensitized Isomerization of Azobenzene. *J. Am. Chem. Soc.* **1965**, *87* (18), 4219–4220.
341. Ronayette, J.; Arnaud, R.; Lemaire, J. Isomérisation Photosensibilisée Par Des Colorants et Photoréduction de l'azobenzène En Solution. II. *Can. J. Chem.* **1974**, *52* (10), 1858–1867.
342. Ronayette, J.; Arnaud, R.; Lebourgeois, P.; Lemaire, J. Isomérisation Photochimique de l'azobenzène En Solution. I. *Can. J. Chem.* **1974**, *52* (10), 1848–1857.
343. Monti, S.; Gardini, E.; Bortolus, P.; Amouyal, E. The Triplet State of

Azobenzene. *Chem. Phys. Lett.* **1981**, *77* (1), 115–119.
344. Bortolus, P.; Monti, S. Cis-Trans Photoisomerization of Azobenzene. Solvent and Triplet Donors Effects. *J. Phys. Chem.* **1979**, *83* (6), 648–652.
345. Monti, S.; Dellonte, S.; Bortolus, P. The Lowest Triplet State of Substituted Azobenzenes: An Energy Transfer Investigation. *J. Photochem.* **1983**, *23* (2), 249–256.
346. Goulet-Hanssens, A. et al. Electrocatalytic Z → E Isomerization of Azobenzenes. *J. Am. Chem. Soc.* **2017**, *139* (1), 335–341.
347. Gagliardi, L. et al. A Theoretical Study of the Lowest Electronic States of Azobenzene: The Role of Torsion Coordinate in the Cis–Trans Photoisomerization. *Theor. Chem. Acc.* **2004**, *111* (2), 363–372.
348. Cembran, A. et al. On the Mechanism of the Cis−trans Isomerization in the Lowest Electronic States of Azobenzene: S0, S1, and T1. *J. Am. Chem. Soc.* **2004**, *126* (10), 3234–3243.
349. Wang, Z. et al. Demonstration of an Azobenzene Derivative Based Solar Thermal Energy Storage System. *J. Mater. Chem. A* **2019**, *7* (25), 15042–15047.
350. Jones, L. B.; Hammond, G. S. Mechanisms of Photochemical Reactions in Solution. XXX.1 Photosensitized Isomerization of Azobenzene. *J. Am. Chem. Soc.* **1965**, *87* (18), 4219–4220.
351. Mercer-Smith, J. A.; Whitten, D. G. Photosensitization of Stilbene Isomerization by Palladium and Platinum Porphyrins, an Intermolecular Quantum Chain Process. *J. Am. Chem. Soc.* **1978**, *100* (9), 2620–2625.
352. Hammond, G. S.; Saltiel, J. Photosensitized Cis-Trans Isomerization of the Stilbenes. *J. Am. Chem. Soc.* **1962**, *84* (24), 4983–4984.
353. Cnossen, A. et al. Driving Unidirectional Molecular Rotary Motors with Visible Light by Intra- And Intermolecular Energy Transfer from Palladium Porphyrin. *J. Am. Chem. Soc.* **2012**, *134* (42), 17613–17619.
354. Fredrich, S.; Morack, T.; Sliwa, M.; Hecht, S. Mechanistic Insights into the Triplet Sensitized Photochromism of Diarylethenes. *Chem. – A Eur. J.* **2020**, *26* (34), 7672–7677.
355. Fredrich, S. et al. Switching Diarylethenes Reliably in Both Directions with Visible Light. *Angew. Chemie Int. Ed.* **2016**, *55* (3), 1208–1212.
356. Hou, L. et al. A General Approach for All-Visible-Light Switching of Diarylethenes through Triplet Sensitization Using Semiconducting Nanocrystals. *Res. Sq.* **2022**.
357. Wyman, G. M.; Zarnegar, B. M.; Whitten, D. G. Excited-State Chemistry of Indigoid Dyes. III. Interaction of Indigo and Thioindigo with Tin(IV) Tetraphenyltetrahydroporphyrin Triplets. Photosensitized Isomerization of Thioindigo. *J. Phys. Chem.* **1973**, *77* (21), 2584–2586.
358. Chibisov, A. K.; Görner, H. Photoprocesses in Spirooxazines and Their

Merocyanines. *J. Phys. Chem. A* **1999**, *103* (26), 5211–5216.
359. Favaro, G.; Aloisi, G. G. Reversible Triplet Energy Transfer between Biacetyl and Norbornadiene Naphthyl Carboxylates. *Zeitschrift für Phys. Chemie* **1988**, *159* (1), 11–19.
360. Chen, J. et al. Light-Harvesting and Photoisomerization in Benzophenone and Norbornadiene-Labeled Poly(Aryl Ether) Dendrimers via Intramolecular Triplet Energy Transfer. *J. Am. Chem. Soc.* **2005**, *127* (7), 2165–2171.
361. Großkopf, J.; Kratz, T.; Rigotti, T.; Bach, T. Enantioselective Photochemical Reactions Enabled by Triplet Energy Transfer. *Chem. Rev.* **2022**, *122* (2), 1626–1653.
362. Neveselý, T.; Wienhold, M.; Molloy, J. J.; Gilmour, R. Advances in the E → Z Isomerization of Alkenes Using Small Molecule Photocatalysts. *Chem. Rev.* **2022**, *122* (2), 2650–2694.
363. Accardo, J. V; Kalow, J. A. Reversibly Tuning Hydrogel Stiffness through Photocontrolled Dynamic Covalent Crosslinks. *Chem. Sci.* **2018**, *9* (27), 5987–5993.
364. Accardo, J. V; McClure, E. R.; Mosquera, M. A.; Kalow, J. A. Using Visible Light to Tune Boronic Acid–Ester Equilibria. *J. Am. Chem. Soc.* **2020**, *142* (47), 19969–19979.
365. Morstein, J.; Awale, M.; Reymond, J.-L.; Trauner, D. Mapping the Azolog Space Enables the Optical Control of New Biological Targets. *ACS Cent. Sci.* **2019**, *5* (4), 607–618.
366. Samanta, S.; Qin, C.; Lough, A. J.; Woolley, G. A. Bidirectional Photocontrol of Peptide Conformation with a Bridged Azobenzene Derivative. *Angew. Chemie Int. Ed.* **2012**, *51* (26), 6452–6455.
367. Tellkamp, T.; Shen, J.; Okamoto, Y.; Herges, R. Diazocines on Molecular Platforms. *European J. Org. Chem.* **2014**, *2014* (25), 5456–5461.
368. Joshi, D. K. et al. Synthesis of Cyclic Azobenzene Analogues. *Tetrahedron* **2012**, *68* (41), 8670–8676.
369. Trads, J. B. et al. Sign Inversion in Photopharmacology: Incorporation of Cyclic Azobenzenes in Photoswitchable Potassium Channel Blockers and Openers. *Angew. Chemie Int. Ed.* **2019**, *58* (43), 15421–15428.
370. Miyajima, D. et al. Delayed Fluorescence from Inverted Singlet and Triplet Excited States for Efficient Organic Light-Emitting Diodes. *Res. Sq.* **2021**.
371. Parker, C. A.; Hatchard, C. G. Triplet-Singlet Emission in Fluid Solutions. Phosphorescence of Eosin. *Trans. Faraday Soc.* **1961**, *57* (0), 1894–1904.
372. Finikova, O. S. et al. Energy and Electron Transfer in Enhanced Two-Photon-Absorbing Systems with Triplet Cores. *J. Phys. Chem. A* **2007**, *111* (30), 6977–6990.
373. Garakyaraghi, S. et al. Delayed Molecular Triplet Generation from Energized Lead Sulfide Quantum Dots. *J. Phys. Chem. Lett.* **2017**, *8* (7),

1458–1463.
374. Bender, J. A. et al. Surface States Mediate Triplet Energy Transfer in Nanocrystal–Acene Composite Systems. *J. Am. Chem. Soc.* **2018**, *140* (24), 7543–7553.
375. Zhao, G. et al. Triplet Energy Migration Pathways from PbS Quantum Dots to Surface-Anchored Polyacenes Controlled by Charge Transfer. *Nanoscale* **2021**, *13* (2), 1303–1310.
376. Massaro, G. et al. Thermally Switchable Molecular Upconversion Emission. *Chem. Mater.* **2016**, *28* (3), 738–745.
377. Duan, P.; Yanai, N.; Kurashige, Y.; Kimizuka, N. Aggregation-Induced Photon Upconversion through Control of the Triplet Energy Landscapes of the Solution and Solid States. *Angew. Chemie Int. Ed.* **2015**, *54* (26), 7544–7549.
378. Goerner, H.; Gruen, H.; Schulte-Frohlinde, D. Laser Flash Photolysis Study of Substituted Azobenzenes. Evidence for a Triplet State in Viscous Media. *J. Phys. Chem.* **1980**, *84* (23), 3031–3039.

PUBLICATIONS

Publication I Durandin, N. A.; Isokuortti, J.; Efimov, A.; Vuorimaa-Laukkanen, E.; Tkachenko, N. V.; Laaksonen, T. Efficient photon upconversion at remarkably low annihilator concentrations in a liquid polymer matrix: when less is more. *Chemical Communications* **2018**, 54, 14029.

Publication II Durandin, N. A.; Isokuortti, J.; Efimov, A.; Vuorimaa-Laukkanen, E.; Tkachenko, N. V.; Laaksonen, T. Critical Sensitizer Quality Attributes for Efficient Triplet-Triplet Annihilation Upconversion with Low Power Density Thresholds. *Journal of Physical Chemistry C.* **2019**, 123, 37, 22865

Publication III Isokuortti, J.; Allu, S. R.; Efimov, A.; Vuorimaa-Laukkanen, E.; Tkachenko, N. V.; Vinogradov, S. A.; Laaksonen, T.; Durandin, N. A. Endothermic and Exothermic Energy Transfer Made Equally Efficient for Triplet-Triplet Annihilation Upconversion. *Journal of Physical Chemistry Letters* **2020**, 11, 1, 318

Publication IV Isokuortti, J.; Kuntze, K.; Virkki, M.; Ahmed, Z.; Vuorimaa-Laukkanen, E.; Filatov, M. A.; Turshatov, A.; Laaksonen, T.; Priimägi, A.; Durandin, N. A. Expanding excitation wavelengths for azobenzene photoswitching into the near-infrared range *via* endothermic triplet energy transfer. *Chemical Science* **2021**, 12, 7504

PUBLICATION I

Efficient photon upconversion at remarkably low annihilator concentrations in a liquid polymer matrix: when less is more

Durandin, N. A.; Isokuortti, J.; Efimov, A.; Vuorimaa-Laukkanen, E.; Tkachenko, N. V.; Laaksonen, T.

Chemical Communications, vol. 54, p. 14029, 2018
DOI: https://doi.org/10.1039/C8CC07592A

ChemComm

COMMUNICATION

View Article Online
View Journal | View Issue

Cite this: *Chem. Commun.*, 2018, **54**, 14029

Received 19th September 2018,
Accepted 21st November 2018

DOI: 10.1039/c8cc07592a

rsc.li/chemcomm

Efficient photon upconversion at remarkably low annihilator concentrations in a liquid polymer matrix: when less is more†

Nikita A. Durandin, * Jussi Isokuortti, Alexander Efimov, Elina Vuorimaa-Laukkanen, Nikolai V. Tkachenko and Timo Laaksonen

A green-to-blue triplet–triplet annihilation upconversion of 24.5% quantum yield was achieved at a remarkably low 600 μM annihilator concentration in a viscous polymer matrix. This was made possible by utilizing a ZnTPP-based photosensitizer with exceptionally long 11 ms phosphorescence lifetime. Higher 3 mM annihilator concentration resulted in lower 24% upconversion quantum yield.

Discovered by Parker and Hatchard in the 1960s,[1–3] triplet–triplet annihilation-based photon upconversion (TTAUC) experiences a resurrection nowadays, as it is able to convert low-energy photons into high-energy ones under non-coherent, low-power excitation light.[4] Thus, the principle can be employed in numerous imperative applications including TTAUC-employed solar cells,[5–7] photocatalysis,[8] bio-imaging[9,10] and phototriggered drug delivery systems.[11–14]

To initialize TTAUC, a photo-excited sensitizer (S) molecule in its triplet state undergoes triplet–triplet energy transfer (TTET) to another molecule, called an annihilator (A). Eventually, two annihilator triplets collide with each other to generate one singlet and one ground state *via* triplet–triplet annihilation (TTA). Consequently, the annihilator singlet state emits the photon of higher energy (lower wavelength) than the one absorbed by a sensitizer, thus generating delayed upconverted fluorescence.[1–3] Thus the TTAUC efficiency depends on four parameters: intersystem crossing efficiency of a sensitizer (Φ_{ISC}), TTET and TTA efficiencies (Φ_{TTET} and Φ_{TTA}), and quantum yield of annihilator fluorescence (Φ_{fl}^{A}) and can be expressed as follows:

$$\Phi_{UC} = \Phi_{ISC} \times \Phi_{TTET} \times \Phi_{TTA} \times \Phi_{fl}^{A} \quad (1)$$

Up to now most commonly used TTAUC sensitizers are noble metal porphyrins, such as Pt(II) and Pd(II) complexes because of their high intersystem crossing efficiency ($\Phi_{ISC} \geq 0.99$).[4,15,16] However, a vast majority of those sensitizers have rather short-living triplet states (up to several hundreds of microseconds), which is detrimental for the initial triplet–triplet energy transfer of TTAUC. Moreover, the rate of the triplet–triplet energy transfer is diffusion-limited and thus viscosity-dependent, which makes it a "bottleneck" for the whole TTAUC in polymeric matrices. A higher concentration of the annihilator makes the TTET process more efficient, but on the other hand results in undesired aggregates and excimer formation.[17,18] This results in a decrease in TTAUC efficacy. Moreover, for soft matter systems high annihilator concentration is extremely challenging or unfeasible.[11,12,19–22] Thus, it is of paramount importance to find sensitizers with a long living triplet state and high Φ_{ISC} to overcome the problems mentioned above.[23,24]

Herein we used a zinc tetraphenylporphyrin derivative, namely, the zinc complex of 2-{3-[10,15,20-tris(3,5-di-*tert*-butylphenyl)-porphyrin-5-yl]phenoxy}ethanol (ZnTPPOH), which takes advantage of the properties of ZnTPP ($\Phi_{ISC} \approx 0.83–0.88$[25,26] and $\tau_T \approx 4$ ms),[27] whilst the *tert*-butyl substituents prevent aggregation.[28,29] It is noteworthy that despite the promising properties of the ZnTPP molecule for TTAUC, quantitative data on ZnTPP-sensitized upconversion remain scarce.[30–32] However, there are a few studies on other Zn-containing porphyrins such as ZnTPTBP[33] and ZnOEP.[34,35]

In contrast to ZnTPPOH, the Pt(II) complex of the same porphyrin (PtTPPOH) with $\Phi_{ISC} \approx 1$ was also utilized as a sensitizer.[36] The use of PtTPPOH is rationalized here as a control molecule with a very similar structure to ZnTPPOH, but with shorter lifetime. In this way, it is possible to evaluate the effect of triplet state lifetimes on the efficiency of TTAUC. 2,5,8,11-Tetra-*tert*-butylperylene (TTBPer) was chosen as the annihilator because of perylene's ability to generate the singlet excited state with unity efficiency *via* TTA. Perylene also has a low enough triplet energy level for efficient TTET.[37] PtTPPOH and ZnTPPOH were prepared by a previously described method[29] and comprehensively characterized (see the ESI†), while TTBPer was purchased from a commercial source (Scheme 1).

Laboratory of Chemistry and Bioengineering, Tampere University of Technology, P.O. Box 541, FI-33101, Tampere, Finland. E-mail: nikita.durandin@tut.fi, nikita.durandin@gmail.com

† Electronic supplementary information (ESI) available: Synthetic procedures and additional characterization results. See DOI: 10.1039/c8cc07592a

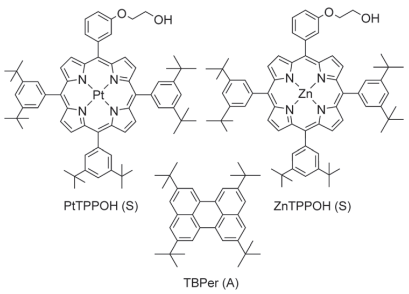

Scheme 1 Molecular structures of PtTPPOH, ZnTPPOH and TTBPer.

Although most studies focus on performing the TTA experiments in organic solvents,[38–44] the sensitizer/annihilator pairs should actually be incorporated in a polymer matrix to anticipate their potential utilization in real applications. In the current study, we introduced our molecules into a poly(ethylene glycol) 200 matrix doped with 30 mM oleic acid (PEG–OA) to simulate *e.g.* soft matter/polymeric device conditions. PEG–OA has been proposed by Castellano and co-workers[45] as a promising medium for TTAUC-based devices due to the low solubility of O_2 in PEG and the prominent oxygen scavenging properties of OA that are both essential for reducing losses associated with oxygen quenching of the triplet state.[46–48]

Fig. 1 depicts the absorption and luminescence spectra of all three molecules in a degassed PEG–OA matrix. It is noteworthy that in parallel to phosphorescence at 796 nm, ZnTPPOH exhibits pronounced fluorescence (λ_{max} = 660 nm) as a result of non-unity intersystem crossing efficacy of the ZnTPP moiety.[25]

Phosphorescence lifetime measurements of the porphyrins in degassed PEG–OA were conducted, followed by quenching experiments with TTBPer. Consequently, Stern–Volmer constants (K_{SV}) and TTET rates (K_{TTET}) were estimated (Fig. 2; eqn (S1) in the ESI†). The intact phosphorescence lifetime of ZnTPPOH shows a dramatic difference of more than 2 orders of magnitude with respect to PtTTPOH. Due to the ultralong 11.0 ms triplet lifetime, the Stern–Volmer constant for ZnTPPOH is about 74 times larger than that for PtTPPOH (2.2×10^5 M^{-1} *vs.* 2980 M^{-1}). However, K_{TTET} is smaller for ZnTPPOH than for PtTPPOH (2×10^7 *vs.* 5×10^7 M^{-1} s^{-1}) which can be explained by the smaller triplet energy gap for the ZnTPPOH/TTBPper pair with respect to PtTPPOH/TTBPer.[49]

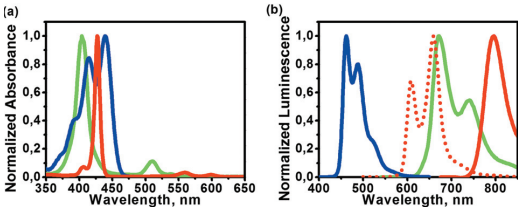

Fig. 1 (a) Normalized absorption and (b) phosphorescence spectra of PtTPPOH (green), ZnTPPOH (red), and TTBPer (blue) in optically dilute (OD ≈ 0.1) PEG–OA solutions. The dashed red line in (b) is the fluorescence spectrum of ZnTPPOH.

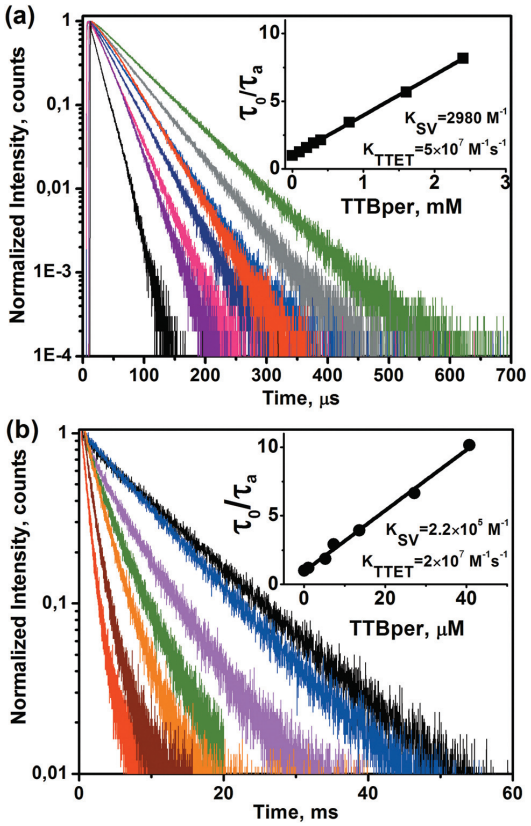

Fig. 2 Time-resolved phosphorescence decays of PtTPPOH (a) and ZnTPPOH (b) excited at 510 nm and 560 nm, respectively, with a Xe μF flash lamp at different TTBPer concentrations. Insets: Corresponding Stern–Volmer plots for the set of concentrations used, where τ_0 and τ_a are the sensitizer triplet lifetime in the absence and presence of particular annihilator concentration.

Based on the phosphorescence lifetime experiments, a TTBPer concentration of 3 mM was chosen for further studies. At this concentration, more than 90% TTET efficiency (Φ_{TTET}) was obtained for both sensitizers. All the solutions were adjusted to have optical densities of 1.0 at the excitation wavelength to utilize 90% of the laser power density. This corresponds to the PtTPPOH and ZnTPPOH concentrations of 100 μM and 294 μM, respectively, according to the molecular extinction coefficients (ε) of PtTPPOH (10^4 M^{-1} cm^{-1}) and ZnTPPOH (3.4×10^3 M^{-1} cm^{-1}) at 532 nm.

To our delight, selective excitation of porphyrins at 532 nm by using a second-harmonic Nd:YAG laser in the presence of TTBPer gave rise to an anti-Stokes blue emission at 460 nm (see the ESI†). The intensity of the upconverted light was measured as a function of laser power density resulting in quadratic-to-linear power dependence (Fig. 3), which corresponds to the annihilation

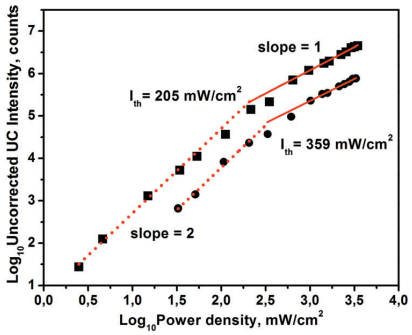

Fig. 3 Double logarithmic plot of the upconverted emission for PtTPPOH/TTBPer (squares) and ZnTPPOH/TTBPer (circles) as a function of power density.

nature of the blue fluorescence. At low power densities (slope = 2) non-radiative triplet decay contributes more to the kinetics of the process. Above the power threshold point (I_{th}) TTA starts to dominate, approaching a maximum for UC fluorescence (slope = 1).[50] The Φ_{UC} values of 29% and 24% for PtTPPOH/TTBPer and ZnTPPOH/TTBPer pairs, respectively, were calculated from the data. The difference in values is related to the difference in Φ_{ISC} for the corresponding porphyrins.[51]

As the Stern–Volmer constant for ZnTPPOH was so high, we were encouraged to investigate the effect of annihilator concentration on UC intensity at constant sensitizer concentration and high power density (3300 mW cm^{-2}). The triplet–triplet energy transfer efficiency (Φ_{TTET}) reached 91% already at 50 μM concentration of the annihilator, and this process has almost no effect on TTAUC efficiency (Φ_{UC}) at higher TTBPer concentrations. At low annihilator concentrations (below 0.1 mM), the observed quadratic dependence of UC intensity, and thus Φ_{UC}, indicates the prevalence of unimolecular and pseudo-first-order annihilator triplet deactivation pathways. However, this is not the case for annihilator concentrations higher than 100 μM. Linear dependence means that TTA is already a dominant mechanism of TTBPer triplet degeneration in the system. A further increase in the annihilator concentration resulted in a plateau thus Φ_{TTA} and consequently whole TTAUC (Φ_{UC}) reached their maximum (eqn (1)). In essence, 600 μM and 1.5 mM of TTBPer were enough to obtain Φ_{UC} of 24.5% and 26.4%, respectively (Fig. 4a).

It is worth mentioning that a higher TTBPer concentration (3 mM) resulted in lower Φ_{UC} (24%). This can be attributed to the fact that higher TTBPer concentration leads to a higher probability of excimer formation. Thus, the quantum yield of monomeric annihilator fluorescence (Φ_{fl}^{A}) decreases resulting in lower Φ_{UC}.[37]

Consequently, the TTAUC sensitization properties of ZnTPPOH have been compared with those of PtTPPOH. Since ε_{532} values of ZnTPPOH and PtTPPOH are substantially different resulting in prominent concentration inequality at identical optical density the annihilator/sensitizer ratio (An/Sen) has been employed to compare the obtained results. Fig. 4b clearly

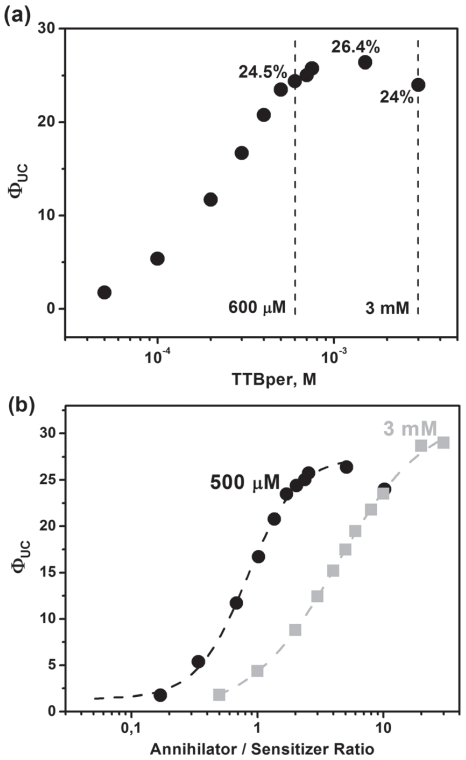

Fig. 4 (a) A plot of the TTAUC quantum yield with respect to the molar concentration of TTBPer used upon excitation of ZnTPPOH at 532 nm; (b) dependence of Φ_{UC} with respect to the An/Sen ratio upon excitation of ZnTPPOH (circles) and PtTPPOH (squares) at 532 nm.

demonstrates the benefits of ZnTPPOH utilization for TTAUC in the An/Sen range *i.e.* from 0.5 to 3. Indeed, when PtTPPOH was able to generate only 4.4% Φ_{UC} ZnTPPOH has already sensitized TTAUC with more than 16.5% quantum yield.

In summary, we report a ZnTPP-based photosensitizer possessing to our knowledge the longest triplet lifetime (11 ms) among the sensitizers used for TTAUC together with a high Φ_{ISC} of 0.75. In the case of ZnTPPOH, this allows us to perform TTET in a more efficient manner by using a lower amount of the annihilator in comparison with widely used expensive Pt(II) porphyrins. As a result, TTAUC with 24.5% Φ_{UC} has been obtained by using only 600 μM of TTBPer even in a viscous polymer matrix. This is in striking contrast to 3 mM annihilator concentration needed for PtTPPOH-sensitized photon upconversion with 29% TTAUC efficiency.

This demonstrates that looking for molecules with long-living triplet lifetimes and high Φ_{ISC} would be extremely important whenever efficient TTAUC is needed, especially in viscous media. Moreover, we stress that overly high annihilator concentrations are deleterious for TTAUC. Our results clearly prove that at lower TTBPer concentrations Φ_{UC} is higher to some extent. This finding can be useful in a variety of

applications, such as sensors, photocatalysis, photovoltaics, and phototriggered drug delivery systems, where the high loading of the molecules is difficult, but a high Φ_{UC} value is still desired.

This work was supported by The Academy of Finland (grant number 316893), fellowship programme of the Centre for International Mobility, (CIMO, decision TM-16-10063, Finland).

Conflicts of interest

There are no conflicts to declare.

References

1 C. A. Parker and C. G. Hatchard, *Proc. R. Soc. London, Ser. A*, 1962, **269**, 574–584.
2 C. A. Parker, *Proc. R. Soc. London, Ser. A*, 1963, **276**, 125–135.
3 C. A. Parker, C. G. Hatchard and T. A. Joyce, *Nature*, 1965, **205**, 1282–1284.
4 T. N. Singh-Rachford and F. N. Castellano, *Coord. Chem. Rev.*, 2010, **254**, 2560–2573.
5 T. F. Schulze and T. W. Schmidt, *Energy Environ. Sci.*, 2015, **8**, 103–125.
6 Y. Y. Cheng, A. Nattestad, T. F. Schulze, R. W. MacQueen, B. Fückel, K. Lips, G. G. Wallace, T. Khoury, M. J. Crossley and T. W. Schmidt, *Chem. Sci.*, 2016, **7**, 559–568.
7 A. Nattestad, Y. Y. Cheng, R. W. MacQueen, T. F. Schulze, F. W. Thompson, A. J. Mozer, B. Fückel, T. Khoury, M. J. Crossley, K. Lips, G. G. Wallace and T. W. Schmidt, *J. Phys. Chem. Lett.*, 2013, **4**, 2073–2078.
8 J.-H. Kim and J.-H. Kim, *J. Am. Chem. Soc.*, 2012, **134**, 17478–17481.
9 O. S. Kwon, H. S. Song, J. Conde, H. Kim, N. Artzi and J.-H. Kim, *ACS Nano*, 2016, **10**, 1512–1521.
10 C. Wohnhaas, V. Mailänder, M. Dröge, M. A. Filatov, D. Busko, Y. Avlasevich, S. Baluschev, T. Miteva, K. Landfester and A. Turshatov, *Macromol. Biosci.*, 2013, **13**, 1422–1430.
11 S. H. C. Askes, A. Bahreman and S. Bonnet, *Angew. Chem., Int. Ed.*, 2014, **53**, 1029–1033.
12 S. H. C. Askes, M. Kloz, G. Bruylants, J. T. M. Kennis and S. Bonnet, *Phys. Chem. Chem. Phys.*, 2015, **17**, 27380–27390.
13 Q. Liu, W. Wang, C. Zhan, T. Yang and D. S. Kohane, *Nano Lett.*, 2016, **16**, 4516–4520.
14 W. Wang, Q. Liu, C. Zhan, A. Barhoumi, T. Yang, R. G. Wylie, P. A. Armstrong and D. S. Kohane, *Nano Lett.*, 2015, **15**, 6332–6338.
15 V. Gray, K. Moth-Poulsen, B. Albinsson and M. Abrahamsson, *Coord. Chem. Rev.*, 2018, **362**, 54–71.
16 J. Zhao, S. Ji and H. Guo, *RSC Adv.*, 2011, **1**, 937–950.
17 W. Zhao and F. N. Castellano, *J. Phys. Chem. A*, 2006, **110**, 11440–11445.
18 C. Bohne, E. B. Abuin and J. C. Scaiano, *J. Am. Chem. Soc.*, 1990, **112**, 4226–4231.
19 S. H. C. Askes, P. Brodie, G. Bruylants and S. Bonnet, *J. Phys. Chem. B*, 2017, **121**, 780–786.
20 S. H. C. Askes, N. L. Mora, R. Harkes, R. I. Koning, B. Koster, T. Schmidt, A. Kros and S. Bonnet, *Chem. Commun.*, 2015, **51**, 9137–9140.
21 S. H. C. Askes, V. C. Leeuwenburgh, W. Pomp, H. Arjmandi-Tash, S. Tanase, T. Schmidt and S. Bonnet, *ACS Biomater. Sci. Eng.*, 2017, **3**, 322–334.
22 S. H. C. Askes, W. Pomp, S. L. Hopkins, A. Kros, S. Wu, T. Schmidt and S. Bonnet, *Small*, 2016, **12**, 5579–5590.
23 J. Peng, X. Jiang, X. Guo, D. Zhao and Y. Ma, *Chem. Commun.*, 2014, **50**, 7828–7830.
24 X. Jiang, X. Guo, J. Peng, D. Zhao and Y. Ma, *ACS Appl. Mater. Interfaces*, 2016, **8**, 11441–11449.
25 A. Harriman, *J. Chem. Soc., Faraday Trans. 1*, 1980, **76**, 1978–1985.
26 J. K. Hurley, N. Sinai and H. Linschitz, *Photochem. Photobiol.*, 1983, **38**, 9–14.
27 H. L. Kee, J. Bhaumik, J. R. Diers, P. Mroz, M. R. Hamblin, D. F. Bocian, J. S. Lindsey and D. Holten, *J. Photochem. Photobiol., A*, 2008, **200**, 346–355.
28 M. Anikin, N. V. Tkachenko and H. Lemmetyinen, *Langmuir*, 1997, **13**, 3002–3008.
29 E. Sariola-Leikas, M. Hietala, A. Veselov, O. Okhotnikov, S. L. Semjonov, N. V. Tkachenko, H. Lemmetyinen and A. Efimov, *J. Colloid Interface Sci.*, 2012, **369**, 58–70.
30 J. A. O'Brien, S. Rallabandi, U. Tripathy, M. F. Paige and R. P. Steer, *Chem. Phys. Lett.*, 2009, **475**, 220–222.
31 R. Rautela, N. K. Joshi, S. Novakovic, W. W. H. Wong, J. M. White, K. P. Ghiggino, M. F. Paige and R. P. Steer, *Phys. Chem. Chem. Phys.*, 2017, **19**, 23471–23482.
32 S. K. Sugunan, U. Tripathy, S. M. K. Brunet, M. F. Paige and R. P. Steer, *J. Phys. Chem. A*, 2009, **113**, 8548–8556.
33 X. Cui, J. Zhao, P. Yang and J. Sun, *Chem. Comm.*, 2013, **49**, 10221.
34 Y. V. Aulin, M. van Sebille, M. Moes and F. C. Grozema, *RSC Adv.*, 2015, **5**, 107896.
35 V. Gray, A. Dreos, P. Erhart, B. Albinsson, K. Moth-Poulsen and M. Abrahamsson, *Phys. Chem. Chem. Phys.*, 2017, **19**, 10931–10939.
36 T. Kobayashi, D. Huppert, K. D. Straub and P. M. Rentzepis, *J. Chem. Phys.*, 1979, **70**, 1720–1726.
37 S. Hoseinkhani, R. Tubino, F. Meinardi and A. Monguzzi, *Phys. Chem. Chem. Phys.*, 2015, **17**, 4020–4024.
38 R. R. Islangulov, D. V. Kozlov and F. N. Castellano, *Chem. Commun.*, 2005, 3776–3778.
39 T. N. Singh-Rachford, A. Nayak, M. L. Muro-Small, S. Goeb, M. J. Therien and F. N. Castellano, *J. Am. Chem. Soc.*, 2010, **132**, 14203–14211.
40 T. N. Singh-Rachford and F. N. Castellano, *J. Phys. Chem. A*, 2009, **113**, 5912–5917.
41 T. N. Singh-Rachford and F. N. Castellano, *J. Phys. Chem. A*, 2008, **112**, 3550–3556.
42 T. N. Singh-Rachford and F. N. Castellano, *J. Phys. Chem. Lett.*, 2010, **1**, 195–200.
43 T. N. Singh-rachford, A. Haefele, R. Ziessel and F. N. Castellano, *J. Am. Chem. Soc.*, 2008, **130**, 16164–16165.
44 F. Deng, W. Sun and F. N. Castellano, *Photochem. Photobiol. Sci.*, 2014, **13**, 813–819.
45 C. Mongin, J. H. Golden and F. N. Castellano, *ACS Appl. Mater. Interfaces*, 2016, **8**, 24038–24048.
46 D. Dzebo, K. Moth-Poulsen and B. Albinsson, *Photochem. Photobiol. Sci.*, 2017, **16**, 1327–1334.
47 M. A. Filatov, S. Baluschev and K. Landfester, *Chem. Soc. Rev.*, 2016, **45**, 4668–4689.
48 N. V. Nazarova, Y. S. Avlasevich, K. Landfester and S. Baluschev, *Dalton Trans.*, 2018, **47**, 8605–8610.
49 K. Sandros, *Acta Chem. Scand.*, 1964, **18**, 2355–2374.
50 A. Haefele, J. Blumhoff, R. S. Khnayzer and F. N. Castellano, *J. Phys. Chem. Lett.*, 2012, **3**, 299–303.
51 C. A. Parker and T. A. Joyce, *Trans. Faraday Soc.*, 1966, **62**, 2785–2792.

PUBLICATION II

Critical Sensitizer Quality Attributes for Efficient Triplet−Triplet Annihilation Upconversion with Low Power Density Thresholds

Durandin, N. A.; Isokuortti, J.; Efimov, A.; Vuorimaa-Laukkanen, E.; Tkachenko, N. V.; Laaksonen, T.

Journal of Physical Chemistry C, vol. 123, p. 22865, 2019
DOI: https://doi.org/10.1021/acs.jpcc.9b08026

THE JOURNAL OF PHYSICAL CHEMISTRY C

Article

Cite This: J. Phys. Chem. C 2019, 123, 22865−22872

pubs.acs.org/JPCC

Critical Sensitizer Quality Attributes for Efficient Triplet−Triplet Annihilation Upconversion with Low Power Density Thresholds

Nikita A. Durandin,* Jussi Isokuortti, Alexander Efimov, Elina Vuorimaa-Laukkanen, Nikolai V. Tkachenko, and Timo Laaksonen

Faculty of Engineering and Natural Sciences, Tampere University, Korkeakoulunkatu 8, 33720 Tampere, Finland

Supporting Information

ABSTRACT: Triplet−triplet annihilation upconversion (TTAUC) is a power density-dependent process where photons of low energy are transformed into high energy ones. The most important attributes of efficient TTAUC are quantum yield Φ_{TTAUC}, power density threshold I_{th} (photon flux at which 50% of Φ_{TTAUC} is achieved), and the upconversion shift of emitted photons (anti-Stokes shift). To date, approaches to balance these parameters have remained unclear. Herein, the cumulative effect of sensitizer triplet lifetime (τ_0^S), sensitizer-annihilator triplet energy gap (ΔE_T), and the total concentration of the sensitizer on the power density threshold at high TTAUC quantum yields is evaluated experimentally using Pt, Pd, and Zn tetraphenylporphyrin derivatives and a tetra-*tert*-butylperylene annihilator, and by kinetic rate modeling. The results suggest that a large energy gap ($\Delta E_T \geq 4\ k_BT$) and long sensitizer triplet lifetime make the triplet−triplet energy transfer (TTET) extremely efficient and allow the utilization of high sensitizer concentrations for low I_{th}. However, for large upconversion shifts, the triplet energy gap should be as small as possible. Smaller energy gap values result in slower forward TTET and faster reverse TTET, which together with high total sensitizer concentration can lead to a quenching of annihilator's triplet state and therefore elevate the I_{th}. In this regard, low concentration of a sensitizer is beneficial, making sensitizers with high molar extinction coefficients preferential. Sensitizers with a long living triplet state and a high molar extinction coefficient can work efficiently and have low I_{th} at 0 k_BT or even negative ΔE_T. Kinetic rate modeling further helps to optimize the parameters for best possible TTAUC performance. Thus, the findings of the study pave the way for the design of TTAUC systems with superior performance, such as high Φ_{TTAUC} at low excitation power densities with large anti-Stokes shift, for, for example, solar-driven photovoltaics, photocatalysis, bioimaging, and safe light-triggered drug-delivery systems.

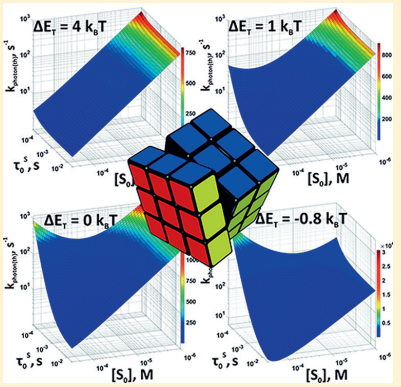

INTRODUCTION

Photon upconversion based on triplet−triplet annihilation represents an attractive approach to turn the photons of higher wavelengths into lower ones by using noncoherent excitation sources.[1−3] Nowadays, the method draws a lot of attention because of its broad applicability, spanning from organic electronics to bionanotechnology.[4−8] The process relies on an interplay between two pairs of photoactive molecules, namely a sensitizer and an annihilator. After the photoexcitation of a sensitizer with photons of low energy, through the processes of triplet−triplet energy transfer (TTET) and triplet−triplet annihilation (TTA), the two annihilator triplet state molecules collide to generate one annihilator singlet state of high energy, which emits the upconverted photon (Scheme 1).[9] Altogether, the TTAUC quantum yield (Φ_{TTAUC}) is a product of five parameters:[9]

$$\Phi_{TTAUC} = \frac{1}{2} \times f \times \Phi_{ISC} \times \Phi_{TTET} \times \Phi_{TTA} \times \Phi_{fl}^{A} \quad (1)$$

where f is the statistical probability to obtain a singlet excited state after TTA, Φ_{ISC} is the intersystem crossing efficiency of a sensitizer, Φ_{TTET} and Φ_{TTA} are TTET and TTA efficiencies, and Φ_A^{fl} is the fluorescence quantum yield of an annihilator.

As is clear from Scheme 1, the TTA efficiency (Φ_{TTA}) relies on the concentration of the generated annihilator triplet state, which makes TTAUC quantum yield (Φ_{TTAUC}) dependent on the power density of the excitation source.[10−12] Recently, the power density threshold (I_{th}), that is, the power density value at which Φ_{TTA} and therefore Φ_{TTAUC} equals to 50% of its maximum for the system under study, has been proposed as a TTAUC figure-of-merit.[13−15] Together with Φ_{TTAUC}, I_{th} value is one of the crucial criteria for the selection of TTAUC sensitizer/annihilator pairs. Indeed, TTAUC systems with high Φ_{TTAUC} that can be obtained at low excitation power densities are of paramount importance, for example, for the next generation of organic electronics and prospective biomedical

Received: August 22, 2019
Published: August 26, 2019

DOI: 10.1021/acs.jpcc.9b08026
J. Phys. Chem. C 2019, 123, 22865−22872

Scheme 1. Jablonski Diagram of the Triplet−Triplet Annihilation Upconversion Process[a]

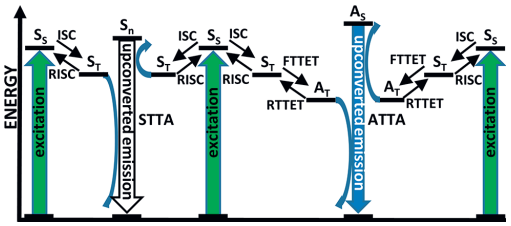

[a]Where S_S and S_n are first and n (either first or second) sensitizer singlet states, A_S is annihilator singlet state, ISC and RISC are intersystem crossing and reverse intersystem crossing processes, S_T is sensitizer triplet state, STTA and ATTA are sensitizer and annihilator triplet−triplet annihilation, and RTTET and FTTET are forward and reverse triplet−triplet energy transfers.

applications. While the way to control Φ_{TTAUC} seems to be straightforward, the methods to fine-tune the excitation power density threshold remain limited.[14−16] This lack of proper methodology strongly hampers the development of TTAUC-based photon management approach toward high performance devices, for example, solar cells.[4]

The expression for I_{th} value was proposed by Monguzzi et al:[15]

$$I_{th} = 2\frac{(k_p)^2}{k_{TTA} \times \alpha(\varepsilon) \times \Phi_{TTET}} \quad (2)$$

where $k_P = 1/\tau_0^A$ and represents the rate constant of all annihilator unimolecular and pseudo-first-order processes such as phosphorescence and quenching with, for example, oxygen (τ_0^A is phosphorescence lifetime of an annihilator), $\alpha(\varepsilon)$ is a sensitizer absorption coefficient, and k_{TTA} is second-order TTA rate constant.

On the basis of eq 2, one can easily modulate I_{th} values by using long-living annihilators. However, only a few annihilators have both high fluorescence quantum yield (Φ_A^{fl}) and high singlet state formation probability via TTA (parameter f in eq 1) that are critical for high Φ_{TTAUC} values.[17−19]

In this respect, the sensitizer choice allows a higher degree of freedom. Up to now, a large variety of sensitizers has been used for TTAUC studies starting from heavy-atom-free molecules toward metalated porphyrinoids and even semiconductor nanocrystals.[20−24] Therefore, we are striving to understand the pathways toward efficient TTAUC in terms of power density threshold through the prism of sensitizer properties.

RESULTS AND DISCUSSION

Sensitizers and Annihilators under Study. A set of metal complexes of 2-{3-[10,15,20-tris(3,5-di*tert*-butylphenyl)-porphyrin-5-yl]phenoxy}ethanol with Pt, Pd or Zn (i.e., PtTPPOH, PdTPPOH, ZnTPPOH) was used as sensitizers (Scheme 2). The substances possess drastically different physicochemical characteristics such as triplet lifetime (τ_0^S), triplet energy level (E_T^S), Φ_{ISC}, and molar extinction coefficient at excitation wavelength of 532 nm (ε_{532}). The last one is responsible for the different sensitizer concentrations [S_0] for ensuring identical absorption coefficient $\alpha(\varepsilon)$ and laser power utilization for all three sensitizers.[14,15] Therefore, the choice of porphyrins allowed us to follow the effect of sensitizer triplet

Scheme 2. Molecular Structures of PtTPPOH, PdTPPOH, and ZnTPPOH and TBPer[a]

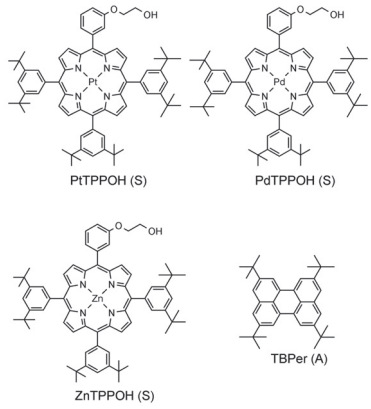

[a]S is sensitizer, and A is annihilator.

lifetimes and energy levels and molar extinction coefficient together with total concentration of the sensitizer on I_{th} and Φ_{TTAUC}.

2,5,8,11-Tetra-*tert*-butylperylene (TBPer) was selected as the annihilator because of perylene's long triplet lifetime, high fluorescence quantum yield, and moderately high triplet state energy (4 ms, 96%, and ∼1.54 eV, respectively). Moreover, the singlet state formation probability via TTA (parameter f) for perylene is approaching unity, while the *tert*-butyl substituents prevent an aggregation making TBPer one of the first-in-class annihilators.[17]

Degassed poly(ethylene glycol)-200 matrix with 30 mM oleic acid (PEG-OA) was employed as the media for experiments. The degassed PEG protects the sensitizer/annihilator system from back oxygen diffusion and allows a moderate degree of mobility for triplet−triplet interactions (TTET and TTA), while OA represents a powerful scavenger for the residual trace oxygen.[19,25]

TTET and TTA Photophysics. To prove the ability of the sensitizers under study to serve as triplet energy donors, time-resolved phosphorescence quenching experiments with TBPer were performed. Efficient TTET occurred and Stern−Volmer constants (K_{SV}) and forward TTET rates (k_{FTTET}) were calculated (see ESI). K_{SV} values were in agreement with the triplet lifetimes of the sensitizers. Short living PtTPPOH showed a Stern−Volmer constant of ∼3×10^3 M^{-1}, while the longer living sensitizers PdTPPOH and ZnTPPOH revealed higher values of 100×10^3 and 220×10^3 M^{-1}, respectively. On the other hand, PtTPPOH and PdTPPOH demonstrated higher forward k_{FTTET} rate constants than did ZnTPPOH (5×10^7 and 6.4×10^7 M^{-1} s^{-1} vs 2.2×10^7 M^{-1} s^{-1}). This fact can be explained in terms of triplet energy gap values for the sensitizer/annihilator pairs (ΔE_T) (Figure 1). Indeed, forward and reverse TTET rate constants (k_{FTTET} and k_{RTTET}) are dependent on the energy gap value through Boltzmann equation:[26]

$$k_{FTTET} = k_D \times \frac{1}{1 + e^{(-\Delta E_T/k_B T)}} \quad (3)$$

DOI: 10.1021/acs.jpcc.9b08026
J. Phys. Chem. C 2019, 123, 22865−22872

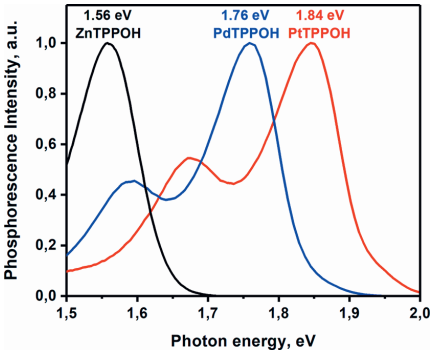

Figure 1. Normalized phosphorescence spectra of PtTPPOH (red), PdTPPOH (blue), and ZnTPPOH (black) in optically dilute (OD_{532} ≈ 0.1) PEG-OA solutions upon excitation at 509, 515, and 560 nm, respectively.

$$k_{RTTET}/k_{FTTET} = e^{(-\Delta E_T/k_B T)} \quad (4)$$

where ΔE_T is sensitizer/annihilator triplet energy gap, k_B is Boltzmann constant, T is the absolute temperature, and k_D is the diffusion constant of a medium. Therefore, higher energy gap makes the forward (FTTET) step enthalpy-driven and diffusion-controlled, hence facilitating the population of annihilator triplet state.

Power density dependences of upconverted light were measured for every sensitizer/annihilator pair. Nd:YAG continuous wave laser emitting at 532 nm was employed to selectively excite the porphyrins. Concentrations of the sensitizers were adjusted to have OD = 1 at the excitation wavelength to utilize 90% of input power density. The annihilator TBPer was used at a fixed 3 mM concentration to obtain at least 90% Φ_{TTET} for all TTAUC pairs. Quantum yields of TTAUC for all of the pairs were calculated by using Rhodamine 6G in ethanol as a reference.[25] Figure 2a clearly shows the strong and weak annihilation regimes, which is an integral feature of TTAUC process described by the equations:[10,12]

$$f_{TTA} = \frac{k_{TTA}[A_T^*]}{k_p + k_{TTA}[A_T^*]} \quad (5)$$

$$\Phi_{TTA} = 1 - \frac{f_{TTA} - 1}{f_{TTA}} \ln(1 - f_{TTA}) \quad (6)$$

where f_{TTA} is the fraction of triplets decaying via TTA deactivation pathway.

It also should be noted that by solving eqs 5 and 6 in terms of power density (which affects the $[A_T^*]$ parameter), one can find the value at which the yield of triplet−triplet annihilation Φ_{TTA} reaches 0.5 of its maximum (see ESI) resulting in the refinement of eq 2:

$$I_{th} = 2.513\frac{(k_p)^2}{k_{TTA} \times \alpha(\varepsilon) \times \Phi_{TTET}} \quad (7)$$

Moreover, if we describe the system with Φ_{TTA} close to its maximum (0.9), the scaling coefficient in eq 7 rises from 2.513 to as high as 36. These values were used to validate the data presented on Figure 2b. The estimated 50% and 90% threshold

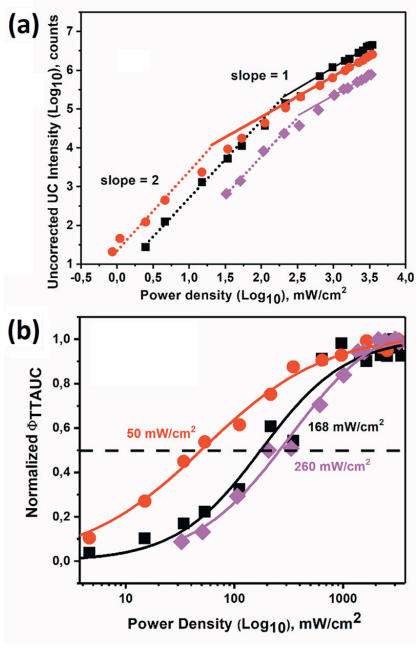

Figure 2. Plot of (a) upconverted fluorescence intensity and (b) normalized Φ_{TTAUC} dependence as a function of the applied power density for 52 μM PdTPPOH/TBPer (red circles); 100 μM PtTPPOH/TBPer (black squares); 294 μM ZnTPPOH/TBPer (magenta diamonds).

values from eq 7 agreed with the experimental results. It is good to remember that as both k_p and k_{TTA} are intrinsic annihilator properties, there is no need to consider these when comparing power thresholds for different sensitizers with slow k_{RTTET} (large ΔE_T).

The upconversion yields and power density thresholds are collected in Table 1. The Φ_{TTAUC} values of 29%, 31%, and 24% for PtTPPOH, PdTPPOH, and ZnTPPOH, respectively, are in good agreement with Φ_{ISC} and Φ_{TTET} efficiencies for these porphyrins. It is noteworthy that the obtained power density thresholds for the three porphyrin/annihilator pairs were obviously different (Figure 2, Table 1), which is not evident from eq 7. According to eq 7, the pair with lowest Φ_{TTET} should have had the highest I_{th}. In striking contrast, the pair with the longest living triplet state sensitizer and more than 0.99 Φ_{TTET}, namely ZnTPPOH/TBPer, shows the highest I_{th} value (258 mW/cm^2), while PtTPPOH and PdTPPOH sensitized upconversion systems revealed lower power density threshold values, that is, 168 and 50 mW/cm^2. According to the equations, there should have been only a slight difference in I_{th} for all of the sensitizer/annihilator pairs since Φ_{TTET} are close for all pairs studied.[15]

One of the reasons for this discrepancy is the large difference in the sensitizer concentrations $[S_0]$ because of different ε_{532} of the porphyrins used in our study. Recently, Schmidt et al. have stressed that a too high sensitizer concentration can be detrimental for the upconversion efficiency regardless of improved power density utilization. At constant power density, the Φ_{TTA} dependence on the sensitizer concentration appeared

DOI: 10.1021/acs.jpcc.9b08026
J. Phys. Chem. C 2019, 123, 22865−22872

Table 1. Characteristics of 2,5,8,11-Tetra-tert-butylperylene TTAUC Sensitized by Different Porphyrins

sensitizer	Φ_{ISC}	τ_0^S, ms	ε_{532}, M^{-1} cm^{-1}	$[S_0]$, μM	E_T^S, eV	ΔE_T, eV (k_BT)[a]	k_{FTTET}, M^{-1} s^{-1}	Φ_{TTET}[b]	Φ_{TTAUC}, %[b]	I_{th}, mW/cm^2[b]
PtTPPOH	1	0.061	10^4	100	1.84	0.3 (11.67)	5×10^7	0.9	29	168
PdTPPOH	1	0.75	1.9×10^4	52	1.76	0.22 (8.56)	6.4×10^7	0.993	31	50
ZnTPPOH	0.75	11.0	3.4×10^3	294	1.56	0.02 (0.78)	2.2×10^7	0.9986	24	260

[a]Triplet energy level of 1.54 eV was utilized for TBPer to calculate the triplet energy gap. [b]3 mM TBPer concentration was used to obtain the data.

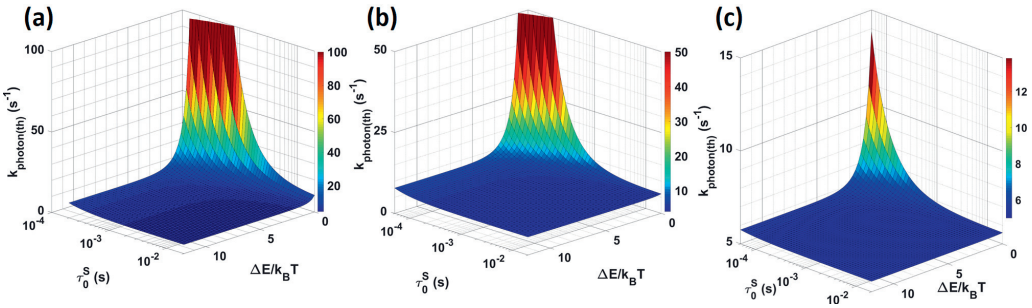

Figure 3. Photon rate thresholds ($k_{photon(th)}$) simulated over several orders of magnitude of τ_0^S and ΔE_T and with (a) $[A_0]$ = 0.5 mM, (b) $[A_0]$ = 3 mM, (c) $[A_0]$ = 30 mM while maintaining a constant sensitizer concentration of $[S_0]$ = 100 μM.

to be parabolic.[27] On the basis of that observation, one may expect that Φ_{TTA} maximum for the systems with excessive sensitizer concentration will be reached at higher I_{th} values,[28] as follows from the eqs 5, 6, and 7.[10,12,27]

In addition, triplet energy gap (ΔE_T) is not identical for the porphyrin/TBPer pairs, resulting in different FTTET and RTTET rate constants (eqs 3 and 4). Together with an excess of sensitizer $[S_0]$, the fast reverse energy transfer can lower the annihilator triplet state concentration, thus suppressing the annihilator TTA process. In good agreement with this, for the ZnTPPOH/TBPer pair, which had the highest sensitizer concentration and smallest triplet energy gap, the I_{th} value is highest in the set. It is therefore clear that reverse TTET must be considered and more detailed description for the I_{th} is needed than the one given by eq 7. Especially considering that low ΔE_T could lead to higher upconversion shifts, which is one of the most desirable properties for TTAUC.

Kinetic Rate Modeling. To shed light on the obtained parameters, we have performed full TTAUC kinetic rate modeling taking into account the processes depicted on the Scheme 1 while varying the sensitizer properties (for details see ESI, page 14). Herein, we have utilized the approach proposed by Schmidt et al.,[16] taking also into account reverse TTET rate constant and sensitizer concentration $[S_0]$. Equilibrium conditions have been applied to solve the set of equations:

$$\frac{dS_3^*}{dt} = -\frac{dS_1^*}{dt} = k_{photon}[S_0]\Phi_{ISC} - k_{nr}[S_T^*] - k_{FTTET}[S_T^*][A_0] + k_{RTTET}[A_T^*][S_0] - k_{TTA}(2[S_T^*]^2 + [S_T^*][A_T^*]) = 0 \quad (8)$$

$$\frac{dA_3^*}{dt} = -\frac{dA_1^*}{dt} = k_{FTTET}[S_T^*][A_0] - k_p[A_T^*] - k_{RTTET}[A_T^*][S_0] - k_{TTA}([A_T^*]^2 + [S_T^*][A_T^*]) = 0 \quad (9)$$

$$\Phi_{TTAUC} = 2\frac{k_{TTA}[A_T^*]^2}{k_{photon}[S_0]} \times \Phi_{fl}^A \quad (10)$$

where $k_{nr} = 1/\tau_0^S$ is the sensitizer's triplet first-order decay constant, $[S_0]$ = total annihilator concentration, $[S^*_T]$ = sensitizer triplet state concentration, $[A_0]$ = total annihilator concentration, $[A^*_S]$ = annihilator singlet state concentration, $[A^*_T]$ = annihilator triplet state concentration, $k_{photon} = \varphi \times \varepsilon'$ is the photon absorption rate (in s^{-1}) in which φ is photon flux (in moles of photons dm^{-2} s^{-1}) and ε' = ln 10 × ε (in M^{-1} dm^{-1}).

For the modeling, the excitation light power was expressed in photon absorption rate (in s^{-1}). The photon absorption rate was recalculated into power density (mW/cm^2) or *vice versa* to compare the results of the modeling with the experimental data. TBPer triplet decay rate constant (k_p) of 250 s^{-1} was utilized based on the literature data,[29] diffusion constant = 5 × 10^7 s^{-1}, Φ_{ISC} = 1, and the triplet−triplet annihilation rate constant (k_{TTA}) of 2.5 × 10^7 s^{-1} (0.5 × k_D) was employed for TTAUC simulations. Maximum Φ_{TTAUC} value of 32% was set to make calculations consistent with performed spectroscopy experiments. Further, photon rate threshold ($k_{photon(th)}$) was calculated as a photon absorption rate resulting in 16% upconversion quantum yield, that is, 50% of Φ_{TTAUC} maximum.

Effect of Sensitizer Lifetime and *S/A* Triplet Energy Gap on TTAUC Photon Rate Threshold. First, the additive effect of sensitizer triplet lifetime (τ_0^S) and *S/A* triplet energy gap (ΔE_T) were examined to address the issue of photon absorption rate threshold. Sensitizer lifetime was varied from 50 μs to 20 ms and ΔE_T values from 12 to 0 k_BT (Figure 3). Other parameters were kept constant.

In essence, sensitizers with triplet lifetimes shorter than 100 μs limit the possibility to use the TTAUC pairs with small ΔE_T (below 3 k_BT) to achieve low $k_{photon(th)}$. On the contrary, a long triplet lifetime of the sensitizer (>5 ms) is extremely beneficial for TTAUC process regardless of ΔE_T values in the simulated conditions, that is, 3 mM TBPer concentration and $[S_0]$ = 100

DOI: 10.1021/acs.jpcc.9b08026
J. Phys. Chem. C 2019, 123, 22865−22872

μM (Figure 3b). Notably, sensitizers with triplet lifetimes longer than 1 ms allow an efficient TTET even with lower amount of annihilator (e.g., 500 μM) while keeping $k_{photon(th)}$ values in the minimum (Figure 3a).

Low annihilator concentrations make TTAUC pairs more sensitive to lower triplet energy gap values (below 2 k_BT, or 0.0514 eV). At small ΔE_T, the reverse TTET process is not negligible. Excessive concentration of the sensitizer in the ground state can react with the triplet state of the annihilator, thus competing with annihilator's TTA. At the same time, the sensitizer triplet−triplet annihilation competes with the forward TTET from sensitizer to the ground state annihilator resulting in a lower concentration of annihilator triplet state and high photon rate thresholds.[30,31]

However, a great excess of the annihilator with respect to the sensitizer, for example, from 3 to 30 mM, makes FTTET more feasible even for the sensitizers with short living triplet states and small ΔE_T, hence suppressing RTTET and resulting in lower $k_{photon(th)}$ values (Figure 3b,c). On the other hand, high $[A_0]$ leads to higher excimer state formation probability, which decreases Φ_A^{fl} and makes TTAUC less efficient (eq 1). Furthermore, solubility issues with high amounts of annihilator may come into play, especially in polymers and nanocarriers.[7,32]

It is further clear from Figure 3 that with high ΔE_T values ($\Delta E_T \geq 4\ k_BT$) and τ_0^s above 200 μs, there are no additional benefits from even longer sensitizer triplet lifetimes.

Effect of Sensitizer Concentration and Lifetime on TTAUC Photon Rate Threshold. An increase in sensitizer concentration $[S_0]$ can improve the photon absorption rate threshold (eq 7) while keeping Φ_{TTAUC} as high as possible. Indeed, a simultaneous increase in both $[S_0]$ and τ_0^s should result in a dramatic increase in the sensitizer triplet state concentration. As a consequence, a decrease in $k_{photon(th)}$ values can be achieved. Keeping this consideration in mind, the response of TTAUC photon rate threshold to the changes in τ_0^S and $[S_0]$ was simulated while keeping ΔE_T fixed.

Figure 4a shows the dynamics of $k_{photon(th)}$ with respect to sensitizer triplet lifetime and total sensitizer concentration at $\Delta E_T = 4\ k_BT$. There is a slight improvement in photon rate threshold (≈ 7.5 vs 5 s^{-1}) upon changing the sensitizer triplet lifetime from 50 μs to 20 ms at $[S_0]$ = 100 μM. However, three-fold increase in $[S_0]$ results in substantial decrease of the photon rate threshold for both τ_0^s values (≈ 3.36 and 1.86 s^{-1}). This offers a way to further improve $k_{photon(th)}$. The same tendency occurs for simulations where $\Delta E_T = 10\ k_BT$ and 7 k_BT were used (ESI). Albeit, the change in photon rate threshold with τ_0^S becomes negligible for all three ΔE_T values when the sensitizer lifetime exceeds 200 μs.

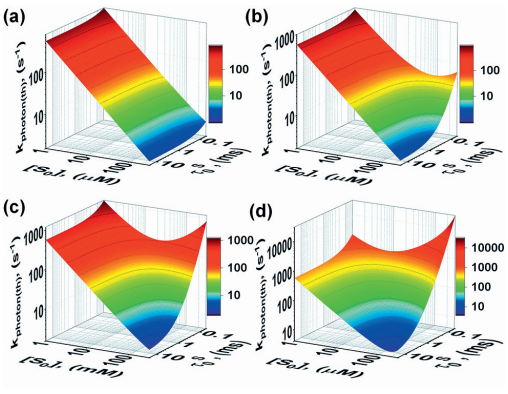

Figure 4. TTAUC photon rate threshold value as a function of sensitizer triplet state lifetime and sensitizer total concentration while keeping $[A_0]$ = 3 mM and (a) $\Delta E_T = 4\ k_BT$, (b) $\Delta E_T = 1\ k_BT$, (c) $\Delta E_T = 0$, (d) $\Delta E_T = -0.8\ k_BT$.

High triplet energy gaps $\Delta E_T > 4\ k_BT$ considerably limit the upconversion shift of emitted photons. Thus, a situation where ΔE_T is close to 0 k_BT is of a special interest. Notably, in this case, the reverse TTET effect may not be neglected *a priori* and must be always taken into account together with the sensitizer total concentration. Hence, a precise analysis of the photon rate threshold behavior with respect to the variations in the sensitizer triplet state lifetime and its total concentration was performed at energy gaps of 1, 0, and −0.8 k_BT (Figure 4b−d).

Our modeling revealed that the $k_{photon(th)}$ dependence on $[S_0]$ and sensitizer lifetime is a parabolic surface with a distinct minimum.[27] The minimum $k_{photon(th)}$ value depends strongly on the sensitizer triplet lifetime resulting in lower photon rate threshold for longer living sensitizers. This is particularly true in the case of a large sensitizer concentration. The $k_{photon(th)}$ initially decreases as sensitizer concentration and triplet lifetime increase due to generation of higher sensitizer triplet state concentrations and hence increased annihilator triplet state concentration through FTTET. However, after reaching a minimum for $k_{photon(th)}$ with respect to the sensitizer concentration, a further increase in $[S_0]$ affects the $k_{photon(th)}$ values negatively. Overly high sensitizer concentrations quench the annihilator triplet states through reverse TTET process, thus increasing the apparent k_p rate constant, which is crucial for low power density threshold (eq 7).

The effect of reverse TTET becomes more pronounced for smaller triplet state energy gaps. For example, in the case of the sensitizer with 100 μs triplet lifetime at $\Delta E_T = 1\ k_BT$, the photon rate threshold of 17 s^{-1} was reached at 167 μM sensitizer concentration. Meanwhile for $\Delta E_T = 0$ and $\Delta E_T = -0.8\ k_BT$, the minimum $k_{photon(th)}$ value was 72 s^{-1} and 295 s^{-1} at $[S_0]$ of 41 μM and 13 μM, respectively. The $k_{photon(th)}$ values are higher and cannot be made smaller with larger sensitizer concentrations. This is in striking contrast with the scenario when a sensitizer with long living triplet state was simulated. The photon rate threshold dramatically improved with respect to the values obtained for short living sensitizers. Moreover, long living sensitizers allowed the utilization of higher total sensitizer concentration without a negative effect on the photon rate threshold. It is important to emphasize that sensitizers with long living triplet lifetimes and negative ΔE_T values can work even better than a short living sensitizer with positive energy gaps. For long living sensitizers, the low photon rate thresholds can be reached at low $[S_0]$ concentrations even at negative triplet energy gaps. A precise analysis of the kinetic parameters for the sensitizer/annihilator pairs with ΔE_T close to 0 k_BT can be used to design functional and efficient TTAUC systems.

Further, we analyzed and compared the results of our simulations with our experimental data. First, we focused on the sensitizer/annihilator pair with the most unexpected result, namely ZnTPPOH/TBPer. Simulations performed at $\Delta E_T = 1\ k_BT$ and $\Delta E_T = 0$ for a molecule with ZnTPPOH properties in

DOI: 10.1021/acs.jpcc.9b08026
J. Phys. Chem. C 2019, 123, 22865−22872

the presence of 3 mM of the annihilator showed $k_{photon(th)}$ values of 2 s^{-1} and 2.5 s^{-1} that corresponded to 58 and 73 mW/cm^2, respectively (Figure 4b,c). These values disagree with the value of 260 mW/cm^2 obtained for ZnTPPOH experimentally. Even at $\Delta E_T = -0.5\ k_BT$, the simulated I_{th} for ZnTPPOH is 112 mW/cm^2 (ESI). Only an energy gap of $-0.8\ k_BT$ (-0.02 eV) gives good agreement between the modeling and the experimental value. Taking this energy gap into account together with the 1.56 eV ZnTPPOH triplet state energy obtained from phosphorescence studies, TBPer triplet state energy of ≥1.58 eV was elucidated in PEG-OA mixture. This value is consistent with results of Northrop et al. and Hall et al. where 1.57 eV triplet energy for perylene was calculated.[33,34] It also proves that efficient TTAUC process with high quantum yield is possible at negative ΔE_T, even though careful kinetic analysis is needed to ensure lowest I_{th} values by adjusting the concentrations.[35,36] By using 1.58 eV TBPer triplet energy level, the energy gaps ΔE_T for PtTPPOH/TBPer and PdTPPOH/TBPer were calculated to be 10 k_BT and 7 k_BT, respectively. The experimentally determined porphyrin/TBPer energy gaps were used to simulate the threshold I_{th}. The values of 70 mW/cm^2, 56 mW/cm^2, and 255 mW/cm^2 were obtained for PtTPPOH, PdTPPOH, and ZnTPPOH, respectively, which are in agreement with the experimental data (Table 1).

To prove the fact that reverse TTET is responsible for the high I_{th} value for ZnTPPOH/TBPer as predicted by our modeling, we have performed the power density dependence experiment with three-times lower ZnTPPOH concentration (OD_{532} = 0.34) keeping 3 mM TBPer concentration. In the absence of reverse TTET, one may expect a rise in I_{th} value due to much lower optical density at the excitation wavelength and hence lower absorption coefficient $\alpha(\varepsilon)$ according to eq 7. Remarkably, for lower ZnTPPOH concentration, we obtained lower I_{th} value (Figure 5), which is already comparable with I_{th}

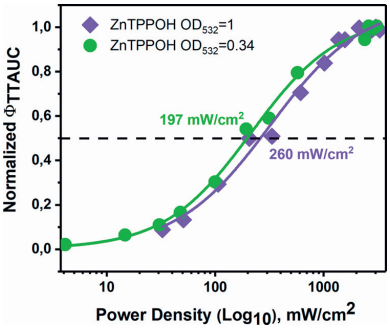

Figure 5. Plot of normalized Φ_{TTAUC} dependence as a function of the applied power density for 294 μM ZnTPPOH/3 mM TBPer (magenta diamonds) and 100 μM ZnTPPOH/3 mM TBPer (green circles).

of PtTPPOH/TBPer pair with large ΔE_T. This photon rate threshold behavior of ZnTPPOH/TBper is in agreement with the results obtained by using kinetic rate modeling (Figure 4c).

Indeed, high sensitizer triplet state concentration promotes the population of annihilator triplet state through FTTET. On the other hand, in the case of ZnTPPOH/TBPer pair, the reverse TTET is enthalpy-driven, and hence, higher annihilator triplet state concentration makes RTTET more favorable. This leads to even faster consumption of annihilator triplets.[35] Consequently, the sensitizer triplet states recover and annihilate with each other with no desired upconverted light generation (Scheme 1).[30,31] Altogether, this requires higher I_{th} values to reach high Φ_{TTAUC} yields.

CONCLUSIONS

Triplet−triplet annihilation upconversion systems with large anti-Stokes shift, high Φ_{TTAUC}, and low power density thresholds are highly desired. In excellent agreement with previous studies, our results indicate that high energy gap between a sensitizer and an annihilator triplet states (more than 4 k_BT) makes forward TTET process enthalpy-driven and diffusion-controlled. This combined with high Φ_{ISC}, long triplet lifetime, and high molecular extinction coefficient of a sensitizer at the excitation wavelength leads to high TTAUC yields and extremely low I_{th} values without any negative effects of high sensitizer concentrations.

However, large anti-Stokes shift is almost impossible for sensitizer/annihilator pairs with high ΔE_T. Even though there are sensitizers with thermally activated delayed fluorescence and strong singlet-to-triplet absorption bands that could solve this issue, their implementation in TTAUC is still limited due to the reverse ISC process.[37−39] Thus, S/A pairs with low ΔE_T must be used to increase the upconversion shifts. In this case, reverse TTET can be controlled via total sensitizer concentration in the system. This is of vital importance for systems utilizing low viscosity medium and annihilators with long living triplet lifetimes, which are more sensitive to a reverse TTET process (see ESI). Hence, preference should be given to the sensitizers with higher molar extinction coefficients and longer triplet lifetimes to neglect the effect of reverse TTET on I_{th}. Moreover, sensitizers with long living triplet states are capable of performing efficient upconversion even at negative triplet energy gaps. Finally, kinetic rate modeling is a powerful tool in the optimization of power density thresholds and upconversion quantum yields by manipulating the concentrations of sensitizer and annihilator.

ASSOCIATED CONTENT

Supporting Information

The Supporting Information is available free of charge on the ACS Publications website at DOI: 10.1021/acs.jpcc.9b08026.

Synthetic procedures and compounds characterization, details of photophysical measurements and calculations (PDF)

AUTHOR INFORMATION

Corresponding Author

*E-mail: nikita.durandin@tuni.fi.

ORCID

Alexander Efimov: 0000-0003-4671-3009
Elina Vuorimaa-Laukkanen: 0000-0002-3610-785X
Nikolai V. Tkachenko: 0000-0002-8504-2335

Notes

The authors declare no competing financial interest.

ACKNOWLEDGMENTS

This work was supported by The Academy of Finland (Grant No. 316893), fellowship programme of the Centre for

DOI: 10.1021/acs.jpcc.9b08026
J. Phys. Chem. C 2019, 123, 22865−22872

International Mobility (CIMO, decision TM-16-10063, Finland).

REFERENCES

(1) Parker, C. A.; Hatchard, C. G. Delayed Fluorescence from Solutions of Anthracene and Phenanthrene. *Proc. R. Soc. A Math. Phys. Eng. Sci.* **1962**, *269*, 574−584.

(2) Parker, C. A. Sensitized P-Type Delayed Fluorescence. *Proc. R. Soc. A Math. Phys. Eng. Sci.* **1963**, *276*, 125−135.

(3) Parker, C. A.; Hatchard, C. G.; Joyce, T. A. Selective and Mutual Sensitization of Delayed Fluorescence. *Nature* **1965**, *205*, 1282−1284.

(4) Schulze, T. F.; Schmidt, T. W. Photochemical Upconversion: Present Status and Prospects for Its Application to Solar Energy Conversion. *Energy Environ. Sci.* **2015**, *8*, 103−125.

(5) Li, C.; Koenigsmann, C.; Deng, F.; Hagstrom, A.; Schmuttenmaer, C. A.; Kim, J.-H. Photocurrent Enhancement from Solid-State Triplet−Triplet Annihilation Upconversion of Low-Intensity. *ACS Photonics* **2016**, *3*, 784−790.

(6) Kim, J.-H.; Kim, J.-H. Encapsulated Triplet−Triplet Annihilation-Based Upconversion in the Aqueous Phase for Sub-Band-Gap Semiconductor Photocatalysis. *J. Am. Chem. Soc.* **2012**, *134*, 17478−17481.

(7) Askes, S. H. C.; Bahreman, A.; Bonnet, S. Activation of a Photodissociative Ruthenium Complex by Triplet-Triplet Annihilation Upconversion in Liposomes. *Angew. Chem., Int. Ed.* **2014**, *53*, 1029−1033.

(8) Borisov, S. M.; Larndorfer, C.; Klimant, I. Triplet-Triplet Annihilation-Based Anti-Stokes Oxygen Sensing Materials with a Very Broad Dynamic Range. *Adv. Funct. Mater.* **2012**, *22*, 4360−4368.

(9) Singh-Rachford, T. N.; Castellano, F. N. Photon Upconversion Based on Sensitized Triplet-Triplet Annihilation. *Coord. Chem. Rev.* **2010**, *254*, 2560−2573.

(10) Bachilo, S. M.; Weisman, R. B. Determination of Triplet Quantum Yields from Triplet−Triplet Annihilation Fluorescence. *J. Phys. Chem. A* **2000**, *104*, 7711−7714.

(11) Schmidt, T. W.; Castellano, F. N. Photochemical Upconversion: The Primacy of Kinetics. *J. Phys. Chem. Lett.* **2014**, *5*, 4062−4072.

(12) Cheng, Y. Y.; Fückel, B.; Khoury, T.; Clady, R. G. C. R.; Tayebjee, M. J. Y.; Ekins-Daukes, N. J.; Crossley, M. J.; Schmidt, T. W. Kinetic Analysis of Photochemical Upconversion by Triplet-Triplet Annihilation: Beyond Any Spin Statistical Limit. *J. Phys. Chem. Lett.* **2010**, *1*, 1795−1799.

(13) Haefele, A.; Blumhoff, J.; Khnayzer, R. S.; Castellano, F. N. Getting to the (Square) Root of the Problem: How to Make Noncoherent Pumped Upconversion Linear. *J. Phys. Chem. Lett.* **2012**, *3*, 299−303.

(14) Monguzzi, A.; Mezyk, J.; Scotognella, F.; Tubino, R.; Meinardi, F. Upconversion-Induced Fluorescence in Multicomponent Systems: Steady-State Excitation Power Threshold. *Phys. Rev. B: Condens. Matter Mater. Phys.* **2008**, *78*, 195112.

(15) Monguzzi, A.; Tubino, R.; Hoseinkhani, S.; Campione, M.; Meinardi, F. Low Power, Non-Coherent Sensitized Photon up-Conversion: Modelling and Perspectives. *Phys. Chem. Chem. Phys.* **2012**, *14*, 4322−4332.

(16) Auckett, J. E.; Chen, Y. Y.; Khoury, T.; Clady, R. G. C. R.; Ekins-Daukes, N. J.; Crossley, M. J.; Schmidt, T. W. Efficient Up-Conversion by Triplet-Triplet Annihilation. *J. Phys. Conf. Ser.* **2009**, *185*, No. 012002.

(17) Hoseinkhani, S.; Tubino, R.; Meinardi, F.; Monguzzi, A. Achieving the Photon Up-Conversion Thermodynamic Yield Upper Limit by Sensitized Triplet−Triplet Annihilation. *Phys. Chem. Chem. Phys.* **2015**, *17*, 4020−4024.

(18) Gray, V.; Dreos, A.; Erhart, P.; Albinsson, B.; Moth-Poulsen, K.; Abrahamsson, M. Loss Channels in Triplet−Triplet Annihilation Photon Upconversion: Importance of Annihilator Singlet and Triplet Surface Shapes. *Phys. Chem. Chem. Phys.* **2017**, *19*, 10931−10939.

(19) Mongin, C.; Golden, J. H.; Castellano, F. N. Liquid PEG Polymers Containing Antioxidants: A Versatile Platform for Studying Oxygen-Sensitive Photochemical Processes. *ACS Appl. Mater. Interfaces* **2016**, *8*, 24038−24048.

(20) Sugunan, S. K.; Greenwald, C.; Paige, M. F.; Steer, R. P. Efficiency of Noncoherent Photon Upconversion by Triplet−Triplet Annihilation: The C60 Plus Anthanthrene System and the Importance of Tuning the Triplet Energies. *J. Phys. Chem. A* **2013**, *117*, 5419−5427.

(21) Zhao, J.; Ji, S.; Guo, H. Triplet−Triplet Annihilation Based Upconversion: From Triplet Sensitizers and Triplet Acceptors to Upconversion Quantum Yields. *RSC Adv.* **2011**, *1*, 937−950.

(22) Yanai, N.; Kimizuka, N. New Triplet Sensitization Routes for Photon Upconversion: Thermally Activated Delayed Fluorescence Molecules, Inorganic Nanocrystals, and Singlet-to-Triplet Absorption. *Acc. Chem. Res.* **2017**, *50*, 2487−2495.

(23) Moor, K.; Kim, J.-H.; Snow, S.; Kim, J.-H. [C70] Fullerene-Sensitized Triplet−Triplet Annihilation Upconversion. *Chem. Commun.* **2013**, *49*, 10829−10831.

(24) Wu, M.; Congreve, D. N.; Wilson, M. W. B.; Jean, J.; Geva, N.; Welborn, M.; Van Voorhis, T.; Bulović, V.; Bawendi, M. G.; Baldo, M. A. Solid-State Infrared-to-Visible Upconversion Sensitized by Colloidal Nanocrystals. *Nat. Photonics* **2016**, *10*, 31−34.

(25) Durandin, N. A.; Isokuortti, J.; Efimov, A.; Vuorimaa-Laukkanen, E.; Tkachenko, N. V.; Laaksonen, T. Efficient Photon Upconversion at Remarkably Low Annihilator Concentrations in a Liquid Polymer Matrix: When Less Is More. *Chem. Commun.* **2018**, *54*, 14029−14032.

(26) Sandros, K.; et al. Transfer of Triplet State Energy in Fluid Solutions. *Acta Chem. Scand.* **1964**, *18*, 2355−2374.

(27) Gholizadeh, E. M.; Frazer, L.; MacQueen, R. W.; Gallaher, J. K.; Schmidt, T. W. Photochemical Upconversion Is Suppressed by High Concentrations of Molecular Sensitizers. *Phys. Chem. Chem. Phys.* **2018**, *20*, 19500−19506.

(28) Zhou, Y.; Ayad, S.; Ruchlin, C.; Posey, V.; Hill, S. P.; Wu, Q.; Hanson, K. Examining the Role of Acceptor Molecule Structure in Self-Assembled Bilayers: Surface Loading, Stability, Energy Transfer, and Upconverted Emission. *Phys. Chem. Chem. Phys.* **2018**, *20*, 20513−20524.

(29) Parker, C. A.; Joyce, T. A. Formation Efficiency and Energy of the Perylene Triplet. *Chem. Commun.* **1966**, *4*, 108b−109.

(30) O'Brien, J. A.; Rallabandi, S.; Tripathy, U.; Paige, M. F.; Steer, R. P. Efficient S2 State Production in ZnTPP−PMMA Thin Films by Triplet−Triplet Annihilation: Evidence of Solute Aggregation in Photon Upconversion Systems. *Chem. Phys. Lett.* **2009**, *475*, 220−222.

(31) Giri, N. K.; Ponce, C. P.; Steer, R. P.; Paige, M. F. Homomolecular Non-Coherent Photon Upconversion by Triplet-Triplet Annihilation Using a Zinc Porphyrin on Wide Bandgap Semiconductors. *Chem. Phys. Lett.* **2014**, *598*, 17−22.

(32) Askes, S. H. C.; Pomp, W.; Hopkins, S. L.; Kros, A.; Wu, S.; Schmidt, T.; Bonnet, S. Imaging Upconverting Polymersomes in Cancer Cells: Biocompatible Antioxidants Brighten Triplet-Triplet Annihilation Upconversion. *Small* **2016**, *12*, 5579−5590.

(33) Northrop, D. C.; Simpson, O. Electronic Properties of Aromatic Hydrocarbons I. Electrical Conductivity. *Proc. R. Soc. London. Ser. A. Math. Phys. Sci.* **1956**, *234*, 124−135.

(34) Hall, G. G.; Lennard-Jones, J. E. The Molecular Orbital Theory of Chemical Valency. XI. Bond Energies, Resonance Energies and Triplet State Energies. *Proc. R. Soc. London. Ser. A. Math. Phys. Sci.* **1952**, *213*, 113−123.

(35) Cheng, Y. Y.; Fückel, B.; Khoury, T.; Clady, R. G. C. R.; Ekins-Daukes, N. J.; Crossley, M. J.; Schmidt, T. W. Entropically Driven Photochemical Upconversion. *J. Phys. Chem. A* **2011**, *115*, 1047−1053.

(36) Goudarzi, H.; Limbu, S.; Cabanillas-González, J.; Zenonos, V. M.; Kim, J. S.; Keivanidis, P. E. Impact of Molecular Conformation on Triplet-Fusion Induced Photon Energy up-Conversion in the Absence of Exothermic Triplet Energy Transfer. *J. Mater. Chem. C* **2019**, *7*, 3634−3643.

DOI: 10.1021/acs.jpcc.9b08026
J. Phys. Chem. C 2019, 123, 22865−22872

(37) Wu, T. C.; Congreve, D. N.; Baldo, M. A. Solid State Photon Upconversion Utilizing Thermally Activated Delayed Fluorescence Molecules as Triplet Sensitizer. *Appl. Phys. Lett.* **2015**, *107*, No. 031103.
(38) Chen, W.; Song, F.; Tang, S.; Hong, G.; Wu, Y.; Peng, X. Red-to-Blue Photon up-Conversion with High Efficiency Based on a TADF Fluorescein Derivative. *Chem. Commun.* **2019**, *55*, 4375−4378.
(39) Amemori, S.; Sasaki, Y.; Yanai, N.; Kimizuka, N. Near-Infrared-to-Visible Photon Upconversion Sensitized by a Metal Complex with Spin-Forbidden yet Strong S0-T1 Absorption. *J. Am. Chem. Soc.* **2016**, *138*, 8702−8705.

DOI: 10.1021/acs.jpcc.9b08026
J. Phys. Chem. C 2019, 123, 22865−22872

PUBLICATION III

Endothermic and Exothermic Energy Transfer Made Equally Efficient for Triplet−Triplet Annihilation Upconversion

Isokuortti, J.; Allu, S. R.; Efimov, A.; Vuorimaa-Laukkanen, E.; Tkachenko, N. V.; Vinogradov, S. A.; Laaksonen, T.; Durandin, N. A.

Journal of Physical Chemistry Letters, vol. 11, p. 318, 2020
DOI: https://doi.org/10.1021/acs.jpclett.9b03466

THE JOURNAL OF PHYSICAL CHEMISTRY Letters

Cite This: J. Phys. Chem. Lett. 2020, 11, 318−324

Letter

pubs.acs.org/JPCL

Endothermic and Exothermic Energy Transfer Made Equally Efficient for Triplet−Triplet Annihilation Upconversion

Jussi Isokuortti,[†] Srinivasa Rao Allu,[‡] Alexander Efimov,[†] Elina Vuorimaa-Laukkanen,[†] Nikolai V. Tkachenko,[†] Sergei A. Vinogradov,[‡] Timo Laaksonen,[†,§] and Nikita A. Durandin*[,†]

[†]Faculty of Engineering and Natural Sciences, Tampere University, Korkeakoulunkatu 8, 33720 Tampere, Finland

[‡]Department of Biochemistry and Biophysics, Perelman School of Medicine, and Department of Chemistry, School of Arts and Sciences, University of Pennsylvania, Philadelphia, Pennsylvania 19104, United States

[§]Division of Pharmaceutical Biosciences, Faculty of Pharmacy, University of Helsinki, Viikinkaari 5 E, 00014 Helsinki, Finland

Supporting Information

ABSTRACT: Expanding the anti-Stokes shift for triplet−triplet annihilation upconversion (TTA-UC) systems with high quantum yields without compromising power density thresholds (I_{th}) remains a critical challenge in photonics. Our studies reveal that such expansion is possible by using a highly endothermic TTA-UC pair with an enthalpy difference of +80 meV even in a polymer matrix 1000 times more viscous than toluene. Carrying out efficient endothermic triplet−triplet energy transfer (TET) requires suppression of the reverse annihilator-to-sensitizer TET, which was achieved by using sensitizers with high molar extinction coefficients and long triplet state lifetimes as well as optimized annihilator concentrations. Under these conditions, the sensitizer-to-annihilator forward TET becomes effectively entropy driven, yielding upconversion quantum yields comparable to those achieved with the exothermic TTA-UC pair but with larger anti-Stokes shifts and even lower I_{th}, a previously unattained achievement.

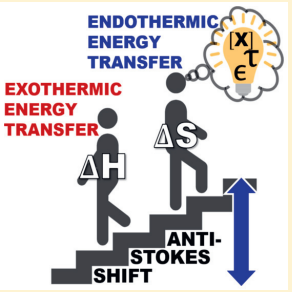

Triplet−triplet annihilation upconversion (TTA-UC), also known as triplet fusion, is capable of upconverting low-energy photons to higher-energy ones through a cascade of photochemical processes (see Scheme 1): A sensitizer molecule absorbs a low-energy photon and undergoes intersystem crossing (ISC) to yield a triplet excited state. This energy is transferred to an annihilator molecule via triplet−triplet energy transfer (TET). Upon encountering each other, two triplet state annihilators can yield one singlet excited annihilator, which will subsequently emit a high-energy photon. This complete process, from absorption to emission, is known as TTA-UC.[1−4] TTA-UC is a promising approach to boost many high-tech fields, for example, in enhancing the efficiency of photovoltaics and photocatalysis, driving chemical reactions and photoactuation, or improving the functions of biomedical devices.[5−20] These applications require efficient upconversion systems, typically meaning a high quantum yield (Φ_{UC}), a large anti-Stokes emission shift, and a low power density threshold (photon flux at which 50% of Φ_{UC} is achieved). The last one is of great importance because Φ_{UC} is power density-dependent[21,22] and many applications, such as photovoltaics and biomedical systems, require low excitation power densities.

Several approaches for maximizing the anti-Stokes shift or upconversion energy shift (UES) have been suggested, for example, employing molecules with a small singlet−triplet gap, exciting the sensitizer directly to its excited triplet state, or utilizing sensitizer/annihilator pairs with small or even negative triplet energy gaps, and even double TTA-UC.[23−33] However, the dilemma of simultaneous expansion of UES and preservation of low power density thresholds and high Φ_{UC} has not been resolved to date. Here, we show that the UES of a TTA-UC system can be increased by decreasing the exothermicity of the triplet energy gap between the sensitizer and annihilator or even by utilizing considerably endothermic sensitizer/annihilator pairs. At the same time, a high Φ_{UC} and low power density threshold are retained with careful consideration of the photochemistry involved and design of the experimental system to efficiently suppress the reverse triplet−triplet energy transfer (RTET) from the annihilator back to sensitizer. This is crucial because RTET is the fundamental cause of low quantum yields in endothermic systems.

For this work, two tetraarylphthalimidoporphyrins (Scheme 1), palladium(II) and zinc(II) *N*-{2,6-di-[(3′(methoxycarbonyl)propyloxy)phenyl]}phthalimido-porphyrin[34] (PdTAPIP and ZnTAPIP, respectively) were used as sensitizers and 9-(4-phenylethynyl)-10-phenylanthracene[35] (PEAP, Scheme 1) as the annihilator for TTA-UC. Measurements were performed in viscous solvents, poly(ethylene glycol)-200 (PEG200) and poly(ethylene glycol)-300 (PEG300) with oleic acid (50 mM) as the oxygen scavenger.

Received: November 23, 2019
Accepted: December 19, 2019
Published: December 19, 2019

DOI: 10.1021/acs.jpclett.9b03466
J. Phys. Chem. Lett. 2020, 11, 318−324

Scheme 1. (Left) Structures of the Sensitizers (ZnTAPIP and PdTAPIP) and the Annihilator (PEAP) Used in This Study; (Right) Jablonski Diagram of TTA-UC[a]

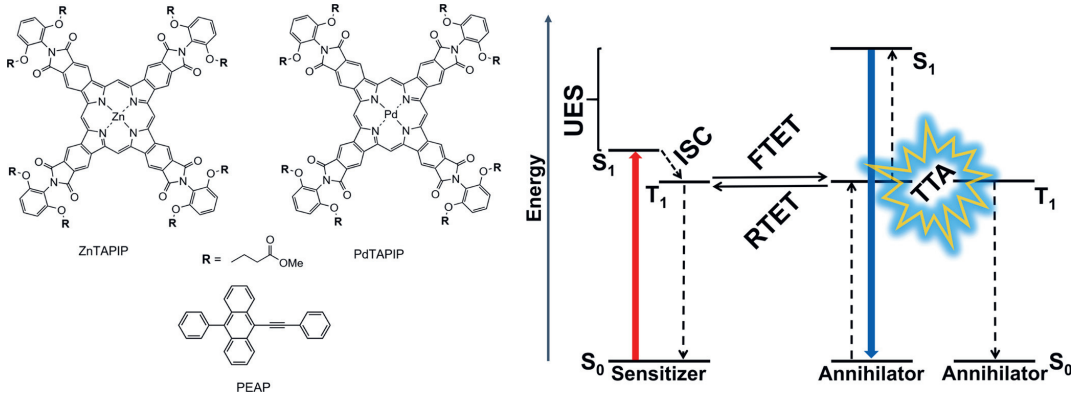

[a]The sensitizer undergoes excitation to a singlet state, followed by ISC to yield an excited triplet state. This energy is then transferred to the annihilator (forward triplet−triplet energy transfer, FTET). Two triplet state annihilators can undergo annihilation, after which an upconverted photon is emitted. The energy difference between the absorbed (red arrow) and emitted (blue arrow) photon is the UES. The relative sensitizer and annihilator triplet energies strongly influence the rates of FTET and RTET.

Liquid PEGs containing oxygen scavengers are versatile and robust matrixes for TTA-UC studies[36] and were used here to emulate the viscosity conditions of soft matter devices, such as polymer micelles or elastomer matrixes. The viscosity of PEG200 at room temperature is 54 cP, and in order to increase the viscosity range, PEG300 was used at −5 °C to yield a viscosity of 520 cP.

As previously reported, the requirements for effective sensitizers are high extinction coefficients, efficient ISC, and long triplet state lifetimes.[4,37,38] Thus, both TAPIPs are very attractive thanks to their outstanding Q-band molar extinction coefficients (ϵ) and long triplet state lifetimes (τ_0), which are given in Table 1. The absorption spectra of both TAPIPs are shown in Figure 1. The large Q-band ϵ and quite small singlet−triplet energy gaps, 0.36 and 0.35 eV for Pd and ZnTAPIP, respectively, are results of the π-extension of the porphyrin macrocycles.[39,40] The ISC efficiency (Φ_{ISC}) of PdTAPIP is about unity.[34] On the basis of ZnTAPIP's fluorescence quantum yield (10% in dimethylacetamide[34] and 9% in PEG200), the upper limit of ZnTAPIP's Φ_{ISC} is 90%, which is in line with the reported values for other Zn porphyrins.[41−43] The total concentrations of the sensitizers were chosen so that at the excitation wavelengths (633 nm for PdTAPIP and 660 nm for ZnTAPIP) the optical density in a 1 cm cuvette was 1 in PEG200 and 2 in PEG300. For PdTAPIP, this meant concentrations 4.2 and 8.4 μM and for ZnTAPIP 5.1 and 10.2 μM in PEG200 and PEG300, respectively.

Table 1. Photophysical Properties of the Sensitizers

sensitizer	Q-band max (nm)	ϵ (M^{-1} cm^{-1})	τ_0 in PEG200 (ms)	τ_0 in PEG300 (ms)	E_T (eV)
PdTAPIP	630	263 500	0.439	0.488	1.61
ZnTAPIP	659	198 500	10.3	17.4	1.53

The triplet excited state energies (E_T) of the TAPIPs in PEG200 were determined from their phosphorescence spectra (Figures S1 and S2) and are given in Table 1. On the basis of these energies, PEAP was chosen as the annihilator due to its high fluorescence quantum yield (76% in hexane[44]), long triplet state lifetime (2.4 ms in toluene[45]), and E_T of 1.49−1.50 eV[44,45] as evaluated with TD-DFT calculations. The fluorescence spectrum of PEAP in PEG200 is shown in Figure 1, and the absorption spectrum together with the molar extinction coefficients is shown in Figures S3 and S4 and Table S1. TD-DFT-calculated E_T of PEAP thus matches closely the E_T of ZnTAPIP to minimize enthalpic energy "loss" in TET, and, in comparison, with the larger difference in triplet state energies between PdTAPIP and PEAP, rapid TET from PdTAPIP would be expected.

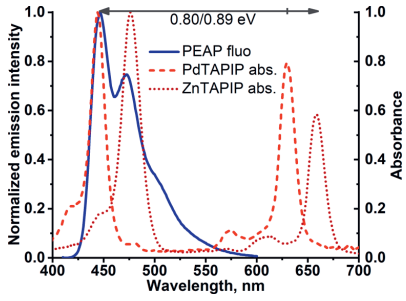

Figure 1. Fluorescence spectrum of PEAP (solid blue) and absorption spectra of PdTAPIP (dashed red) and ZnTAPIP (dotted dark red) in PEG200. The arrow indicates the UES achieved with both TAPIPs and PEAP as annihilator.

To evaluate the forward triplet−triplet energy transfer (FTET) rate constants from sensitizer to annihilator (k_{FTET}) for each upconversion system, the phosphorescence lifetimes of the TAPIPs in the presence of different [PEAP] were measured in both solvents. The resulting Stern−Volmer plots along with the calculated values of k_{FTET} are shown in Figure 2. The phosphorescence decays of both TAPIPs with and without PEAP in both solvents are shown in Figures S7−S10.

DOI: 10.1021/acs.jpclett.9b03466
J. Phys. Chem. Lett. 2020, 11, 318−324

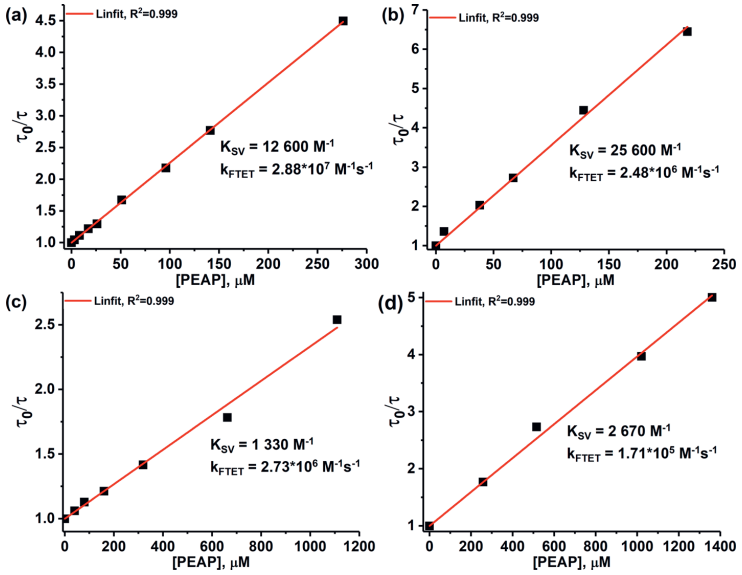

Figure 2. Stern–Volmer plots of PdTAPIP (a) and ZnTAPIP (b) in PEG200 and PdTAPIP (c) and ZnTAPIP (d) in PEG300 with the resulting Stern–Volmer constants (K_{SV}) and FTET rate constants (k_{FTET}).

The rate of FTET follows the Boltzmann distribution and can be written as $k_{FTET} = \frac{k_{diff}}{1 + \exp\left(-\frac{\Delta E_T}{k_B T}\right)}$,[46] where k_{diff} is the diffusion rate constant (approximately 5×10^7 M^{-1} s^{-1} in PEG200[47]) and ΔE_T is the triplet energy gap between the sensitizer and the annihilator at temperature T. Thus, by using the k_{FTET} values obtained from the quenching studies, ΔE_T for both pairs can be estimated as 0.01 eV (0.4 k_BT at room temperature) for PdTAPIP/PEAP and −0.08 eV (−3 k_BT) for ZnTAPIP/PEAP.[48] This also means that the TD-DFT-calculated E_T of PEAP (1.49–1.50 eV) underestimates the real energy, which we determine to be closer to 1.6 eV. Therefore, FTET from PdTAPIP to PEAP is slightly exothermic, but the energy transfer from ZnTAPIP to PEAP is considerably endothermic. The rate constant of RTET can be calculated as $k_{RTET} = k_{FTET} \exp\left(-\frac{\Delta E_T}{k_B T}\right)$.[46] For ZnTAPIP/PEAP, this gives $k_{RTET} \approx 5 \times 10^7$ M^{-1} s^{-1}, a fully diffusion-controlled rate in the viscous PEG200, which in turn can be used to evaluate the ratio $k_{RTET}/k_{FTET} \approx 20$. For PdTAPIP/PEAP, $k_{RTET} \approx 1.9 \times 10^7$ M^{-1} s^{-1} and $k_{RTET}/k_{FTET} \approx 0.7$. Thus, RTET should be expected from PEAP back to both sensitizers, and the effect of RTET on TTAUC performance has to be taken into account, especially in the case of ZnTAPIP.

Due to substantial RTET, the efficiency of TET that results in successful annihilation and upconversion, i.e., apparent TET efficiency (Φ_{TET}), cannot be solely determined from the FTET rate constants. Thus, we monitored how [PEAP] affects the upconverted emission intensity (I_{UC}). At constant excitation intensity, I_{UC} depends on the quantum yield of upconversion $\Phi_{UC} = f\Phi_{ISC}\Phi_{TTA}\Phi_{fluo}\Phi_{TET}$,[49] where f is the so-called spin-statistical factor,[45,50,51] Φ_{TTA} is the efficiency of triplet–triplet annihilation, and Φ_{fluo} is the annihilator's fluorescence quantum yield. Here Φ_{UC} is multiplied by 2 to make the maximum theoretical quantum yield 100%. By comparing the projected efficiency of FTET ($\Phi_{FTET} = \frac{k_{FTET}[A]}{\frac{1}{\tau_0} + k_{FTET}[A]}$, where τ_0 is the unquenched triplet lifetime of the sensitizer) and I_{UC}, the effect of RTET in each system becomes clearly observable (Figure 3).

As evident from Figure 3, despite the large endothermic energy gap, the FTET from ZnTAPIP to PEAP is very efficient thanks to the ultralong triplet state lifetime of the sensitizer. Indeed, 90% Φ_{FTET} is reached from ZnTAPIP with a lower [PEAP] than that from PdTAPIP. However, the much faster

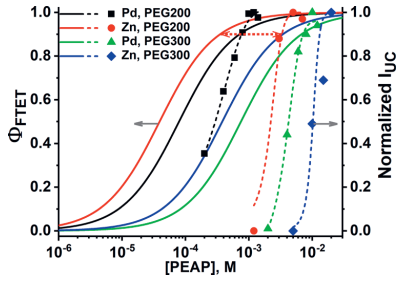

Figure 3. Comparison between the projected FTET efficiency (Φ_{FTET}, in solid lines, left axis) and the measured upconversion emission intensity of each upconversion system (I_{UC}, geometric markers and dashed lines, right axis) at a given annihilator concentration. The dashed red arrow shows the discrepancy between the projected FTET efficiency and the UC emission. The arrow illustrates the difference between the concentrations that yield 90% Φ_{FTET} and 90% of the maximum UC emission intensity with ZnTAPIP in PEG200. The emission intensities were normalized by each system's maximum value due to the differences in Φ_{ISC} and Φ_{fluo}.

DOI: 10.1021/acs.jpclett.9b03466
J. Phys. Chem. Lett. 2020, 11, 318–324

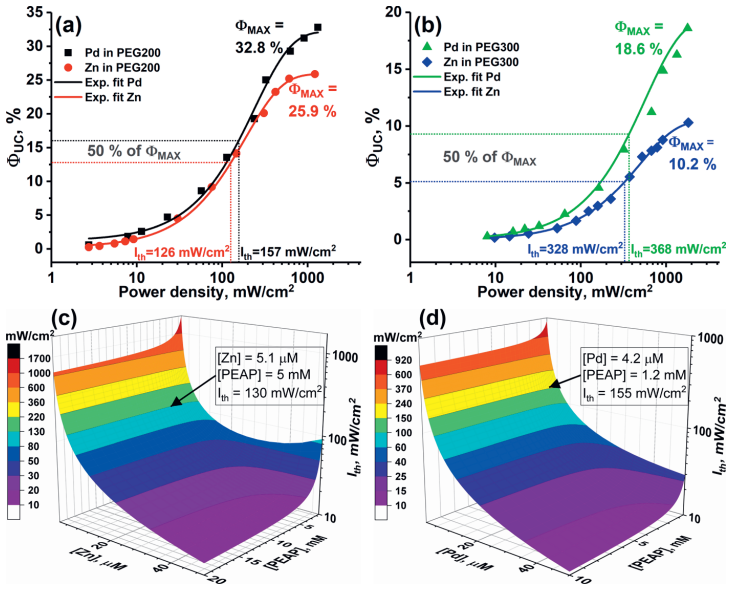

Figure 4. Quantum yields of upconversion (Φ_{UC}) as a function of power density in PEG200 (a) and in PEG300 (b). The upconverted fluorescence spectra are shown in Figures S15 and S16. I_{th} was determined from the sigmoidal fit (Exp. fit) as half of the determined maximum quantum yield (Φ_{MAX}). The kinetic rate models of ZnTAPIP/PEAP (c) and PdTAPIP/PEAP (d) in PEG200 show how I_{th} of both systems depends on the total sensitizer ([Zn] or [Pd]) and annihilator ([PEAP]) concentrations. The text boxes highlight the I_{th} values obtained with the model using the experimental concentrations of sensitizer and annihilator.

Table 2. Properties of the Upconversion Systems Presented

sensitizer	viscosity (cP)	ΔE_T (k_BT)	[S_0] (μM)	[PEAP] (mM)	I_{th} (mW/cm^2)	Φ_{UC} (%)	$\Phi_{UC}^{corrected}$ (%)[a]
PdTAPIP	54	0.4	4.2	1.2	157	18.8	32.8
	520		8.4	10	368	9.6	18.6
ZnTAPIP	54	−3	5.1	5	126	11.6	25.9
	520		10.2	20	328	2.1	10.2

[a]$\Phi_{UC}^{corrected}$ is the quantum yield of upconversion with correction for reabsorbed photons.

RTET in the case of the endothermic ZnTAPIP/PEAP pair makes the apparent TET efficiency Φ_{TET} considerably smaller. RTET causes a striking difference between the concentrations that yield high Φ_{FTET} and the concentrations resulting in high apparent Φ_{TET} and consequently high I_{UC} (because $I_{UC} \propto \Phi_{UC} \propto \Phi_{TET}$) for the ZnTAPIP systems (highlighted with the red arrow in Figure 3). With ZnTAPIP as the sensitizer, 90% Φ_{FTET} occurs at [PEAP] = 0.35 mM, but the emission intensity reaches its maximum with [PEAP] = 5 mM. Conversely, the performance of the PdTAPIP/PEAP pair follows the projected FTET efficiencies more closely: 90% Φ_{FTET} is yielded with [PEAP] = 0.7 mM, and the maximum emission intensity is achieved with [PEAP] = 1.2 mM. This is because the effect of RTET is much smaller and the apparent TET efficiency is more directly determined by the FTET efficiency. The PEG300-based systems show the same trend: 90% Φ_{FTET} is attained with [PEAP] of 3.4 and 6.8 mM, and the maximum emission intensity is reached with [PEAP] of 20 and 10 mM, when using ZnTAPIP or PdTAPIP as sensitizers, respectively. While a larger [PEAP] is required to attain the same upconversion efficiency for ZnTAPIP, these results give us important information regarding the concentration required to attain the maximum Φ_{UC} for each system. On the basis of these results, it is possible to design a system where the adverse effect of RTET is minimized and the full potential of endothermic TET pairs can be realized.

The requirement for higher annihilator concentration to yield efficient TET from ZnTAPIP to PEAP can be explained with reference to entropy. Because TET from ZnTAPIP to PEAP is endothermic, high annihilator concentrations are needed to provide an entropic driving force. Cheng et al. have shown that the change of entropy in FTET is $\Delta S = k_B \ln\left(\frac{[A_0][S_T]}{[S_0][A_T]}\right)$,[30] where [$A_0$], [$A_T$], [$S_0$], and [$S_T$] are the ground and triplet state concentrations of the annihilator and sensitizer, respectively. Thus, by increasing the annihilator ground state concentration, the process becomes exergonic and FTET is promoted over RTET. The equation also reveals that low [S_0] and high [S_T] are needed for large ΔS, emphasizing the requirement for a sensitizer with high molar extinction coefficient and long triplet state lifetime.

To further study the performance of our TTA-UC systems, we measured the quantum yields of upconversion and determined the excitation power density thresholds (I_{th}) for each system using [PEAP] that yielded the maximum upconversion emission intensity (Figure 4 and Table 2). At

DOI: 10.1021/acs.jpclett.9b03466
J. Phys. Chem. Lett. 2020, 11, 318−324

power densities higher than I_{th}, the upconversion emission intensity of the system has a linear dependence on the power density. At power densities lower than I_{th}, the upconversion emission intensity has a quadratic dependence on the excitation power density (Figures S11–S14).[22] At I_{th}, the annihilator triplet states decay via annihilation and spontaneous pathways at equal rates, and the quantum yield of upconversion is half of the maximum quantum yield of the system.[21,22,52] The well-known equation for I_{th} by Monguzzi et al. shows that $I_{th} = \frac{2(k_A^T)^2}{\gamma_{TT}\alpha(\lambda)\Phi_{TET}}$,[52] where k_A^T is the spontaneous decay rate of the annihilator triplet state, γ_{TT} is the second-order decay rate of TTA and $\alpha(\lambda)$ is the absorption coefficient of the sensitizer at the excitation wavelength. Thus, for systems using the same annihilator and the same optical densities, determining I_{th} provides a reliable evaluation for the efficiency of apparent TET.

To our delight, when comparing the I_{th} values of the systems, it is clear that RTET was successfully suppressed and apparent TET is efficient for all systems with the concentrations used. Exceptionally, the endothermic ZnTAPIP/PEAP pair exhibits even lower I_{th} values than the exothermic PdTAPIP/PEAP pair. To the best of our knowledge, an endothermic pair has not exhibited as efficient TET as an exothermic pair. Thus, our results demonstrate that exothermic TET is not required for efficient TTA-UC.

To corroborate these experimental findings and to further study the effect of both sensitizer and annihilator concentrations on I_{th}, we applied our kinetic rate model[53] (equations and parameters are presented in the Supporting Information) to both sensitizer/annihilator pairs. The simulations confirmed that with the endothermic ZnTAPIP/PEAP pair it is indeed possible to attain the same or even lower I_{th} than that with the exothermic PdTAPIP/PEAP pair. Furthermore, the model corroborated the experimental findings by the fact that the utilized experimental conditions (sensitizer and annihilator ground state concentrations and diffusion rate constant) yielded I_{th} values of 130 and 155 mW/cm^2 in PEG200 (Figure 4) and 335 and 336 mW/cm^2 in PEG300 (Figures S17 and S18) for ZnTAPIP- and PdTAPIP-sensitized systems, respectively. In the Supporting Information, we also provide simulation results (Figures S19 and S20) in a less viscous environment (e.g., toluene). Generally, kinetic rate modeling shows that for an upconversion system with substantially endothermic TET a long triplet state lifetime and high annihilator ground state concentration are extremely beneficial for reducing the I_{th}.

From the equation $I_{th} = \frac{2(k_A^T)^2}{\gamma_{TT}\alpha(\lambda)\Phi_{TET}}$, a simple approach for reducing I_{th} for a given pair of sensitizer/annihilator is to increase α (which is proportional to ϵ and $[S_0]$) of the system by increasing the sensitizer ground state concentration. However, overly high sensitizer ground state concentrations are deleterious even in exothermic cases due to quenching of the annihilator triplet state and quenching of the sensitizer triplet state via sensitizer–sensitizer TTA.[53–56] Increasing the sensitizer ground state concentration would require also a higher annihilator ground state concentration to suppress RTET, especially in the case of the endothermic ZnTAPIP/PEAP pair: at higher [ZnTAPIP], the I_{th} depends strongly on the [PEAP], as we can see in Figure 4c. Consequently, a higher annihilator ground state concentration will also increase the probability of excimer formation and thus decrease the fluorescence quantum yield of the annihilator, which will, in turn, decrease the Φ_{UC}.[47,51] This effect is observable in our systems as Φ_{UC} drops when higher [PEAP] is utilized in PEG300 (Figure 4a,b and Table 2). Thus, a sensitizer with high ϵ is thus decisive for efficient TTA-UC built upon endothermic sensitizer/annihilator pairs.

The designer of an upconversion system with large UES thus needs to choose whether to strive for as low as possible I_{th} or as high as possible Φ_{UC}. The upconversion systems presented here exhibit balanced performance even in viscous media with high maximum quantum yields (33 and 26%), low-power density thresholds (160 and 130 mW/cm^2), and large UESs (0.80 and 0.89 eV) for exothermic and highly endothermic TET pairs, respectively. These features are attributed to high annihilator concentration (enabled by high solubility), low sensitizer concentration (while still harvesting excitation light completely, enabled by high ϵ), and long sensitizer triplet lifetime. These properties collectively lead to entropically suppressed RTET and make TET exergonic. Thus, after carefully selecting sensitizer and annihilator molecules with outstanding properties and optimizing their concentrations, we have shown that utilizing sensitizer/annihilator pairs with a negative triplet energy gap is a viable approach for expanding UES without compromising the power density threshold and Φ_{UC}.

■ ASSOCIATED CONTENT

Supporting Information

The Supporting Information is available free of charge at https://pubs.acs.org/doi/10.1021/acs.jpclett.9b03466.

Absorption and luminescence spectra of the molecules, phosphorescence decays of the sensitizers, and experimental and kinetic rate modeling results and details (PDF)

■ AUTHOR INFORMATION

Corresponding Author

*E-mail: nikita.durandin@tuni.fi.

ORCID

Alexander Efimov: 0000-0003-4671-3009
Elina Vuorimaa-Laukkanen: 0000-0002-3610-785X
Nikolai V. Tkachenko: 0000-0002-8504-2335
Sergei A. Vinogradov: 0000-0002-4649-5534
Nikita A. Durandin: 0000-0002-5734-7377

Author Contributions

The manuscript was written through contributions of all authors. All authors have given approval to the final version of the manuscript.

Notes

The authors declare no competing financial interest.

■ ACKNOWLEDGMENTS

This work was supported by The Academy of Finland (Grant No. 316893). Support of Grants EB018464 and EB027397 from the NIH USA (SAV) is gratefully acknowledged.

■ REFERENCES

(1) Parker, C. A.; Hatchard, C. G. Delayed Fluorescence from Solutions of Anthracene and Phenanthrene. *Proc. R. Soc. London. Ser. A. Math. Phys. Sci.* **1962**, *269* (1339), 574–584.

DOI: 10.1021/acs.jpclett.9b03466
J. Phys. Chem. Lett. 2020, 11, 318–324

(2) Parker, C. A.; Hatchard, C. G. Sensitised Anti-Stokes Delayed Fluorescence. *Proc. Chem. Soc.* **1962**, 386−387.
(3) Parker, C. A.; Hatchard, C. G.; Joyce, T. A. Selective and Mutual Sensitization of Delayed Fluorescence. *Nature* **1965**, *205* (4978), 1282−1284.
(4) Singh-Rachford, T. N.; Castellano, F. N. Photon Upconversion Based on Sensitized Triplet-Triplet Annihilation. *Coord. Chem. Rev.* **2010**, *254* (21−22), 2560−2573.
(5) Nattestad, A.; Cheng, Y. Y.; MacQueen, R. W.; Schulze, T. F.; Thompson, F. W.; Mozer, A. J.; Fückel, B.; Khoury, T.; Crossley, M. J.; Lips, K.; et al. Dye-Sensitized Solar Cell with Integrated Triplet−Triplet Annihilation Upconversion System. *J. Phys. Chem. Lett.* **2013**, *4* (12), 2073−2078.
(6) Cheng, Y. Y.; Nattestad, A.; Schulze, T. F.; MacQueen, R. W.; Fückel, B.; Lips, K.; Wallace, G. G.; Khoury, T.; Crossley, M. J.; Schmidt, T. W. Increased Upconversion Performance for Thin Film Solar Cells: A Trimolecular Composition. *Chem. Sci.* **2016**, *7* (1), 559−568.
(7) Baluschev, S.; Yakutkin, V.; Wegner, G.; Miteva, T.; Nelles, G.; Yasuda, A.; Chernov, S.; Aleshchenkov, S.; Cheprakov, A. Upconversion with Ultrabroad Excitation Band: Simultaneous Use of Two Sensitizers. *Appl. Phys. Lett.* **2007**, *90* (18), 181103.
(8) Kim, J.-H.; Kim, J.-H. Encapsulated Triplet−Triplet Annihilation-Based Upconversion in the Aqueous Phase for Sub-Band-Gap Semiconductor Photocatalysis. *J. Am. Chem. Soc.* **2012**, *134* (42), 17478−17481.
(9) Islangulov, R. R.; Castellano, F. N. Photochemical Upconversion: Anthracene Dimerization Sensitized to Visible Light by a RuII Chromophore. *Angew. Chem., Int. Ed.* **2006**, *45* (36), 5957−5959.
(10) Börjesson, K.; Dzebo, D.; Albinsson, B.; Moth-Poulsen, K. Photon Upconversion Facilitated Molecular Solar Energy Storage. *J. Mater. Chem. A* **2013**, *1* (30), 8521−8524.
(11) Jiang, Z.; Xu, M.; Li, F.; Yu, Y. Red-Light-Controllable Liquid-Crystal Soft Actuators via Low-Power Excited Upconversion Based on Triplet−Triplet Annihilation. *J. Am. Chem. Soc.* **2013**, *135* (44), 16446−16453.
(12) Wohnhaas, C.; Mailänder, V.; Dröge, M.; Filatov, M. A.; Busko, D.; Avlasevich, Y.; Baluschev, S.; Miteva, T.; Landfester, K.; Turshatov, A. Triplet−Triplet Annihilation Upconversion Based Nanocapsules for Bioimaging Under Excitation by Red and Deep-Red Light. *Macromol. Biosci.* **2013**, *13* (10), 1422−1430.
(13) Kwon, O. S.; Song, H. S.; Conde, J.; Kim, H.; Artzi, N.; Kim, J.-H. Dual-Color Emissive Upconversion Nanocapsules for Differential Cancer Bioimaging In Vivo. *ACS Nano* **2016**, *10* (1), 1512−1521.
(14) Liu, Q.; Yin, B.; Yang, T.; Yang, Y.; Shen, Z.; Yao, P.; Li, F. A General Strategy for Biocompatible, High-Effective Upconversion Nanocapsules Based on Triplet−Triplet Annihilation. *J. Am. Chem. Soc.* **2013**, *135* (13), 5029−5037.
(15) Timko, B. P.; Dvir, T.; Kohane, D. S. Remotely Triggerable Drug Delivery Systems. *Adv. Mater.* **2010**, *22* (44), 4925−4943.
(16) Askes, S. H. C.; Bahreman, A.; Bonnet, S. Activation of a Photodissociative Ruthenium Complex by Triplet-Triplet Annihilation Upconversion in Liposomes. *Angew. Chem., Int. Ed.* **2014**, *53* (4), 1029−1033.
(17) Askes, S. H. C.; Kloz, M.; Bruylants, G.; Kennis, J. T. M.; Bonnet, S. Triplet−Triplet Annihilation Upconversion Followed by FRET for the Red Light Activation of a Photodissociative Ruthenium Complex in Liposomes. *Phys. Chem. Chem. Phys.* **2015**, *17* (41), 27380−27390.
(18) Wang, W.; Liu, Q.; Zhan, C.; Barhoumi, A.; Yang, T.; Wylie, R. G.; Armstrong, P. A.; Kohane, D. S. Efficient Triplet−Triplet Annihilation-Based Upconversion for Nanoparticle Phototargeting. *Nano Lett.* **2015**, *15* (10), 6332−6338.
(19) Liu, Q.; Wang, W.; Zhan, C.; Yang, T.; Kohane, D. S. Enhanced Precision of Nanoparticle Phototargeting in Vivo at a Safe Irradiance. *Nano Lett.* **2016**, *16* (7), 4516−4520.
(20) Ravetz, B. D.; Pun, A. B.; Churchill, E. M.; Congreve, D. N.; Rovis, T.; Campos, L. M. Photoredox Catalysis Using Infrared Light via Triplet Fusion Upconversion. *Nature* **2019**, *565* (7739), 343−346.
(21) Monguzzi, A.; Mezyk, J.; Scotognella, F.; Tubino, R.; Meinardi, F. Upconversion-Induced Fluorescence in Multicomponent Systems: Steady-State Excitation Power Threshold. *Phys. Rev. B: Condens. Matter Mater. Phys.* **2008**, *78* (19), 195112.
(22) Haefele, A.; Blumhoff, J.; Khnayzer, R. S.; Castellano, F. N. Getting to the (Square) Root of the Problem: How to Make Noncoherent Pumped Upconversion Linear. *J. Phys. Chem. Lett.* **2012**, *3* (3), 299−303.
(23) Chen, W.; Song, F.; Tang, S.; Hong, G.; Wu, Y.; Peng, X. Red-to-Blue Photon up-Conversion with High Efficiency Based on a TADF Fluorescein Derivative. *Chem. Commun.* **2019**, *55* (30), 4375−4378.
(24) Wang, Z.; Zhao, J.; Di Donato, M.; Mazzone, G. Increasing the Anti-Stokes Shift in TTA Upconversion with Photosensitizers Showing Red-Shifted Spin-Allowed Charge Transfer Absorption but a Non-Compromised Triplet State Energy Level. *Chem. Commun.* **2019**, *55* (10), 1510−1513.
(25) Sasaki, Y.; Amemori, S.; Kouno, H.; Yanai, N.; Kimizuka, N. Near Infrared-to-Blue Photon Upconversion by Exploiting Direct S−T Absorption of a Molecular Sensitizer. *J. Mater. Chem. C* **2017**, *5* (21), 5063−5067.
(26) Fan, C.; Wei, L.; Niu, T.; Rao, M.; Cheng, G.; Chruma, J. J.; Wu, W.; Yang, C. Efficient Triplet−Triplet Annihilation Upconversion with an Anti-Stokes Shift of 1.08 EV Achieved by Chemically Tuning Sensitizers. *J. Am. Chem. Soc.* **2019**, *141* (38), 15070−15077.
(27) Yanai, N.; Kozue, M.; Amemori, S.; Kabe, R.; Adachi, C.; Kimizuka, N. Increased Vis-to-UV Upconversion Performance by Energy Level Matching between a TADF Donor and High Triplet Energy Acceptors. *J. Mater. Chem. C* **2016**, *4* (27), 6447−6451.
(28) Yanai, N.; Kimizuka, N. New Triplet Sensitization Routes for Photon Upconversion: Thermally Activated Delayed Fluorescence Molecules, Inorganic Nanocrystals, and Singlet-to-Triplet Absorption. *Acc. Chem. Res.* **2017**, *50* (10), 2487−2495.
(29) Goudarzi, H.; Limbu, S.; Cabanillas-González, J.; Zenonos, V. M.; Kim, J.-S.; Keivanidis, P. E. Impact of Molecular Conformation on Triplet-Fusion Induced Photon Energy up-Conversion in the Absence of Exothermic Triplet Energy Transfer. *J. Mater. Chem. C* **2019**, *7* (12), 3634−3643.
(30) Cheng, Y. Y.; Fückel, B.; Khoury, T.; Clady, R. G. C. R.; Ekins-Daukes, N. J.; Crossley, M. J.; Schmidt, T. W. Entropically Driven Photochemical Upconversion. *J. Phys. Chem. A* **2011**, *115* (6), 1047−1053.
(31) Penconi, M.; Ortica, F.; Elisei, F.; Gentili, P. L. New Molecular Pairs for Low Power Non-Coherent Triplet−Triplet Annihilation Based Upconversion: Dependence on the Triplet Energies of Sensitizer and Emitter. *J. Lumin.* **2013**, *135*, 265−270.
(32) Monguzzi, A.; Meinardi, F. Second-Order Photochemical Upconversion in Organic Systems. *J. Phys. Chem. A* **2014**, *118* (8), 1439−1442.
(33) Li, L.; Zeng, Y.; Chen, J.; Yu, T.; Hu, R.; Yang, G.; Li, Y. Thermally Activated Delayed Fluorescence via Triplet Fusion. *J. Phys. Chem. Lett.* **2019**, *10*, 6239−6245.
(34) Esipova, T. V.; Rivera-Jacquez, H. J.; Weber, B.; Masunov, A. E.; Vinogradov, S. A. Stabilizing G-States in Centrosymmetric Tetrapyrroles: Two-Photon-Absorbing Porphyrins with Bright Phosphorescence. *J. Phys. Chem. A* **2017**, *121* (33), 6243−6255.
(35) Fudickar, W.; Linker, T. Why Triple Bonds Protect Acenes from Oxidation and Decomposition. *J. Am. Chem. Soc.* **2012**, *134* (36), 15071−15082.
(36) Mongin, C.; Golden, J. H.; Castellano, F. N. Liquid PEG Polymers Containing Antioxidants: A Versatile Platform for Studying Oxygen-Sensitive Photochemical Processes. *ACS Appl. Mater. Interfaces* **2016**, *8* (36), 24038−24048.
(37) Schulze, T. F.; Schmidt, T. W. Photochemical Upconversion: Present Status and Prospects for Its Application to Solar Energy Conversion. *Energy Environ. Sci.* **2015**, *8* (1), 103−125.
(38) Zhao, J.; Ji, S.; Guo, H. Triplet−Triplet Annihilation Based Upconversion: From Triplet Sensitizers and Triplet Acceptors to Upconversion Quantum Yields. *RSC Adv.* **2011**, *1* (6), 937−950.

DOI: 10.1021/acs.jpclett.9b03466
J. Phys. Chem. Lett. 2020, 11, 318−324

(39) Esipova, T. V.; Rivera-Jacquez, H. J.; Weber, B.; Masunov, A. E.; Vinogradov, S. A. Two-Photon Absorbing Phosphorescent Metalloporphyrins: Effects of π-Extension and Peripheral Substitution. *J. Am. Chem. Soc.* **2016**, *138* (48), 15648−15662.
(40) Zach, P. W.; Freunberger, S. A.; Klimant, I.; Borisov, S. M. Electron-Deficient Near-Infrared Pt(II) and Pd(II) Benzoporphyrins with Dual Phosphorescence and Unusually Efficient Thermally Activated Delayed Fluorescence: First Demonstration of Simultaneous Oxygen and Temperature Sensing with a Single Emitter. *ACS Appl. Mater. Interfaces* **2017**, *9* (43), 38008−38023.
(41) Harriman, A. Luminescence of Porphyrins and Metalloporphyrins. Part 1.—Zinc(II), Nickel(II) and Manganese(II) Porphyrins. *J. Chem. Soc., Faraday Trans. 1* **1980**, *76* (0), 1978−1985.
(42) Rogers, J. E.; Nguyen, K. A.; Hufnagle, D. C.; McLean, D. G.; Su, W.; Gossett, K. M.; Burke, A. R.; Vinogradov, S. A.; Pachter, R.; Fleitz, P. A. Observation and Interpretation of Annulated Porphyrins: Studies on the Photophysical Properties of Meso-Tetraphenylmetalloporphyrins. *J. Phys. Chem. A* **2003**, *107* (51), 11331−11339.
(43) Harriman, A.; Porter, G.; Richoux, M.-C. Photosensitised Reduction of Water to Hydrogen Using Water-Soluble Zinc Porphyrins. *J. Chem. Soc., Faraday Trans. 2* **1981**, *77* (5), 833−844.
(44) Zhong, F.; Zhao, J. Phenyleneanthracene Derivatives as Triplet Energy Acceptor/Emitter in Red Light Excitable Triplet-Triplet-Annihilation Upconversion. *Dyes Pigm.* **2017**, *136*, 909−918.
(45) Gray, V.; Dreos, A.; Erhart, P.; Albinsson, B.; Moth-Poulsen, K.; Abrahamsson, M. Loss Channels in Triplet−Triplet Annihilation Photon Upconversion: Importance of Annihilator Singlet and Triplet Surface Shapes. *Phys. Chem. Chem. Phys.* **2017**, *19* (17), 10931−10939.
(46) Sandros, K. Transfer of Triplet State Energy in Fluid Solutions. III. Reversible Energy Transfer. *Acta Chem. Scand.* **1964**, *18*, 2355−2374.
(47) Durandin, N. A.; Isokuortti, J.; Efimov, A.; Vuorimaa-Laukkanen, E.; Tkachenko, N. V.; Laaksonen, T. Efficient Photon Upconversion at Remarkably Low Annihilator Concentrations in a Liquid Polymer Matrix: When Less Is More. *Chem. Commun.* **2018**, *54* (99), 14029−14032.
(48) Gray, V.; Küçüköz, B.; Edhborg, F.; Abrahamsson, M.; Moth-Poulsen, K.; Albinsson, B. Singlet and Triplet Energy Transfer Dynamics in Self-Assembled Axial Porphyrin−Anthracene Complexes: Towards Supra-Molecular Structures for Photon Upconversion. *Phys. Chem. Chem. Phys.* **2018**, *20* (11), 7549−7558.
(49) Gray, V.; Dzebo, D.; Abrahamsson, M.; Albinsson, B.; Moth-Poulsen, K. Triplet−Triplet Annihilation Photon-Upconversion: Towards Solar Energy Applications. *Phys. Chem. Chem. Phys.* **2014**, *16* (22), 10345−10352.
(50) Groff, R. P.; Merrifield, R. E.; Avakian, P. Singlet and Triplet Channels for Triplet-Exciton Fusion in Anthracene Crystals. *Chem. Phys. Lett.* **1970**, *5* (3), 168−170.
(51) Hoseinkhani, S.; Tubino, R.; Meinardi, F.; Monguzzi, A. Achieving the Photon Up-Conversion Thermodynamic Yield Upper Limit by Sensitized Triplet−Triplet Annihilation. *Phys. Chem. Chem. Phys.* **2015**, *17* (6), 4020−4024.
(52) Monguzzi, A.; Tubino, R.; Hoseinkhani, S.; Campione, M.; Meinardi, F. Low Power, Non-Coherent Sensitized Photon up-Conversion: Modelling and Perspectives. *Phys. Chem. Chem. Phys.* **2012**, *14* (13), 4322−4332.
(53) Durandin, N. A.; Isokuortti, J.; Efimov, A.; Vuorimaa-Laukkanen, E.; Tkachenko, N. V.; Laaksonen, T. Critical Sensitizer Quality Attributes for Efficient Triplet-Triplet Annihilation Upconversion with Low Power Density Thresholds. *J. Phys. Chem. C* **2019**, *123* (37), 22865−22872.
(54) Gholizadeh, E. M.; Frazer, L.; MacQueen, R. W.; Gallaher, J. K.; Schmidt, T. W. Photochemical Upconversion Is Suppressed by High Concentrations of Molecular Sensitizers. *Phys. Chem. Chem. Phys.* **2018**, *20* (29), 19500−19506.
(55) O'Brien, J. A.; Rallabandi, S.; Tripathy, U.; Paige, M. F.; Steer, R. P. Efficient S2 State Production in ZnTPP−PMMA Thin Films by Triplet−Triplet Annihilation: Evidence of Solute Aggregation in Photon Upconversion Systems. *Chem. Phys. Lett.* **2009**, *475* (4), 220−222.
(56) Giri, N. K.; Ponce, C. P.; Steer, R. P.; Paige, M. F. Homomolecular Non-Coherent Photon Upconversion by Triplet−Triplet Annihilation Using a Zinc Porphyrin on Wide Bandgap Semiconductors. *Chem. Phys. Lett.* **2014**, *598*, 17−22.

DOI: 10.1021/acs.jpclett.9b03466
J. Phys. Chem. Lett. 2020, 11, 318−324

PUBLICATION IV

Expanding excitation wavelengths for azobenzene photoswitching into the near-infrared range via endothermic triplet energy transfer

Isokuortti, J.; Kuntze, K.; Virkki, M.; Ahmed, Z.; Vuorimaa-Laukkanen, E.; Filatov, M. A.; Turshatov, A.; Laaksonen, T.; Priimägi, A.; Durandin, N. A.

Chemical Science, vol. 12, p. 7504, 2021
DOI: https://doi.org/10.1039/D1SC01717A

Chemical Science

ROYAL SOCIETY OF CHEMISTRY

EDGE ARTICLE

View Article Online
View Journal | View Issue

Cite this: *Chem. Sci.*, 2021, **12**, 7504

All publication charges for this article have been paid for by the Royal Society of Chemistry

Expanding excitation wavelengths for azobenzene photoswitching into the near-infrared range *via* endothermic triplet energy transfer†

Jussi Isokuortti,[a] Kim Kuntze,[a] Matti Virkki,[a] Zafar Ahmed,[a] Elina Vuorimaa-Laukkanen,[a] Mikhail A. Filatov,[b] Andrey Turshatov,[c] Timo Laaksonen,[ad] Arri Priimagi*[a] and Nikita A. Durandin*[a]

Developing azobenzene photoswitches capable of selective and efficient photoisomerization by long-wavelength excitation is an enduring challenge. Herein, rapid isomerization from the *Z*- to *E*-state of two *ortho*-functionalized bistable azobenzenes with near-unity photoconversion efficiency was driven by triplet energy transfer upon red and near-infrared (up to 770 nm) excitation of porphyrin photosensitizers in catalytic micromolar concentrations. We show that the process of triplet-sensitized isomerization is efficient even when the sensitizer triplet energy is substantially lower (>200 meV) than that of the azobenzene used. This makes the approach applicable for a wide variety of sensitizer-azobenzene combinations and enables the expansion of excitation wavelengths into the near-infrared spectral range. Therefore, indirect excitation *via* endothermic triplet energy transfer provides efficient and precise means for photoswitching upon 770 nm near-infared light illumination with no chemical modification of the azobenzene chromophore, a desirable feature in photocontrollable biomaterials.

Received 26th March 2021
Accepted 25th April 2021

DOI: 10.1039/d1sc01717a

rsc.li/chemical-science

Introduction

Light is a versatile, non-invasive and efficient stimulus with high spatial and temporal resolution and facile modulation. Photoswitches, of which azobenzenes are arguably the most common class, enable the control of functional materials with light.[1,2] The photoswitching of azobenzenes is based on their reversible *trans*(*E*)-to-*cis*(*Z*) isomerization. Depending on their structure, azobenzenes have varying *Z*-isomer thermal lifetimes and varying degrees of spectral separation between the absorption bands of the isomers. Conventional azobenzenes absorb ultraviolet or visible light with relatively high energy, which limits their applicability for emerging fields such as solar energy harvesting,[3] 3D printing,[4] photosensors,[5] photoactuation[6] and photocatalysis.[7] When compared to longer wavelengths, UV excitation is hampered by, for example, its limited solar availability, non-specific absorption, and harmfulness to organic materials and live cells.[8] Moreover, due to the optical properties of biological tissue, photoswitching systems capable of operating under red or even near-infrared (NIR) light are of particular interest for biomedicine.[9–14]

Developing azobenzenes suitable for these aforementioned fields in terms of properties such as red-shifted excitation wavelengths, spectral resolution of *E*- and *Z*-isomers and thermal stability of the *Z*-isomer, requires structural modification;[15] a complex approach that generally involves extensive computational studies and synthesis. For example, *ortho*-functionalization of azobenzenes is an established approach to create photoswitches with a long *Z*-lifetime,[16,17] which is required for efficient photoswitching in both directions and precise control of the isomer composition. Despite recent advances, creating bistable red-absorbing azobenzenes remains a challenge, since red-shifting typically leads to drastically decreased thermal stability of the *Z*-isomer. Furthermore, there are no reports on bistable NIR-absorbing azobenzenes.[18,19]

Indirect excitation, *i.e.*, excitation that does not rely on the thermal relaxation or absorption bands of the *E*- and *Z*-isomers, but instead makes use of a proxy molecule to absorb light-activation signals, may overcome the foregoing issues of azobenzenes while retaining their beneficial intrinsic properties such as bistability and robustness. Intriguingly, indirect excitation allows tailoring and expansion of the photoswitching properties of the system without structural modification, even beyond the capabilities of the azobenzene itself. Isomerization by indirect excitation can be effected in various ways, such as photoinduced electron transfer,[20–22] two-photon absorption

[a]*Faculty of Engineering and Natural Sciences, Tampere University, FI-33101, Tampere, Finland. E-mail: arri.priimagi@tuni.fi; nikita.durandin@tuni.fi*
[b]*School of Chemical and Pharmaceutical Sciences, Technological University Dublin, City Campus, Kevin Street, Dublin 8, Ireland*
[c]*Institute of Microstructure Technology, Karlsruhe Institute of Technology, Hermann-von-Helmholtz-Platz 1, 76344 Eggenstein-Leopoldshofen, Germany*
[d]*Drug Research Program, Division of Pharmaceutical Biosciences, Faculty of Pharmacy, University of Helsinki, FI-00014, Helsinki, Finland*

† Electronic supplementary information (ESI) available. See DOI: 10.1039/d1sc01717a

induced energy transfer,[23] photon upconversion[24,25] and triplet sensitization.[26–30]

Triplet-sensitized *Z*-to-*E* isomerization of azobenzenes is an especially viable approach for indirect excitation due to its reversibility, non-destructivity and near-unity conversion efficiency.[26,29,31] Triplet sensitization has also been utilized to isomerize other types of photoswitches, such as overcrowded alkenes,[32] diarylethenes,[33] stilbenes[34] and indigos.[35] However, in previous reports triplet sensitizers have been excited in the UV-to-yellow (<580 nm) range, while the capabilities of potent red and NIR-absorbing triplet sensitizers, such as porphyrins, have not been utilized in azobenzene photoswitching. Thus, we set out to study this orthogonal excitation pathway for bistable azobenzenes and explore the wavelength limits of triplet-sensitized photoisomerization and how it improves the efficiency and control over photoswitching.

Here we demonstrate triplet-sensitized *Z*-to-*E* isomerization of azobenzenes under red and NIR excitation and establish its efficiency *via* kinetics studies. We have employed a NIR-absorbing porphyrin, PdNP (Pd(II)*meso*-tetraphenyltetranaphthoporhyrin[36–38]) and two commercially available red-absorbing porphyrins, PdP and PtP (Pd(II) and Pt(II)*meso*-tetraphenyltetrabenzoporphyrin, see Chart 1), as triplet photosensitizers. The sensitizers were used in combination with tetrafluoroazobenzene (TFA[39,40]) and fluoropyrrolidineazobenzene (FPA,[41] see Chart 1). Both *ortho*-functionalized azobenzenes exhibit efficient photoisomerization (>80% conversion to both *Z*- and *E*-isomers) under visible light and remarkably long thermal half-lives (days). TFA requires blue light (410 nm) for *Z*-to-*E* photoisomerization. In contrast, *Z*-FPA absorbs red light, albeit weakly, and thus it was used to compare photoisomerization under direct and triplet-sensitized excitation.

Results and discussion

Triplet energy transfer studies

All experiments were conducted in dimethyl sulfoxide (DMSO). Since triplet sensitizers generate reactive oxygen species under illumination, bis(methylthio)methane was added as an oxygen scavenger.[42] To study the triplet energy transfer (TET) from PdP and PtP to the azobenzenes, we performed quenching studies by measuring the phosphorescence lifetimes of both sensitizers in the presence of *E*- or *Z*-isomers of both azobenzenes. The resulting Stern–Volmer plots of the quenching studies are shown in Fig. 1.

The Stern–Volmer rate constant (K_{SV}) yielded by the linear fit on the quenching data was then used to evaluate the rate constant of triplet energy transfer:

$$k_{TET} = \frac{K_{SV}}{\tau_0}, \quad (1)$$

where τ_0 is the unquenched phosphorescence lifetime of the sensitizer (260 μs and 46 μs for PdP and PtP, respectively). The quenching experiments are discussed in more detail in the ESI.† k_{TET} values were then used to calculate the triplet energy gap (ΔE_T) between the sensitizer and azobenzene triplet states:[43]

$$\frac{\Delta E_T}{k_B T} = \ln\left(\frac{k_{diff}}{k_{TET}} - 1\right), \quad (2)$$

where k_B is the Boltzmann constant, T is the temperature and k_{diff} ($= 1.1 \times 10^9$ M^{-1} s^{-1}) is the diffusion rate constant of the system (see the ESI†). Finally, the obtained ΔE_T values were used together with the sensitizer triplet energies (1.55 and 1.61 eV for PdP and PtP, respectively, see Fig. S3†) to evaluate the triplet energies (E_T) of both *E*- and *Z*-isomers of the azobenzenes. To our knowledge, these are the first reported triplet state energies of *ortho*-substituted azobenzenes. The k_{TET}, ΔE_T and E_T values of each pair are given in Table 1.

Interestingly, the *Z*-isomer of TFA has higher E_T than the *E*-isomer, which appears contrary to the unsubstituted azobenzene (E_T of *Z*-isomer 29 kcal mol^{-1} *i.e.* 1.29 eV), whereas the E_T values of *E*-TFA and *E*-FPA are comparable to the previously reported values for unsubstituted and *para*-substituted azobenzenes (33–35 kcal mol^{-1} *i.e.* 1.43–1.52 eV).[44,45] The kinetics studies results also reveal the

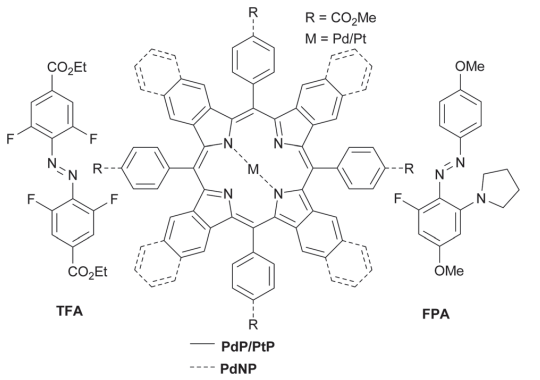

Chart 1 Sensitizers and azobenzenes used in this study.

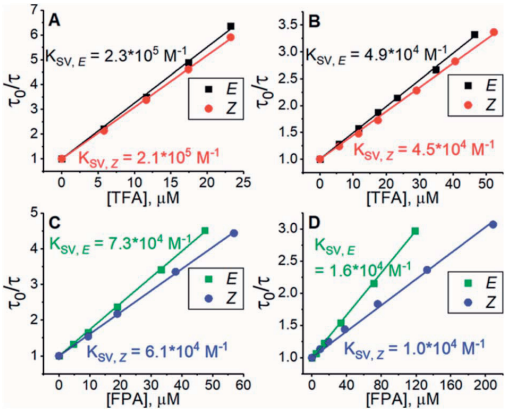

Fig. 1 Results of phosphorescence quenching. Stern–Volmer plots and the corresponding K_{SV} values of (A) TFA and PdP, (B) TFA and PtP, (C) FPA and PdP and (D) FPA and PtP.

Table 1 Rate constant of triplet energy transfer (k_{TET}), the triplet energy gap (ΔE_T) between the sensitizer and azobenzene, and the triplet energy (E_T) of the azobenzene derived from the quenching results

Pair	k_{TET} (M^{-1} s^{-1})	ΔE_T (k_BT)	ΔE_T (meV)	E_T (eV)
E-TFA/PdP	8.7×10^8	−1.3	−34	1.49–1.52
E-TFA/PtP	1.1×10^9	−4.7	−120	
Z-TFA/PdP	8.1×10^8	−1.0	−26	1.52–1.56
Z-TFA/PtP	9.7×10^8	−2.0	−52	
E-FPA/PdP	2.8×10^8	1.1	29	1.58–1.63
E-FPA/PtP	3.6×10^8	0.7	18	
Z-FPA/PdP	2.4×10^8	1.3	34	1.58–1.65
Z-FPA/PtP	2.2×10^8	1.4	36	

thermodynamics between the sensitizer and azobenzene: triplet energy transfer from both PdP and PtP appears exothermic for TFA (negative ΔE_T), while the lower values of k_{TET} between the sensitizers and FPA indicate endothermic energy transfer (positive ΔE_T).

Triplet-sensitized isomerization with red light

To study the effect of the triplet energies on photoisomerization, we employed both PdP and PtP for photoswitching of TFA and FPA. In agreement with previous works,[26,28,29] *E*-to-*Z* isomerization was negligible on excitation of the sensitizer. This was observed although k_{TET} of the *E*-isomer is larger than for the *Z*-isomer for both TFA and FPA. However, after isomerizing the azobenzenes to their *Z*-configuration by direct excitation of the *E*-isomer (525 nm for TFA and 405 nm for FPA), rapid and nearly complete *Z*-to-*E* isomerization could be readily induced under 640 nm excitation using catalytic amounts (1.8 μM *i.e.* 1.2 mol% with respect to the azobenzene) of each sensitizer (see Fig. 2). An exponential function was fitted to the isomerization data to determine the rates of isomerization ($r_{Z\to E}$). The resulting fits are shown in Fig. S12–S16.† The rates of *Z*-to-*E* isomerization are clearly increased by several orders of magnitude by indirect excitation *via* the triplet energy transfer route. For example, the photoisomerization rate for FPA by triplet sensitization was over 100 times faster than that under 640 nm direct excitation (3.10 min^{-1} *versus* 0.028 min^{-1}). As expected, no isomerization of TFA without sensitizers was observed under 640 nm excitation. Notably, the sensitized photoswitching of FPA, for which TET is endothermic and thus slower, occurs as rapidly as photoswitching of TFA.

The conversion efficiency of sensitized *Z*-to-*E* isomerization ($\Phi_{Z\to E}$) was determined from the curves as the ratio of initial (dark) and final (achieved upon sensitization) absorbances. All values were close to unity, and only a minor difference in the conversion efficiency was observed between TFA and FPA. $r_{Z\to E}$ and $\Phi_{Z\to E}$ values of each sensitizer/azobenzene pair are shown in Table 2.

Surprisingly, the sensitizers appear to catalyze the *Z*-to-*E* isomerization of FPA even in the dark (see Fig. S18†). This increase in the rate of the thermal isomerization is especially pronounced with PtP as the contribution of the dark reaction to the overall observed rate is 31% (0.15 min^{-1}). In case of FPA/PdP, the contribution is only *ca.* 2% (0.06 min^{-1}). Also, the free base of the porphyrin (H_2P) catalyzes the isomerization of FPA in the dark (0.09 min^{-1}). This catalytic effect is perhaps a result of ground state coordination[46–48] between *Z*-FPA and the porphyrin. FPA has three π donors in *ortho*- and *para*-positions and only one electron-withdrawing fluorine substituent, increasing the affinity of the azo bridge to an electron-deficient site such as a metal cation. This effect is not observed with the drastically electron-poorer TFA, which supports this explanation.

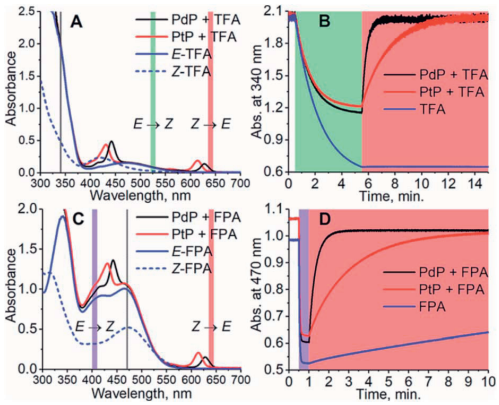

Fig. 2 The absorption spectra of the photoswitching systems consisting of PdP and PtP and TFA (A) and FPA (C) and their photoisomerization curves (B) and (D). The concentration of the azobenzene was 150 μM and the concentration of the sensitizer was 1.2 mol% of the azobenzene, *i.e.* 1.8 μM. The colored sections indicate the wavelength and time ranges used for photoswitching. The excitation light is on during the times indicated by the representative colors. Gray lines in (A) and (C) indicate the wavelength used for monitoring the isomerization. The observed partial *E*-to-*Z* isomerization of the azobenzenes, especially in case of TFA due to its small molar extinction coefficient at 525 nm, is caused by the competitive absorption of the azobenzene and the sensitizer.

Table 2 Rates ($r_{Z\to E}$) and efficiency ($\Phi_{Z\to E}$) of the photoisomerization under 640 nm excitation

Pair	TFA/PdP	TFA/PtP	FPA/PdP	FPA/PtP
$r_{Z\to E}$ (min^{-1})	3.10	0.50[a]	3.10	0.49[a]
$\Phi_{Z\to E}$ (%)	99	99	96	96

[a] The smaller $\Phi_{Z\to E}$ yielded by PtP results mainly from a smaller spectral overlap between the absorption and the excitation (see Fig. 2).

Mechanism of triplet-sensitized isomerization

To better understand the observed results of triplet-sensitized photoswitching and the considerably increased isomerization rates, we conducted an analysis of the underlying reaction mechanisms that can be described with the following set of equations:[26,29]

$$^3S^* + E - \text{Azo} \xrightarrow{k_{\text{TET-}E}} S + {}^3\text{Azo}^* \quad (3)$$

$$^3S^* + Z - \text{Azo} \xrightarrow{k_{\text{TET-}Z}} S + {}^3\text{Azo}^* \quad (4)$$

$$^3\text{Azo}^* \xrightarrow{k_{\text{ISC-}E}} E\text{-Azo} \quad (5)$$

$$^3\text{Azo}^* \xrightarrow{k_{\text{ISC-}Z}} Z\text{-Azo} \quad (6)$$

where S is the sensitizer, superscript 3 is the triplet state, ISC is the intersystem crossing between the singlet and triplet states and k denotes the rate constant of each process. $k_{\text{TET-}E}$ and $k_{\text{TET-}Z}$ are determined experimentally and given in Table 1. It is also important to notice, that ^{3}Azo* can be considered as a common state between the isomers, since there is no energy barrier associated with the CNNC twist in the triplet manifold.[49,50] While there are no direct observations reported on the triplet lifetime of azobenzenes, the commendable computational work[49] by Cembran *et al.* estimates $k_{\text{ISC-}E}$ as 10^{11} s^{-1}. The ultrafast ISC results from the degeneracy between the minimum of the triplet state and the intersection between the triplet state and ground state of *E*-Azo. Since the photostationary composition yielded by sensitized isomerization can be derived from the equations above as[26,29]

$$\frac{[E\text{-Azo}]}{[Z\text{-Azo}]} = \frac{k_{\text{TET-}Z}}{k_{\text{TET-}E}} \frac{k_{\text{ISC-}E}}{k_{\text{ISC-}Z}}, \quad (7)$$

we can use $\Phi_{Z\rightarrow E}$ and the TET results to estimate relative $k_{\text{ISC-}Z}$ for TFA (10^9 s^{-1}) and FPA (3×10^9 s^{-1}), corresponding roughly to 1–3% of $k_{\text{ISC-}E}$. This also explains why triplet sensitization of azobenzenes leads almost exclusively to the formation of the *E*-isomer.[26,29,49]

Based on the isomerization kinetics, even endothermic TET (as is the case with FPA) is apparently capable of driving isomerization efficiently. This indicates that the whole process of triplet-sensitized isomerization is largely entropy-driven,[51,52] since the rate of the isomerization is fairly decoupled from the change in enthalpy involved in TET. The change in entropy (ΔS) of TET is[51]

$$\Delta S = k_{\text{B}} \ln\left(\frac{[Z - \text{Azo}]\left[^3S^*\right]}{[S]\left[^3\text{Azo}^*\right]}\right). \quad (8)$$

The ultrafast crossing between the triplet state and the ground state of *E*-Azo (eqn (5)) leads to $[^3\text{Azo}^*] \ll [Z\text{-Azo}]$, $[^3S^*]$, $[S]$ and ensures a large entropy component in the triplet-sensitized isomerization. This also effectively eliminates the azobenzene-to-sensitizer reverse TET.[52] Therefore, even photosensitizers with considerably lower triplet energies are still capable of sensitizing the *Z*-to-*E* isomerization of azobenzenes, which enables the expansion of excitation wavelengths to the deeper red and even into NIR regions.

Triplet-sensitized isomerization with near-infrared light

Prompted by this finding, we combined TFA with PdNP, a sensitizer with a triplet energy of 1.30 eV and strong absorption in the NIR region (see Fig. S2 and S4†). The triplet energy gap of this pair is thus ≥220 meV, *i.e.*, 8.5 $k_{\text{B}}T$, and as a result, TET is highly endothermic. Nonetheless, photoisomerization under 740 nm excitation was, to our delight, efficient despite this remarkably high endothermic energy gap (see Fig. 3). PdNP was capable of sensitizing isomerization of TFA even under 770 nm excitation ($r_{Z\rightarrow E}$ = 0.93 min^{-1}, see Fig. S14†).

Thanks to the bistable nature and rapid triplet-sensitized isomerization of TFA under NIR excitation, the isomer composition can be precisely controlled by modulating the excitation dose (duration and/or intensity). This stepwise photoisomerization by dosed excitation is shown in Fig. 4. Repeatable cyclic switching between isomers is also typically desired for applications of photoswitching. This can be achieved in triplet-sensitized photoswitching systems by alternating excitation of the azobenzene and sensitizer as shown in Fig. 4 No discernible change in the rate of sensitized isomerization and only a slight

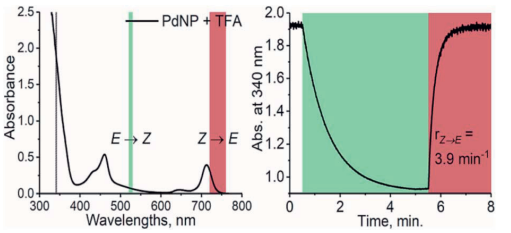

Fig. 3 Absorption spectrum of PdNP and TFA (left) and the photoisomerization curve (right) under 525 nm (green color) and 740 nm (dark red) excitation with the resulting rates of isomerization.

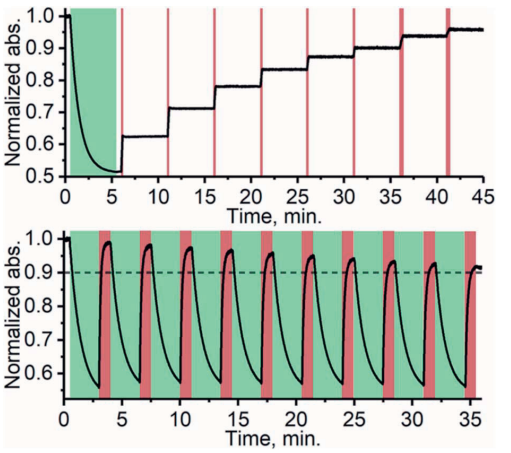

Fig. 4 Stepwise photoisomerization (above) of TFA by exciting PdNP with 10 s (last two were 20 s) doses of 740 nm excitation (dark red bars) in 5 min intervals. Cyclic photoswitching (below) of TFA/PdNP with 10 cycles of alternating 525 nm (direct excitation of *E*-TFA, green sections) and 740 nm (excitation of PdNP, dark red sections) excitation wavelengths.

decrease in efficiency (less than 10%, likely due to photobleaching) was observed in 10 cycles. Photoswitching is achievable even in the presence of oxygen (Fig. S19†), when the effects of singlet oxygen generated by the photosensitizer are mitigated by employing oxygen-scavengers.

Conclusions

We have shown that photoisomerization of bistable *ortho*-functionalized azobenzenes *via* triplet energy transfer is rapid with near-unity efficiency under red and near-infrared (up to 770 nm) excitation. Detailed studies of the kinetics indicate that triplet-sensitized isomerization is largely entropy-driven. Thus, even sensitizers with triplet energies considerably lower than those of the azobenzenes used are still capable of effectively sensitizing the isomerization. This was confirmed by using an azobenzene/sensitizer pair with an endothermic triplet energy gap of over 200 meV between them. The major entropy-factor involved in the process also projects that this excitation pathway is efficient for any azobenzene. This expands the properties of photoswitching systems without chemically modifying the photoswitch itself. Combined with the desirable use of red/NIR excitation, precise control of isomer composition, and repeatable cyclic isomerization, we envision that this approach will emerge as a potent tool for low-energy photoswitching in light-responsive materials.

Conflicts of interest

There are no conflicts to declare.

Acknowledgements

The authors gratefully acknowledge financial support from the Academy of Finland (Grant No. 316893) and the European Research Council (ERC Starting Grant Project PHOTOTUNE, decision number 679646). K. Kuntze is grateful for financial support from the Tampere University graduate school. This work was conducted as part of the Academy of Finland Flagship Programme, Photonics Research and Innovation (PREIN), Decision Number 321065.

Notes and references

1 A. Goulet-Hanssens, F. Eisenreich and S. Hecht, *Adv. Mater.*, 2020, **32**, 1905966.
2 D. Dattler, G. Fuks, J. Heiser, E. Moulin, A. Perrot, X. Yao and N. Giuseppone, *Chem. Rev.*, 2020, **120**, 310–433.
3 L. Dong, Y. Feng, L. Wang and W. Feng, *Chem. Soc. Rev.*, 2018, **47**, 7339–7368.
4 D. Ahn, L. M. Stevens, K. Zhou and Z. A. Page, *ACS Cent. Sci.*, 2020, **6**, 1555–1563.
5 X. Zhou, T. Zifer, B. M. Wong, K. L. Krafcik, F. Léonard and A. L. Vance, *Nano Lett.*, 2009, **9**, 1028–1033.
6 J. Boelke and S. Hecht, *Adv. Opt. Mater.*, 2019, **7**, 1900404.
7 B. M. Neilson and C. W. Bielawski, *ACS Catal.*, 2013, **3**, 1874–1885.
8 M. Zayat, P. Garcia-Parejo and D. Levy, *Chem. Soc. Rev.*, 2007, **36**, 1270–1281.
9 M. Dong, A. Babalhavaeji, S. Samanta, A. A. Beharry and G. A. Woolley, *Acc. Chem. Res.*, 2015, **48**, 2662–2670.
10 M. J. Fuchter, *J. Med. Chem.*, 2020, **63**, 11436–11447.
11 D. Bléger and S. Hecht, *Angew. Chem., Int. Ed.*, 2015, **54**, 11338–11349.
12 S. Samanta, A. A. Beharry, O. Sadovski, T. M. McCormick, A. Babalhavaeji, V. Tropepe and G. A. Woolley, *J. Am. Chem. Soc.*, 2013, **135**, 9777–9784.
13 I. M. Welleman, M. W. H. Hoorens, B. L. Feringa, H. H. Boersma and W. Szymański, *Chem. Sci.*, 2020, **11**, 11672–11691.
14 K. Hüll, J. Morstein and D. Trauner, *Chem. Rev.*, 2018, **118**, 10710–10747.
15 H. M. D. Bandara and S. C. Burdette, *Chem. Soc. Rev.*, 2012, **41**, 1809–1825.
16 D. Bléger, J. Schwarz, A. M. Brouwer and S. Hecht, *J. Am. Chem. Soc.*, 2012, **134**, 20597–20600.
17 M. J. Hansen, M. M. Lerch, W. Szymanski and B. L. Feringa, *Angew. Chem., Int. Ed.*, 2016, **55**, 13514–13518.
18 M. Dong, A. Babalhavaeji, C. V Collins, K. Jarrah, O. Sadovski, Q. Dai and G. A. Woolley, *J. Am. Chem. Soc.*, 2017, **139**, 13483–13486.
19 D. B. Konrad, G. Savasci, L. Allmendinger, D. Trauner, C. Ochsenfeld and A. M. Ali, *J. Am. Chem. Soc.*, 2020, **142**, 6538–6547.
20 A. Goulet-Hanssens, M. Utecht, D. Mutruc, E. Titov, J. Schwarz, L. Grubert, D. Bléger, P. Saalfrank and S. Hecht, *J. Am. Chem. Soc.*, 2017, **139**, 335–341.
21 A. Goulet-Hanssens, C. Rietze, E. Titov, L. Abdullahu, L. Grubert, P. Saalfrank and S. Hecht, *Chem*, 2018, **4**, 1740–1755.
22 G. L. Hallett-Tapley, C. D'Alfonso, N. L. Pacioni, C. D. McTiernan, M. González-Béjar, O. Lanzalunga, E. I. Alarcon and J. C. Scaiano, *Chem. Commun.*, 2013, **49**, 10073–10075.
23 J. Moreno, M. Gerecke, L. Grubert, S. A. Kovalenko and S. Hecht, *Angew. Chem., Int. Ed.*, 2016, **55**, 1544–1547.
24 Z. Jiang, M. Xu, F. Li and Y. Yu, *J. Am. Chem. Soc.*, 2013, **135**, 16446–16453.
25 L. Wang, H. Dong, Y. Li, C. Xue, L.-D. Sun, C.-H. Yan and Q. Li, *J. Am. Chem. Soc.*, 2014, **136**, 4480–4483.
26 L. B. Jones and G. S. Hammond, *J. Am. Chem. Soc.*, 1965, **87**, 4219–4220.
27 J. Ronayette, R. Arnaud, P. Lebourgeois and J. Lemaire, *Can. J. Chem.*, 1974, **52**, 1848–1857.
28 J. Ronayette, R. Arnaud and J. Lemaire, *Can. J. Chem.*, 1974, **52**, 1858–1867.
29 P. Bortolus and S. Monti, *J. Phys. Chem.*, 1979, **83**, 648–652.
30 A. Goulet-Hanssens, C. Rietze, E. Titov, L. Abdullahu, L. Grubert, P. Saalfrank and S. Hecht, *Chem*, 2018, **4**, 1740–1755.
31 A. Cembran, F. Bernardi, M. Garavelli, L. Gagliardi and G. Orlandi, *J. Am. Chem. Soc.*, 2004, **126**, 3234–3243.

32 A. Cnossen, L. Hou, M. M. Pollard, P. V Wesenhagen, W. R. Browne and B. L. Feringa, *J. Am. Chem. Soc.*, 2012, **134**, 17613–17619.
33 S. Fredrich, T. Morack, M. Sliwa and S. Hecht, *Chem.–Eur. J.*, 2020, **26**, 7672–7677.
34 J. A. Mercer-Smith and D. G. Whitten, *J. Am. Chem. Soc.*, 1978, **100**, 2620–2625.
35 G. M. Wyman, B. M. Zarnegar and D. G. Whitten, *J. Phys. Chem.*, 1973, **77**, 2584–2586.
36 J. E. Rogers, K. A. Nguyen, D. C. Hufnagle, D. G. McLean, W. Su, K. M. Gossett, A. R. Burke, S. A. Vinogradov, R. Pachter and P. A. Fleitz, *J. Phys. Chem. A*, 2003, **107**, 11331–11339.
37 V. V Rozhkov, M. Khajehpour and S. A. Vinogradov, *Inorg. Chem.*, 2003, **42**, 4253–4255.
38 O. S. Finikova, S. E. Aleshchenkov, R. P. Briñas, A. V Cheprakov, P. J. Carroll and S. A. Vinogradov, *J. Org. Chem.*, 2005, **70**, 4617–4628.
39 D. Bléger, J. Schwarz, A. M. Brouwer and S. Hecht, *J. Am. Chem. Soc.*, 2012, **134**, 20597–20600.
40 C. Knie, M. Utecht, F. Zhao, H. Kulla, S. Kovalenko, A. M. Brouwer, P. Saalfrank, S. Hecht and D. Bléger, *Chem.–Eur. J.*, 2014, **20**, 16492–16501.
41 Z. Ahmed, A. Siiskonen, M. Virkki and A. Priimagi, *Chem. Commun.*, 2017, **53**, 12520–12523.
42 D. Dzebo, K. Moth-Poulsen and B. Albinsson, *Photochem. Photobiol. Sci.*, 2017, **16**, 1327–1334.
43 K. Sandros, *Acta Chem. Scand.*, 1964, **18**, 2355–2374.
44 S. Monti, E. Gardini, P. Bortolus and E. Amouyal, *Chem. Phys. Lett.*, 1981, **77**, 115–119.
45 S. Monti, S. Dellonte and P. Bortolus, *J. Photochem.*, 1983, **23**, 249–256.
46 A. Nakamura, K. Doi, K. Tatsumi and S. Otsuka, *J. Mol. Catal.*, 1976, **1**, 417–429.
47 S. Ciccone and J. Halpern, *Can. J. Chem.*, 1959, **37**, 1903–1910.
48 Z. Wang, R. Losantos, D. Sampedro, M. Morikawa, K. Börjesson, N. Kimizuka and K. Moth-Poulsen, *J. Mater. Chem. A*, 2019, **7**, 15042–15047.
49 A. Cembran, F. Bernardi, M. Garavelli, L. Gagliardi and G. Orlandi, *J. Am. Chem. Soc.*, 2004, **126**, 3234–3243.
50 L. Gagliardi, G. Orlandi, F. Bernardi, A. Cembran and M. Garavelli, *Theor. Chem. Acc.*, 2004, **111**, 363–372.
51 Y. Y. Cheng, B. Fückel, T. Khoury, R. G. C. R. Clady, N. J. Ekins-Daukes, M. J. Crossley and T. W. Schmidt, *J. Phys. Chem. A*, 2011, **115**, 1047–1053.
52 J. Isokuortti, S. R. Allu, A. Efimov, E. Vuorimaa-Laukkanen, N. V. Tkachenko, S. A. Vinogradov, T. Laaksonen and N. A. Durandin, *J. Phys. Chem. Lett.*, 2020, **11**, 318–324.